



Calhoun: The NPS Institutional Archive
DSpace Repository

Theses and Dissertations

1. Thesis and Dissertation Collection, all items

2014-12

Modeling the Performance of a Laser for Tracking an Underwater Dynamic Target

Dill, Thomas J.

Florida Atlantic University

<http://hdl.handle.net/10945/44418>

Downloaded from NPS Archive: Calhoun



Calhoun is a project of the Dudley Knox Library at NPS, furthering the precepts and goals of open government and government transparency. All information contained herein has been approved for release by the NPS Public Affairs Officer.

Dudley Knox Library / Naval Postgraduate School
411 Dyer Road / 1 University Circle
Monterey, California USA 93943

<http://www.nps.edu/library>

Modeling the Performance of a Laser for Tracking an Underwater Dynamic Target

by

Thomas J. Dill

A Thesis Proposal Submitted to the Faculty of
The College of Engineering and Computer Science
in Partial Fulfillment of the Requirements for the Degree of
Master of Science

Florida Atlantic University

Boca Raton, Florida

December 2014

Copyright 2014 by Thomas J. Dill

Modeling the Performance of a Laser for Tracking an Underwater Dynamic Target

by

Thomas J. Dill

This thesis was prepared under the direction of the candidate's thesis advisor, Dr. Karl von Ellenrieder, Department of Ocean and Mechanical Engineering, and has been approved by the members of his supervisory committee. It was submitted to the faculty of the College of Engineering and Computer Science and was accepted in partial fulfillment of the requirements for the degree of Master of Science.

SUPERVISORY COMMITTEE:



Karl von Ellenrieder, Ph.D.

Thesis Advisor



Pierre-Philippe Beaujean, Ph.D.

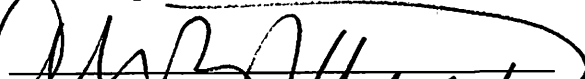


William A. Venezia, Ph.D.




Jayad Hashemi, Ph.D.

Chair, Department of Ocean and Mechanical Engineering



Mohammad Ilyas, Ph.D.

Dean, College of Engineering and Computer Science



Deborah L. Floyd, Ed.D.

Interim Dean, Graduate College

11/14/2014

Date

Acknowledgements

I wish to thank my committee members for their guidance, expertise, and support throughout this thesis work. George Valdez who was a dedicated partner in underlying research and developed the prototype hardware on which the concepts for this thesis revolve. Dr. Fraiser Dagleish who provided extensive background in current laser research, aiding development of the fundamentals for an underwater tracking application. Dr. Philippe-Pierre Beaujean who offered encouragement and a significant source of knowledge at critical junctures in the process. Many thanks to Meredith King for reading, re-reading, and reading again the research proposal and final thesis, lending her skills to questioning every word, comma, and period. Special thanks to my advisor, Dr. Karl von Ellenrieder, for his continual support and advice to bring me back into the research world after a decade of absence and encouraging completion of this thesis. Finally, much thanks to Dr. William Venezia for providing a research opportunity which leveraged many strengths, improved weaknesses, and an interesting topic applicable beyond my academic pursuits. I am sincerely grateful to you all.

Abstract

Author: Thomas J Dill
Title: Modeling the Performance of a Laser for Tracking an Underwater Dynamic Target
Institution: Florida Atlantic University
Thesis Advisor: Dr. Karl von Ellenrieder
Degree: Master of Science Ocean and Mechanical Engineering
Year: 2014

Options for tracking dynamic underwater targets using optical methods is currently limited. This thesis examines optical reflectance intensities utilizing Lambert's Reflection Model and based on a proposed underwater laser tracking system. Numerical analysis is performed through simulation to determine the detectable light intensities based on relationships between varying inputs such as angle of illumination and target position. Attenuation, noise, and laser beam spreading are included in the analysis. Simulation results suggest optical tracking exhibits complex relationships based on target location and illumination angle. Signal to Noise Ratios are a better indicator of system capabilities than received intensities. Signal reception does not necessarily confirm target capture in a multi-sensor network.

Dedication

To my fiancée, Meredith, for your love, dedication, and support through our life together. I couldn't be successful without you. Thank you for all the time and support you've given me to complete my studies. I love you.

Modeling the Performance of a Laser for Tracking an Underwater Dynamic Target

List of Tables	ix
List of Figures	x
Nomenclature	xvi
1 Introduction.....	1
1.1 Development of an Optical Based Tracking System	3
1.2 Foundations and Applications.....	7
1.3 Problem Statement	8
2 Literature Review.....	10
2.1 Light Attenuation	11
2.2 Laser Range Detection Methods.....	13
2.3 Optical Noise	14
2.4 Signal Processing.....	15
2.5 Reflection Modeling	17
3 Approach.....	20
3.1 Lambert’s Model.....	20
3.2 Environmental Effects	22
3.3 Range Estimation	25
3.4 Simulation Geometry	27
3.5 Simulation Cases.....	30

3.6 Simulation Construction	31
4 Results.....	33
4.1 Case II Results	34
4.1.1 Ideal Transmission	34
4.1.2 Attenuation at Constant Depth	36
4.1.3 Signal to Noise Ratio.....	37
4.2 Case III Results	40
4.2.1 Ideal Transmission	40
4.2.2 Attenuation at Constant Depth	42
4.2.3 Signal to Noise Ratio.....	43
4.3 Case IV Results.....	45
4.3.1 Ideal Transmission	45
4.3.2 Single Sensor Attenuated Model.....	47
4.3.3 Signal to Noise Ratio.....	49
4.4 Case V Results	50
4.4.1 Ideal Transmission	50
4.4.2 Multi-Sensor Attenuated Model.....	53
4.4.3 Signal to Noise Ratio.....	56
4.5 Additional Characteristics and Trends.....	59
4.5.1 Tendency of Illumination	59
4.5.2 Average Intensity Response	61
4.5.3 Average SNR Results.....	63
4.6 Range Estimation	65

4.7 Target Tracking.....	69
4.7.1 Laser Power.....	69
4.7.2 Detector Distribution.....	70
5 Conclusions.....	72
Appendices.....	76
Appendix A Case V Intensity Results	77
Appendix B Case V SNR Results.....	87
References.....	92

List of Tables

Table 1: Characteristics of the prototype underwater laser tracking system	5
Table 2 Detector geometry path lengths	71

List of Figures

Figure 1: Conceptual Operation of the Laser Tracking System	6
Figure 2: Laser attenuation over $k = 0:1.25$. Resulting intensity is mapped against the range [m] of travel.....	24
Figure 3: Simulation geometry for transmitter-target-detector relationship.....	28
Figure 4: Simulation geometry, dynamic cases with target movement and laser scanning	29
Figure 5 Case II: Target illumination and reflection intensities for ideal attenuation, $k = 0$ and depth $z = 10$ meters. Results are for a single scan point of the target at each position starting at 1 meter from the transmitter-detector baseline to 21 meters	35
Figure 6 Case II: Intensity delivered to target and sensor at depth $z = 30$ meters and varying attenuation coefficient, $k = 0, 0.25, 1$. The top graph is target illumination and the bottom is reflection intensity.	36
Figure 7 Case II: SNR for constant depth, $z = 30$, and varying attenuation $k = 0, 0.25$, and 1.....	38
Figure 8 Case II: SNR with constant attenuation, $k = 0.25$, and varying depth, $z = 10, 20$, and 30 meters	39
Figure 9 Case III: Laser intensity at the target and sensor under ideal environmental conditions, $k = 0$, at depth $z = 30$ meters. Target is located 1 [m] from the transmitter-sensor baseline.....	40

Figure 10 Case III: Intensity levels for varying angles of illumination and reflection with increasing attenuation at depth $z = 30$ meters. Top graph is target irradiance and bottom graph is intensity at the sensor. Target is located 1 [m] from the transmitter-sensor baseline..... 42

Figure 11 Case III: SNR for increasing attenuation, $k = 0, 0.25,$ and 1, at constant depth, $z = 30$ meters. Target distance is 1 [m] from transmitter-detector baseline.... 43

Figure 12 Case III: SNR at constant attenuation, $k = 0.25,$ and varying depth, $z = 10,$ 20, and 30 meters. Target distance is 1 [m] from transmitter-detector baseline..... 44

Figure 13 Case IV: Ideal transmission with no attenuation, $k = 0,$ at depth $z = 30$ meters. Performance combines varying target position, 1 to 21 meters, and laser scan per position. Curves are plotted Intensity vs Angle with curves on the left of the graph representing results for farthest positions and curves on the right representing closest positions to the transmitter-detector baseline. Arrows in the graphs represent the direction for increasing target position. 46

Figure 14 Case IV: Target illumination and reflected intensities per position with no attenuation, $k = 0,$ and depth $z = 30$ meters. Arrow indicates direction for increasing target position. 47

Figure 15 Case IV: Illumination and reflection intensity responses for $k = 0.25$ and $z = 30$ meters. Arrows indicate direction for increasing target position..... 48

Figure 16 Case IV: SNR for attenuation $k = 0.25$ at depth $z = 30$ meters. Arrow indicates direction for increasing target position. 49

Figure 17 Case V: Target and detector intensity under ideal conditions: attenuation, $k = 0$ at depth $z = 30$ meters. Results at position 1, $r = 1$ meter from baseline is on

the far right, while results at position 21, $r = 21$ meters from baseline is on the far left. Top graph is illumination intensity and the bottom graph is intensity incident at the sensors. Arrow in the upper graph indicates direction of increasing target position for both illumination and reflection..... 51

Figure 18 Case V: Illumination and reflection matched sets for ideal transmission. Arrow indicates direction for increasing target position..... 52

Figure 19 Case V: Illumination and reflection intensities with no attenuation, $k = 0$, at depth $z = 30$ plotted along three axes showing position, angle, and magnitude..... 53

Figure 20 Case V: Multi-sensor attenuated intensity response with attenuation, $k = 0.25$, and depth, $z = 30$ [m]. Top graph is target irradiance and the bottom graph is the intensity response at the sensors. Arrow indicates direction of increasing target position for both illumination and reflection. 54

Figure 21 Case V: General relationship between illuminated and reflected intensities at sensors 1 and 2 in an attenuating environment, $k = 0.25$ and 1, at depth $z = 30$. Arrow indications direction of increasing target position..... 55

Figure 22 Case V: Illuminated and reflection intensities with attenuation, $k = 0.25$ at depth $z = 30$ along 3 axes showing position, angle, and magnitude..... 56

Figure 23 Case V: SNR response curve for attenuation $k = 0.25$ at depth $z = 30$ [m]. Arrow indicates direction of increasing target position..... 57

Figure 24 Case V: SNR response curve for a potential tracking condition considering the described laser parameters. Attenuation, $k = 0.75$ at depth $z = 60$ [m]. Arrow indicates direction of increasing target position. 58

Figure 25 Tendency of illumination for the laser with increasing attenuation factor across all positions and angles. Region 1 is dominated by illumination area through beam divergence, region 2 cosine of the illumination angle, and region 3 attenuation.....	60
Figure 26 Average target illumination with increasing attenuation at constant depth. Top graph is target irradiance, middle is sensor 1 response, and the bottom is sensor 2 response.	61
Figure 27 Difference in the average intensity responses for various attenuation levels at depth $z = 30$ [m]. Top: Difference between illumination and sensor 1. Middle: Difference between illumination and sensor 2. Bottom: Difference between sensors.....	62
Figure 28 Average SNR results for increasing attenuation results and constant depth, $z = 30$ [m]. Top: SNR for sensor 1. Middle: SNR sensor 2. Bottom: Difference between the sensors.....	63
Figure 29 Average SNR results for increasing depth and constant attenuation, $k = 0.25$. Top: SNR sensor 1. Middle: SNR sensor 2. Bottom: Sensor difference.	64
Figure 30 Range estimation results from detected intensity results in Case V, multi-sensor. No attenuation and beam divergence.....	67
Figure 31 Range estimate error. Error is normalized to target distance from the transmitter-sensor baseline. No attenuation and beam divergence.	68
Figure 32 Case V illumination and intensity results for increasing attenuation at depth $z = 10$ [m]. From top to bottom $k = 0, 0.25, 0.5, 0.75, 1$	78

Figure 33 Case V illumination and intensity results for increasing attenuation at depth $z = 20$ [m]. From top to bottom $k = 0, 0.25, 0.5, 0.75, 1$	79
Figure 34 Case V illumination and intensity results for increasing attenuation at depth $z = 30$ [m]. From top to bottom $k = 0, 0.25, 0.5, 0.75, 1$	80
Figure 35 Case V illumination and intensity results for increasing attenuation at depth $z = 40$ [m]. From top to bottom $k = 0, 0.25, 0.5, 0.75, 1$	81
Figure 36 Case V illumination and intensity results for increasing attenuation at depth $z = 50$ [m]. From top to bottom $k = 0, 0.25, 0.5, 0.75, 1$	82
Figure 37 Case V illumination and intensity results for increasing attenuation at depth $z = 60$ [m]. From top to bottom $k = 0, 0.25, 0.5, 0.75, 1$	83
Figure 38 Case V 3D illumination and intensity results for increasing attenuation at depth $z = 10$ [m]. From top to bottom, left to right $k = 0, 0.25, 0.5, 0.75, 1$	83
Figure 39 Case V 3D illumination and intensity results for increasing attenuation at depth $z = 20$ [m]. From top to bottom, left to right $k = 0, 0.25, 0.5, 0.75, 1$	84
Figure 40 Case V 3D illumination and intensity results for increasing attenuation at depth $z = 30$ [m]. From top to bottom, left to right $k = 0, 0.25, 0.5, 0.75, 1$	84
Figure 41 Case V 3D illumination and intensity results for increasing attenuation at depth $z = 40$ [m]. From top to bottom, left to right $k = 0, 0.25, 0.5, 0.75, 1$	85
Figure 42 Case V 3D illumination and intensity results for increasing attenuation at depth $z = 50$ [m]. From top to bottom, left to right $k = 0, 0.25, 0.5, 0.75, 1$	85
Figure 43 Case V 3D illumination and intensity results for increasing attenuation at depth $z = 60$ [m]. From top to bottom, left to right $k = 0, 0.25, 0.5, 0.75, 1$	86

Figure 44 Case V: Multi-sensor SNRs for attenuation $k = 0$ and (from top to bottom, left to right) depth $z = 10, 20, 30, 40, 50$ and 60 [m].....	87
Figure 45 Case V: Multi-sensor SNRs for attenuation $k = 0.25$ and (from top to bottom, left to right) depth $z = 10, 20, 30, 40, 50$ and 60 [m]	88
Figure 46 Case V: Multi-sensor SNRs for attenuation $k = 0.5$ and (from top to bottom, left to right) depth $z = 10, 20, 30, 40, 50$ and 60 [m]	89
Figure 47 Case V: Multi-sensor SNRs for attenuation $k = 0.75$ and (from top to bottom, left to right) depth $z = 10, 20, 30, 40, 50$ and 60 [m]	90
Figure 48 Case V: Multi-sensor SNRs for attenuation $k = 1$ and (from top to bottom, left to right) depth $z = 10, 20, 30, 40, 50$ and 60 [m].....	91

Nomenclature

Acronyms

AUV	Autonomous Underwater Vehicle
CA-CFAR	Cell Averaged Constant False Alarm Rate
CFAR	Constant False Alarm Rate
CPOA	Closest Point of Approach
CUT	Cell Under Test
InGaN	Indium Gallium Nitride
LADAR	Laser Radar
LiDAR	Light Detection and Ranging
N-P	Neyman-Pearson Lemma
NSWCCD	Naval Surface Warfare Center Carderock
PMT	Photo-multiplier tube
RADAR	Radio Detection and Ranging
SFOMF	South Florida Ocean Measurement Facility
SNR	Signal-to-Noise Ratio
TDOA	Time Difference of Arrival
TOA	Time of Arrival
TOF	Time of Flight

Symbols

E	Irradiance
E_{θ}	Irradiance at illumination angle
E_{RN}	Reflection intensity normal to target
$E_{\theta R}$	Reflection intensity at reflection angle theta
I_{att}	Attenuated intensity
I_0	Initial intensity, no attenuation
E_{rec}	Intensity received at sensor
E_{noise}	Noise intensity
Φ	Emitted power
Ω	Beam solid angle at target
$d\Omega_{sensor}$	Solid angle subtended by sensor onto the target
$d\Omega_{element}$	Solid angle subtended by target element onto sensor
$\Omega_{refl\ ratio}$	Solid angle ratio over reflection path length
A	Beam area at target
$dA_{element}$	Illuminated area element of target
dA_{sensor}	Effective area of sensor, light sensitive
θ_{illum}	Illumination angle
θ_R	Reflection angle
k	Total attenuation coefficient
$k_{scatter}$	Scattering attenuation coefficient
$k_{absorption}$	Absorption attenuation coefficient
N_{sensor}	Noise at sensor

P	Power
SR	Solar radiance
bw	Filter bandwidth
r	Range, distance of signal travel
r_{beam}	Laser beam radius
z	Depth

1 Introduction

Optical systems deployed in a total immersive underwater environment have created a niche of options for alternative acquisition methods in the areas of imagery, measurement, and communications. These developments, however, have not included an optical alternative to track underwater objects. Insufficient information is available in existing literature describing optical laser tracking applications, however, the broad scope of information highlighted issues that a system would need to overcome for accurate operation. Many of these challenges are endemic of any water based optical system and broadly applicable to the field, but some issues are unique to the tracking problem. A differentiating basis between tracking and other optic systems is necessary to identify the problems which are universally similar and those which are different.

Systems for imagery, communications, and general measurement are in continuous development and researchers are advancing capabilities on a regular basis. At the most basic level, these systems fundamentally operate under stationary conditions or gather information in an instantaneous snapshot where motion of the subject is not considered. Even in the case of LIDAR imaging, where a laser maybe placed on a mobile platform, the object of interest is often stationary and angles of transmission and reception can be planned to optimize system performance. Transmission and reception angles of the laser is a key performance characteristic of the system. Additionally, travel time for the laser path can generally be controlled through sensor placement with respect to the object of interest. Contrasted with a volumetric scanning and tracking system, where illumination

and reflection angles are important considerations, the laser azimuth and elevation are constantly changing to acquire an unknown object at an unknown location within the volume. Transmission angles may be known, but reflection angles from the target as well as travel time for the light between the transmitter, target, and sensor are unknown. Determining performance of the laser as it illuminates an object of interest at varying angles and range is the central and critical problem differentiating the tracking system from other water deployed optics systems. Defining laser performance against dynamic target movement is crucial information for system design and operations to maximize opportunities for target capture.

Common challenges exist for underwater optical systems in general which are equally applicable to the tracking system. Attenuation through absorption and scattering of the laser by the environment and target is an important consideration which impacts the intensity of light arriving at a detecting sensor. Combined intensities of ambient light noise and target reflection are important aspects in overall signal recognition. Ambient light adding to the noise floor generally correlates to deployed depth of the system, necessitating comparison of the performance response to an estimated noise level. Normalizing the performance to a Signal-to-Noise Ratio (SNR) at designated attenuation levels makes the estimated curve a useful tool for design and calibration.

Analysis of a number of parameters, both common and unique, to a tracking system, determine performance characteristics of an optical system designed and deployed for this purpose. These parameters include angles of transmission and reflection, distance between system and target, attenuation of the environment, and depth of the deployed system. This thesis examines and develops the performance of a laser using these parameters as they

might be considered for an underwater optical tracking system. The end result is a series of performance curves developed through numerical simulation which can aid in design and operation of optical tracking methods.

1.1 Development of an Optical Based Tracking System

This thesis is predicated on a technology demonstration prototype in development by the US Navy's Naval Surface Warfare Center Carderock Division (NSWCC), Dania Beach Detachment at the South Florida Ocean Measurement Facility (SFOMF) to research optical methods for underwater tracking. Although design of the system suggests probable geometries and configurations which are considered in simulation, modeling seeks to answer more fundamental questions concerning performance of a laser illuminating a moving target underwater. The central objective to further system development is understanding energy changes received after reflection by considering variables such as angles of illumination, range, signal attenuation, and noise level.

Initial test and operation of the system constrains the parameters of the simulation. Requirements for power and data restrict preliminary deployment and use of the system in shallow coastal waters. The mathematical simulation developed, however, can equally be used to estimate responses for both coastal and deep water analysis, though the results presented are currently limited to coastal analysis to coincide with prototype testing requirements. As development continues the simulation can be adapted for additional requirements and environments.

Probable targets for tracking are identified for operational tests of the system, including a candidate from Florida Atlantic University's (FAU) available REMUS 100 platforms. For the simulation these targets are not considered for a number of reasons.

First, the fundamental analysis required to understand performance of the laser suggests a simple target is a necessary starting point to construct the theoretical principles for understanding the central issues. A Lambertian plate was selected as the model target for this reason. Second, realistic target geometries, materials, and coatings all have an effect on scattering and absorption of the signal. These parameters vary by target and are not considered in this study, therefore they are left for future consideration after developmental concepts are operationally proven. Third, realistic reflection is a combination of both spectral and Lambertian principles. Spectral reflection is not considered because most probable targets will not exhibit true spectral reflection (angle of incidence equals angle of reflection), and complicates geometries necessary for evaluation. Utilizing a Lambertian reflection model, reflected energy is dispersed and can be detected from any angle provided there is line-of-sight observation between the area of target illumination and the sensor. Additionally, dispersion of light by a target through the Lambertian model is ideal due to uniformity and simplicity for this study, though other dispersive models could have been used.

The Navy's technology prototype operates by rapidly scanning a volume with a narrow beam, Indium Gallium-Nitride (InGaN) green solid state laser and detecting scattered light from a target by a four sensor photo-multiplier tube network spatially separated from the transmitter. The simulation mirrors these design choices, allowing for a set separation distance between the two components. Separation can be changed to explore the change in intensity of light as desired. The simulation assumes there is no additive noise on the sensor from backscattering, due to the bi-static design choice.

Proposed parameters for the prototype system are listed in Table 1 and Figure 1 graphically describes the operational concept of the system and accompanying geometric relationships necessary for tracking an object.

Design Characteristics	
Laser Wavelength	520 nm (Green)
Laser Operation	CW
Power	50 mW, CW mode
Modulating Frequency	40 MHz
Carrier Frequency	575 THz
Field of View from the Horizontal Axis	0-40 degrees
Field of View about Vertical Axis	360 degrees
Scan Rate (Elevation)	19800 deg/s (3300 RPM)
Scan Rate (Azimuth)	1080 deg/s (180 RPM)
Range Detection Method	Phase shift sensor – sensor relationship

Table 1: Characteristics of the prototype underwater laser tracking system

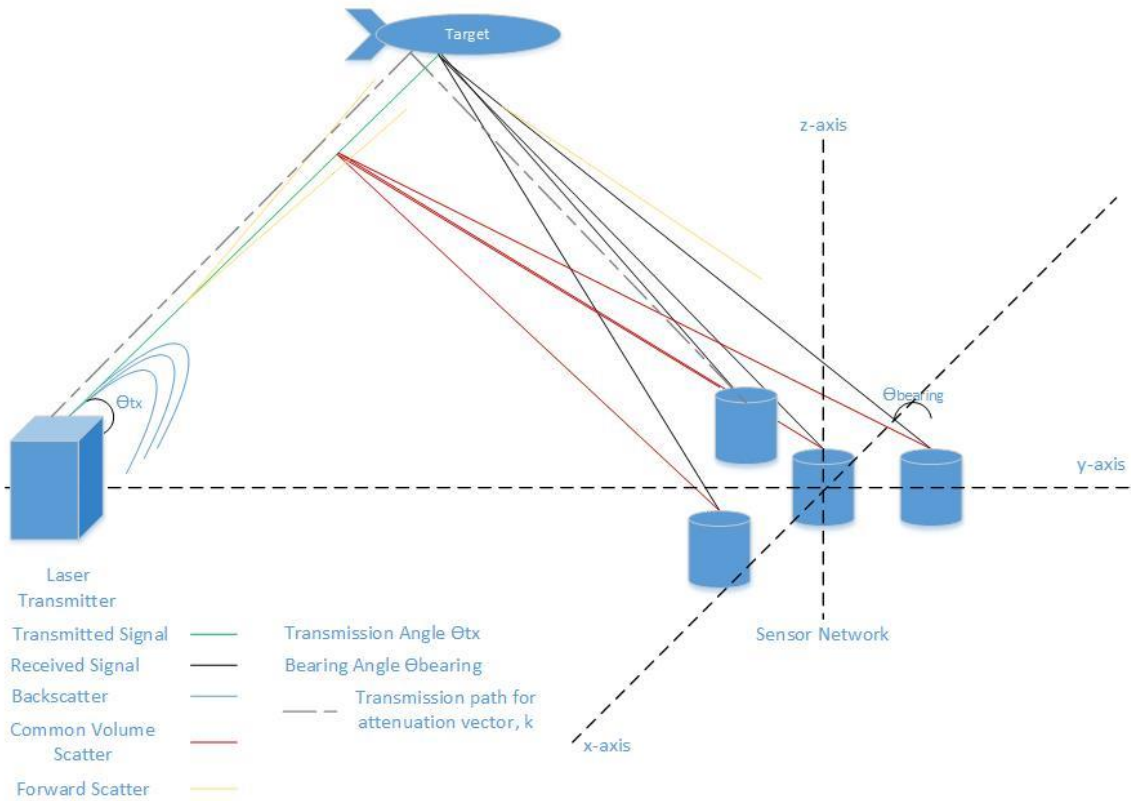


Figure 1: Conceptual Operation of the Laser Tracking System

Experimental validation of the hardware and operational concept of the tracking system are beyond the scope of this study. The connection between the numerical simulation developed for this thesis and the US Navy system is a theoretical analysis of expected laser performance reflected off a target over a series of ranges at differing angles of illumination. Radiative transfer of energy delivered by the laser, reflected by the target, and detected by a sensor network are important theoretical concepts necessary for continued development of optical tracking in a water environment. As a tool, this simulation should suggest sensor sensitivities necessary to detect a target over varying ranges and angles of illumination. Throughout the numerical analysis described, properties

of the prototype system are applied as the starting point for developing this application. This does not mean the simulation cannot be applied to analyze other configurations, it only means the parameters chosen to narrow the variability of possibilities reflect prototype configurations to enhance and compliment the current active research endeavor and develop a better understanding of theory governing operations and capability of the suggested system.

1.2 Foundations and Applications

Ocean laser systems developed as alternative solutions to typical ocean measurement problems. These solutions are often grounded in terrestrial counterparts. Military and commercial applications of terrestrial laser systems resulted in robust measurement, communications, and imaging systems. Terrestrial application and development surpasses marine development due to availability of mature, robust non-optical methods which have been in use for decades. Compounding the issue is limited effectiveness of light transmission in air as opposed to water. The use of lasers in air is much broader with fewer limitations than those used in water.

Waterborne laser tracking systems are a new concept, but have foundations in existing technologies. Understanding how common water optics problems relate to tracking applications is critical to develop viable technology and system implementations for commercial and defense use. Optics based tracking could be used as an alternative to acoustic and magnetic methods in a variety of situations where ambient noise precludes use of typical methods or the subject of interest (target) has unique sensitivities. With additional development, optical tracking could be used on application such as novel deep sea systems or managing a constellation of AUVs requiring high resolution precision in

relative location to one another. Leveraging development in other optical applications is an important start to realizing underwater tracking technologies.

1.3 Problem Statement

The objective of this research is to develop a computational model which is used to analyze energy transfer between a laser transmitter, target, and optical sensor. Development of the model is critical to understanding theoretical principles involved in tracking a dynamic target through an optical transmitter-sensor network in an underwater environment. Performance curves developed through numerical analysis can be used as a design aided tool for laser and sensor selection as well as processing techniques necessary to differentiate signal responses at various target ranges, angles of illumination, and environmental attenuation factors.

Providing a basis for the study is the US Navy prototype laser tracking system, which is used to narrow system related variable parameters such as laser power, operation, and transmitter-sensor geometry. The simulation is thus intended as both an immediate tool to aid in design choices for prototype development and theoretical understanding of expected responses of a laser applied to an underwater tracking problem.

The study represents a fundamental analysis of associated principles by idealizing reflection responses through a Lambertian framework as opposed to other options such as a spectral or mixed model. Environmental factors such as attenuation and ambient light are estimates based on noted values available in literature for typical conditions in coastal waters and solar irradiance on the ocean surface. Reflection responses are based on incidence with a flat plate, neglecting edge effects or more complex geometries of real targets presented by the wide variety of underwater vehicles available in the market. In-

depth analysis of these complex variables is left for additional research. Main components of this study are focused on energy levels received at a sensor, based on varying target range and illumination angle.

Development of this novel, optical method for tracking underwater targets necessitates fundamental understanding of the interaction between a dynamically moving object and intensified, directed light. Analysis of the simulations can be used to suggest appropriate power levels for specific ranging requirements, improve signal to noise ratio, or describe geometric relationships between the system and target resulting in maximum or minimum confidence in target capture.

2 Literature Review

Prior to conceptual design of the US Navy prototype and research conducted for this thesis, development of a laser based underwater tracking system was non-existent. Several researchers, however, have conducted studies to adapt optics for water applications and improve those systems over the years. Literature reviewed for this study did not reveal another tracking system, but did result in various technologies, techniques, and theories which could be adopted and adapted for the proposed application. Though, not exhaustive in the extent of techniques which could be implemented, the literature presents a broad scope of current laser application research and principles which are applicable or could be adapted for the end purpose of underwater optical based tracking.

Laser tracking, traditionally, has numerous applications in defense and commercial sectors. Research to simultaneously acquire, track, and image potential targets on the battlefield have increased over the last decade and now feature applications in both scanning and non-scanning systems [1]. The vast majority of defense related optical tracking research, however, is limited to terrestrial applications, with no known similar research applied in the marine environment. Marine applications have focused primarily on imaging and communications. LiDAR systems, both ship and airborne, have successfully been deployed to map littoral bottom features [2]. This application has extended into additional research in robust systems for enhanced imaging of structures, archeological findings, and other objects. Additional applications include communications and hydrographic analysis of the water column.

2.1 Light Attenuation

Attenuation is the primary environmental phenomenon effecting light transmission in water. Widely known and well documented, attenuation reduces the amplitude of the energy signal from the source along the path of travel. The effects are typically more pronounced for electromagnetic energy, including the visible spectrum, in water compared to atmospheric conditions due to density of the medium. There are two primary components of attenuation in water: absorption and scattering.

Absorption of the visible light spectrum at varying amounts results in only a few useful wavelengths for laser operations, depending on ranging requirements. For distance ranging, blue-green and blue-violet wavelengths are the most useful. Local environmental conditions are critical in determining which laser wavelengths are appropriate for an application. For the intended depth and application of the system, a blue-green wavelength laser is most appropriate due to characteristics in the littoral environment. Models of light attenuation in water typically use principles such as the Beer-Lambert Law [3] along with the e-folding principle described by Farr et al for deep water laser communications in [4]. These principles are useful for determining expected received signal attributes when combined with available local data, such as light attenuation measurements found in [5].

Scattering of the laser due to medium density, particulate, and biological factors is also well-documented. Three descriptions of scattering with reference to signal transmission are cited. Scattering based on particle size: Rayleigh, Mie, etc occur and are expected depending on particulate matter suspended in the medium or turbidity level. Scattering can also be classified based on photon path of travel after interaction with mass in the medium. Under this classification scheme scattering is referenced to the intended

direction for signal transmission, and is identified as back, forward, or common volume scattering [6]. Various methods are used to compensate for scattering in systems. Most often careful selection of the geometries between the transmitter, target, and receiver is considered, but this approach cannot entirely negate scattering effects and can add to the background noise the system must accommodate. The Naval Air Systems Command considered geometries where the transmitter and target were in close proximity and the receiver was a distance behind the transmitter to eliminate backscatter at the receiver, but forward scattering still occurred [7]. This highlights a common solution: spatial separation of the transmitter and receiver is used to eliminate backscatter additives to the noise floor at the receiver. Since backscatter has no interaction with the intended object or target, it carries no useable information for imaging or communications applications. By extension, this would have adverse effects on tracking by reducing the SNR or creating a false positive target capture if the backscattered signal carried sufficient energy. In circumstances where spatial separation is used to limit or eliminate backscattering, common volume scattering and forward scattering can still be received by the system. Additional methods exist to reduce scattering effects and optimize characteristics of the received signal. Range gated systems are useful in reducing the additives of scattering to the noise floor by linking the transmitter and receiver so the aperture of the receiver is open for reception over a finite period of time [8]. Use of a range gated system typically requires some knowledge of the Time-of-Flight (TOF) for the signal between transmitter, target, and sensor. For the prototype tracking system, use of a range gated sensor is not considered at this time.

2.2 Laser Range Detection Methods

Thus far, the applications described tend to be robust and mature, but research continues to improve capability through different methods of laser transmission and noise reduction [7]. Range determination, although not the primary intent of these applications can be calculated using simple signal processing techniques to calculate the time between signal transmission and reception across several sensors. Therefore, an underwater rangefinder is not a difficult advancement from existing technologies, but the concept is crucial to track within the medium volume.

Various methods to retrieve information from the laser are also quite robust, including Time-of-Flight (TOF) and Phase Shift Detection (PSD) [9][10]. The methods have been used and proven for years in a variety of radio wave and terrestrial laser system applications. They are fundamental, established principles that also apply to the operational theory of an underwater tracking system. Additionally, hyperbolic positioning systems, such as the type used for mobile phone location and acoustics can increase accuracy of the target position and reduce the effects of ambient noise by calculating the Time Difference of Arrival (TDOA) by determining signal path delay between sensors [9][11]. Specifically, [12] demonstrates the mathematical calculation to derive both bearing angle and range location data from signal information. Furthermore, techniques for using this type of receiver system have been modeled to develop a 3D location solution for an electromagnetic emitter without knowledge of the emitter's range data based on signal reception by a sensor field, [13].

Although these techniques are not used directly for this study, it is well described by the literature that a multi-sensor array is necessary to establish a fix in a three

dimensional space. To develop laser performance data, there is value in understanding intensity differences a spatially distributed multi-sensor array will experience. Not incidentally, this type of array is also chosen for the prototype system, so the implementation in the study provides direct information for the initial system.

2.3 Optical Noise

Operating lasers in water is accompanied by the problems of attenuation and scattering as previously described. Scattering in particular adds to the optical noise floor received by the acquisition sensor in addition to the ambient noise level created by light penetrating from the surface. As previously described, additive noise due to scattering can be reduced through design layout of the system. Bi-static layouts of the transmitter and receiver, as opposed to a mono-static system are a proven method to reduce noise in similar imaging systems [3]. This study considers spatial separation between the transmitter and sensor array to minimize additive noise effects. In the simulation, however, common volume scatter is not considered, assuming the additive levels are insignificant compared to the level of ambient noise in littoral environments or insufficient to greatly affect the SNR.

Implemented in the hardware design is the use of a physical optical filter, a common method to reduce light noise. Acting as a band-pass filter, it allows specific wavelengths of light to pass through while rejecting others. Optical filtering effects ambient light levels incident on the sensor, by removing visible light outside the pass band. This in turn effects the noise model used to estimate those ambient levels. The most significant source of noise in a littoral operating environment is sunlight incident on the ocean surface. Readily available data and notes indicate light intensity at the ocean surface is approximately 1367

$W/m^2/nm$ [14]. Noise is modeled, for the study, using this estimate and integrating over the wavelength bandwidth of the optical filter. The noise is assumed to be isotropic passing through the depth of the water column.

2.4 Signal Processing

Signal Processing techniques have been applied successfully in laser rangefinders to improve overall performance of the detecting element of the system. Methods to improve SNR are common and used to enhance signals for further processing in a wide variety of applications, not limited to laser rangefinders. Several examples of target detection algorithms adopted from radar theory and applied to laser systems to further improve system response exist.

Improving the SNR is one of the best methods to improve system performance. Differential and smooth-filtering methods have both proved experimentally successful to improve SNRs in pulsed laser range systems, decreasing the detectable ratio, [15]. Estimating SNR is a critical consideration in system design, which can suggest signal processing methods to extract desired range data. In particular, based on SNR, designers can consider different threshold detection methods to maximize target acquisition and minimize false positives as both the target and laser continuously vary in relationship to one another during the search process.

A variety of threshold methods exist in radio, acoustic, and optical applications. One method proved and used for optical detection is implemented in a pulsed system, developed by Li et al, adopted Neyman-Pearson (N-P) criterion for target detection. This is a binary hypothesis used to develop a likelihood ratio to favor one hypothesis over the other, implemented as a Constant False Alarm Rate (CFAR). Establishing an appropriate

CFAR with N-P criteria causes detection probability to directly relate to the SNR [15]. In [16] Mourad and Pramod demonstrated CFAR detection theory applied to a fusion rule set for decentralized, multi-sensor detection systems. Using this method they demonstrate a process to integrate multiple threshold detection decisions at individual sensors to determine if a detection will be processed at a central data hub.

Signal detection in RADAR systems, specifically CFAR, is a data-dependent, probability process, based on relative powers of a received signal and the background noise. For CFAR, this is the normalized power related to a noise estimate calculated over several sample bins. A signal is present if the cell under test (CUT) contains a signal greater than a threshold level, adjusted by the relative noise level measured over several samples. As a RADAR procedure, this method is well developed in several adaptive algorithms, though research continues on improving techniques through selective statistical methods [17][18]. This process is applicable to the laser tracking process. In order to apply and develop an appropriate detection method, analysis of the SNR of the light signal through the tracking process is necessary. While this thesis does not seek to apply signal detection algorithms to differentiate between target acquisition and some other phenomenon in the environment, it does seek to provide an understanding into the ratios of signal to noise in order to further develop these methods in follow on studies.

Thorough research into a tracking problem would be amiss if existing RADAR processes and techniques were not explored for applicability to the underwater tracking problem. In all regards, this is basically a radar problem with an optical detection scheme and a different medium. Signal detection algorithms are commonly used in radar to measure the quality of signals present at the receiver, and these techniques can be adapted

for this application. Algorithms relate a SNR to target recognition and through mathematical analysis leverage that relationship to improve probability and reliability of the process. These processes take into account clutter and electrical interference, but in cases where these elements cannot be removed, degradation to probability recognition is taken into account. If neither of these conditions apply, it is necessary to discard the measurement if an interfering signal exists. Additionally, correlating multiple measurements can improve recognition performance and increase certainty that the received signal is, in fact, a target [19].

Unfortunately, without another optical tracking system available to test theory in this application, determining suitable methods to improve operations using this characteristic are not directly known, though other fields suggest parallels which can be leveraged for options. A significant determination in this research is estimating the SNR of a received signal as geometries vary based on changing range of the target and sweep of the laser. Using this signal relationship, several possibilities for signal processing can be used in the design of the system.

2.5 Reflection Modeling

The key component in target tracking is signal interaction with a target of interest. Acquisition relies on detecting energy illuminating and reflected by the target. Several reflection models exist to describe how energy radiates from an object, though there are primarily two types. Spectral reflection describes traditional reflection where the angles of energy illumination and reflection are equal, with respect to an axis normal to the target. A second type is described by Lambertian reflectance where energy is dispersed from the point of illumination outward in all directions. Energy observed in this second case is equal

regardless of the angle from which the illuminated point is being observed. In reality, with real world targets, reflection is a combination of these two descriptions and there are a number of other models which attempt to realistically describe reflection. A Lambertian model is considered here for two primary reasons, it is a well understood method and in the early stages of system development with no other analysis it is difficult to determine if other models are more appropriate. The spectral model is not useful due to the conditions of reflectance based on geometry of the system. To detect pure spectral reflection, the angles between the transmitter, target, and detector would need to remain constant, defeating key considerations in the purpose of this research.

In [20] Oren and Nayar describe the attributes of Lambertian surfaces, principally the primary characteristic of brightness, which is independent of viewing angle. Additionally, they describe another important aspect of the model, where brightness decreases at the terminal boundaries of an object. Both aspects are important in rendering this initial simulation for the tracking problem. Observer angle independence simplifies the reflection model to produce a constant output at any one point of illumination and allows the model to neglect scattering effects at terminal boundaries of the target, since they are assumed to be zero.

Janecek and Moses confirm these known attributes in [21], with descriptions of Lambertian Reflectance and Lambert's Cosine Law. In their analysis of optical reflection measurements, they generalize the Lambertian Model, showing relative reflection intensity at a maximum at the normal to an incident surface and falling off towards the perpendicular to the normal, or the target surface. These generalizations and experimental results provide

an expectation for the output of the laser performance model through the series of tracking simulations.

3 Approach

The objective of this research is to produce a theoretical model to determine the energy reflected from a dynamic, underwater target. The model is based off Lambertian reflectance theory, simplifying the nature of diffuse reflection and neglecting scattering edge effects of the target. Key environmental considerations are attenuation of the transmitted and reflected signals and ambient noise represented by diffuse down welling sunlight from the water surface. A series of cases were designed to test applicable theory in a progressive simulation construct by incrementing the complexity of target motion and number of sensors. Finally, to correlate the signal results to the problem of target tracking, range to target is estimated based on received energy under ideal environmental conditions.

3.1 Lambert's Model

The basis of the developed simulation is the Lambertian Reflection model. As previously discussed, this model describes diffuse reflection from a point of illumination and is independent of the angle of observation.

Fundamental in the reflection model is determining the energy illuminating the target. Irradiance incident on a target element is a function of the emitted power (P , watts), area of the beam (A , square meters), and angle of illumination (θ_{illum} , radians). Irradiance, E , is described in equation 1 and 2:

$$E = \frac{P}{A} \text{ [W/m}^2\text{]} \quad (1)$$

$$E_{\theta} = E \cos \theta_{illum} \text{ [W/m}^2\text{]} \quad (2)$$

Since irradiance is proportional to the cosine of the illumination angle, the intensity of energy delivered will decrease as the angle between the target normal and illumination increases [22]. This has broader implications on situations where the tracking system is in close proximity to the target, because the sweep of angle measures will have a broader range than at farther distances, the magnitude of energy delivered to the target will correspondingly vary. At farther target ranges, where the angle sweep varies less during target illumination, a smaller range of delivered energy results. An inverse relationship exists for the illumination area. As range increases, beam divergence results in a larger illuminated area on the target, causing irradiance to decrease. These factors when combined influence the total irradiance of the target, which in turn effects the reflection intensity incident on the sensor network.

Reflection intensity is governed by a relationship describing the illuminated target area and an observer. To determine the intensity observed by the detector the area and solid angle of the illuminated target element ($dA_{element}$, $d\Omega_{element}$ respectively) as well as the area and solid angle of the sensor (dA_{sensor} , $d\Omega_{sensor}$ respectively) must be considered. The angle of observation (θ_R) is also considered, but factors out of the equation, equating the intensity of any angle of observation to observation of the target from a ray emitted normal from the target. Equations 3 and 4 summarize the Lambertian model for reflection from the normal, E_{RN} (3) and an observation angle in relation to the normal, E_{θ_R} (4):

$$E_{RN} = \frac{Ed\Omega_{sensor}dA_{element}}{d\Omega_{element}dA_{sensor}} [\text{W/m}^2] \quad (3)$$

$$E_{\theta_R} = \frac{Ed\Omega_{sensor}dA_{element} \cos \theta_R}{d\Omega_{element}dA_{sensor} \cos \theta_R} = \frac{Ed\Omega_{sensor}dA_{element}}{d\Omega_{element}dA_{sensor}} [\text{W/sr}^*\text{m}^2] \quad (4)$$

These four equations form the basis of the numerical analysis performed in the simulations. Two provisions are necessary for implementation in the simulation, target movement and a scanning laser. When these dynamic aspects are considered with the governing reflection equations the resulting intensity at the target and sensor will not be constant from scan point to scan point, due to a change in the angle parameter as energy is delivered. For any one illuminated point, however, the observed intensity at any observation angle from the target normal to the target boundary terminus will be equal at any point along a circle whose circumference includes the illuminated point. Since the detector system is fixed, only the angle of observation resulting in the shortest target-sensor transmission distance is considered for the corresponding solid angles subtended. Additionally, in the multi-sensor consideration the sensors lie on circles with varying radius, this results in varying the subtended solid angles and observed areas, so slight variation between sensor results is expected dependent on the length of spacing.

3.2 Environmental Effects

Environmental effects due to attenuation and noise have two primary consequences on the delivered signal to the target and subsequently to the detector. These effects generally result in a diminished amount of energy delivered and therefore a reduced SNR.

Attenuation is a result of scattering and absorption of a signal's energy due to interaction with matter present in the environment. Energy absorption directly results in

amplitude reduction of the signal, whereas scattering can diminish the signal through de-intensification. A common assumption is to consider scattering and absorption in a single effect. Since actual environmental conditions such as suspended particle size and plankton distributions are unknown, they are not considered in this research, therefore the basic assumption is used. The attenuation coefficient, k , is thus the sum of the scattering and absorption coefficients, shown in equation 5.

$$k = k_{scatter} + k_{absorption} \quad (5)$$

Attenuation is typically applied through e-folding, causing exponential decay over the path length of the signal, which is equivalent to the illumination distance, r . Equation 6 describes the process of attenuation, specifically for the illumination intensity of the target, I_{att} . I_0 , is the delivered intensity with no attenuation. Application is the same for the intensity incident on the sensor network received from target reflection. Figure 2 shows simple attenuation of the laser over a theoretical range of operation using various values for k .

$$I_{att} = I_0 e^{-kr} \text{ [W/m}^2\text{]} \quad (6)$$

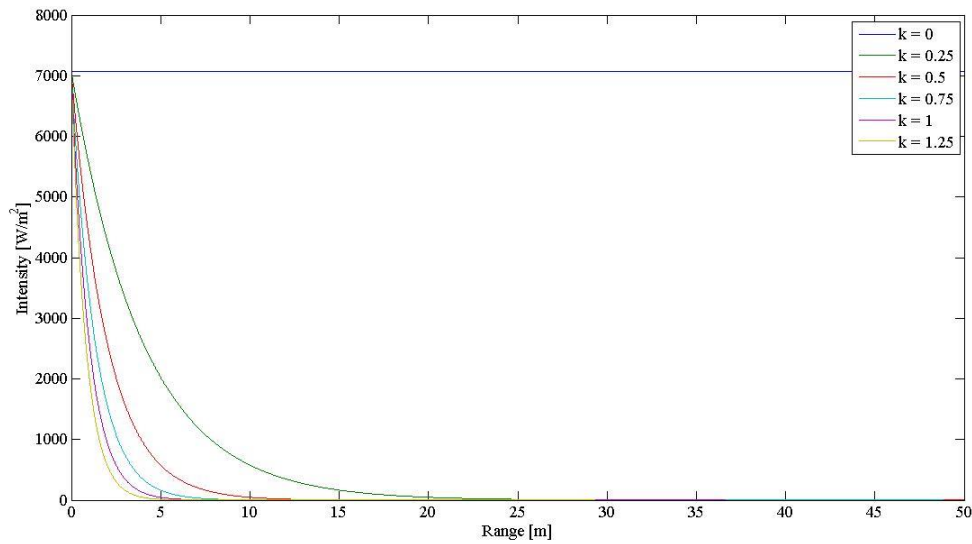


Figure 2: Laser attenuation over $k = 0:1.25$. Resulting intensity is mapped against the range [m] of travel.

The second environmental consideration is noise which has the result of reducing the amplitude of a received signal when compared to the total noise power. Noise can mask the signal altogether in a combined relative high noise, low signal power situation. As discussed in the literature review, the main noise component expected and considered in this simulation is solar radiance down-welling to the system's deployment depth. The magnitude of solar radiance (SR) at the ocean's surface is estimated at $1367 \text{ [W/m}^2\text{/nm]}$ within the visible spectrum. For system deployment, the associated water column to depth, (z) acts as a filter, reducing the intensity of light at the sensor. Also, an optical filter employed in the system design will reduce incident noise by limiting the noise to wavelengths within a specific bandwidth (bw , in nm). In equation 6, the ambient noise (N) estimated at the sensor is modeled.

$$N_{sensor} = SR * bw * e^{-kz} \text{ [W/m}^2\text{]} \quad (7)$$

The Signal-to-Ratio, SNR, is calculated using equation 8: It provides signal characterization to compare the signal to the noise level detected at depth.

$$SNR = 10 \log \frac{E_{rec}}{E_{noise}} \text{ [dB]} \quad (8)$$

A combination of these effects will result in reduced range resolution during tracking. In circumstances of extreme detection range, where the signal is most highly attenuated, and high ambient noise levels, range ambiguity may result. Analysis should show, where ambiguity is a possibility and signal processing methods can be selected to minimize the effects.

3.3 Range Estimation

The ultimate goal in any tracking system is to retrieve range, bearing, and altitude information from signals interacting with a target. This constitutes target acquisition. Various methods exist to retrieve this information based on TOF, TDOA, path delay calculations, or other methods which are beyond the scope of this initial study. The range estimate does not consider these methods because the study is limited to the intensity response at the sensors. Instead the estimate is made based on relating received intensity to laser transmission power. This is a limited approach to determine range because many of the effects impacting detected intensity require range to estimate. Solid angles and attenuation are only two of the many values based on range. When beam spreading is considered in the simulation, area of illumination becomes range dependent. The approach

described is thus limited to the ideal case where attenuation and beam spreading are not considered. An estimation basis still requires knowledge of the noise level and SNR. Two additional assumptions for the calculation are: normal signal incidence with the sensor effective area and the reflection path occurs over the most direct route between the target and sensor. Using Lambert's Cosine Law, received intensity is devolved to the illumination intensity.

$$E = E_{\theta_R} * \frac{d\Omega_{element} dA_{sensor}}{d\Omega_{sensor} dA_{element}} \quad (9)$$

In the equation dA_{sensor} is the fixed valued of the sensor area and $dA_{element}$ is fixed due to the assumption which neglects beam spreading under ideal conditions. This leaves the solid angles as a varying condition based on the range of reflection. Since beam spreading is neglected it can be assumed the solid angles result in a stable ratio, $\Omega_{refl\ ratio}$, which is constant over the operational range of the tracking system. Finally, the radiance equation is substituted into the equation for E , relating the received intensity back to the known quantities for laser power and illumination angle. Here the angle of transmission, θ_{tx} , of the laser from the emitter is assumed to be zero degrees.

$$E_{\theta_R} * \frac{d\Omega_{element} dA_{sensor}}{d\Omega_{sensor} dA_{element}} = \frac{\Phi * \cos \theta_{ill}}{\Omega A \cos \theta_{tx}} \quad (10)$$

Elimination of common variables and substituting for the solid angles results in a single equation relating the illumination range to the received intensity.

$$r = \frac{r_{beam}}{\tan(\cos^{-1}(\frac{-P*\Omega_{reflratio}*A}{2\pi \cos \theta_{illum}})+1))} \text{ [m]} \quad (11)$$

With the extraction of the illumination range, target range can be determined from any reference using geometric relationships to solve for the required distance. This method, however is limited to ideal conditions since attenuation and beam spreading are considered ideal in the analysis. More exact methods, such as the ones described in the opening of this subsection, can accurately fix a target to a specific coordinate location within a certain confidence level and margin of error. This exact analysis, is described in literature for other applications and left for future research.

3.4 Simulation Geometry

Important in the analysis is geometry of the transmitter-target-detector relationship. This geometry is relatively arbitrary, but limited by realistic considerations to make the system useful in an operational deployment. These considerations are system connections to supporting infrastructure, laser power, and average attenuation in the environment. Using these parameters, transmitter-detector spacing is additionally confined to a distance that can acquire and track a target. In practice the simulation can suggest what maximum spacing could be, but for the study transmitter-detector spacing is selected at 5 meters. The simulation is designed so spacing is easily changed by the user with minimal adjustment to the code.

Basic geometry is shown below in figure 3. This covers the static target cases covered in the study. For the cases where the transmitter is scanning, laser motion is indicated in a counterclockwise direction. The Lambertian plate used for the target is 1 meter long with the midpoint aligned with the midpoint of the transmitter-detector baseline.

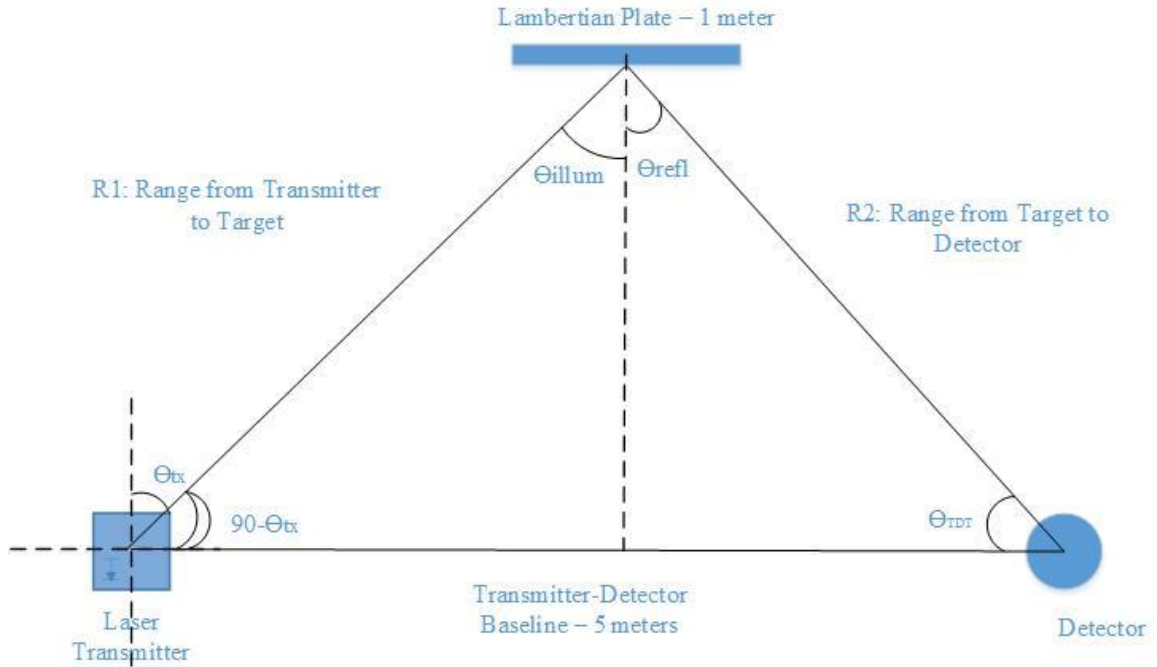


Figure 3: Simulation geometry for transmitter-target-detector relationship

For dynamic cases the geometry is similar. The transmitter-detector baseline and target length remain at 5 and 1 meters, respectively. Midpoints on the baseline and target lie in the same plane along a straight vertical line. Figure 4 shows these relationships with addition of a second sensor to demonstrate the multiple sensor case. Varying triangular geometry due to laser scanning and target positions is also shown. In the dynamic cases with target movement, the target is given a velocity, $v(t) = 1 \text{ m/s}$ and is scanned at each position.

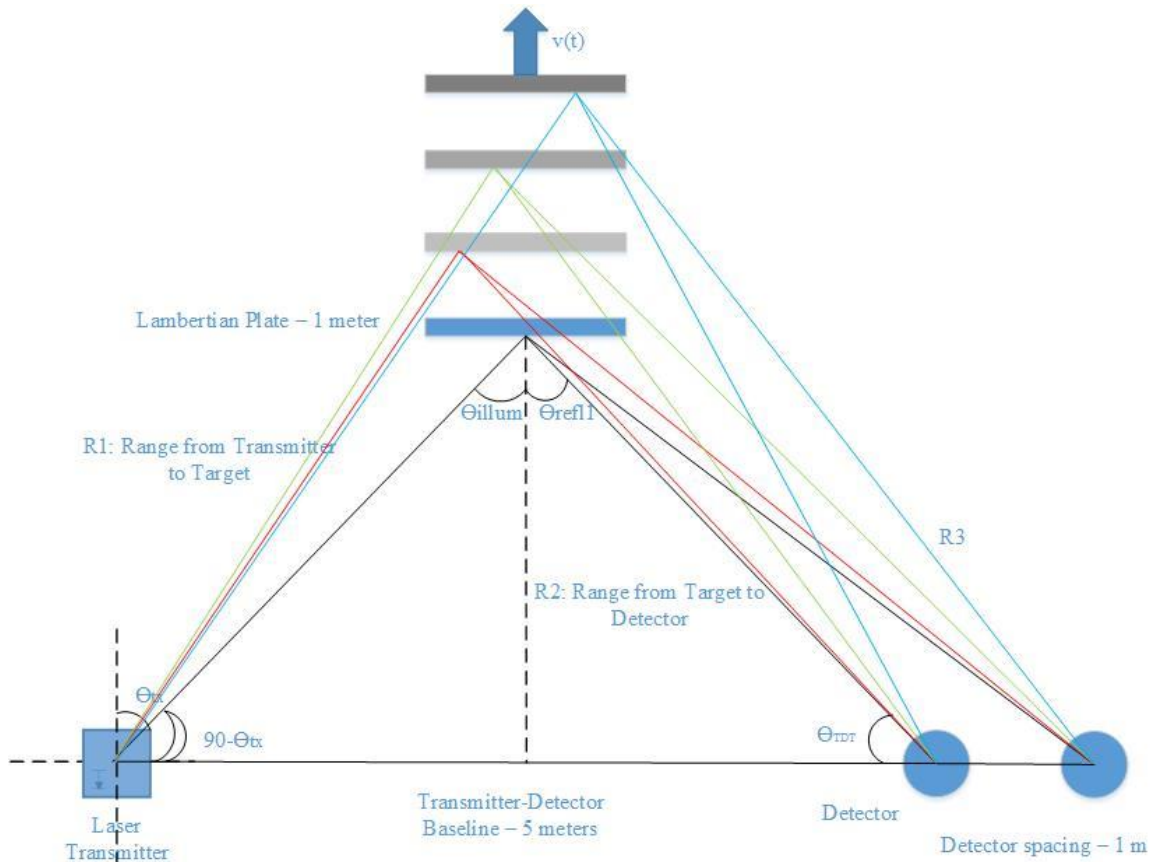


Figure 4: Simulation geometry, dynamic cases with target movement and laser scanning

In both sets of geometry, static and dynamic, ranges and angles are calculated using common geometric relationships and trigonometry. Length of r_1 is easily calculated using right triangle relationships. For r_2 and r_3 the lengths are more easily determined using the Law of Cosines (12).

$$c^2 = a^2 + b^2 - 2ab\cos(C) \quad (12)$$

The geometric relationship between the transmitter, target, and detector is a critical element in the analysis of laser performance. It is a significant factor which determines the

path length of the signal, the dependent variable for attenuation impacting signal loss and the end SNR. It is a factor which cannot be ignored.

3.5 Simulation Cases

To fully develop concepts resulting in performance analysis of the laser, a number of cases were considered. These cases successively built upon concepts in the previous case, developing a simulation for each additional parameter concerned. The five cases developed are described below.

Case I: This is a static case for all components in the relationship: transmitter, target, and detector. It is used to establish the mathematical method necessary to calculate the intensities of the laser, received signal, and noise under the simplest conditions. With no moving components in the case, it is the least interesting and useful. It does however, establish a basis for the magnitude of results under the proposed geometry of the interaction. Due to the limited nature of this case, results are not covered in section 4.

Case II: Building on Case I, this case adds a motion component to the simulation. The target moves in a linear manner at constant velocity away from the transmitter-sensor baseline. Illumination occurs at the midpoint of the target, resulting in a different incident angle at each position the target is measured. The angles of incidence and reflection are equal for single sensor analysis. Maintaining illumination at the midpoint of the target ensures interaction at every position, rather than a fixed angle for the laser with respect to the system baseline which would result in the target moving out of the laser path.

Case III: Here the target is once more static, at a fixed distance from the transmitter-sensor baseline. Instead of moving the target, the laser is scanned across the target to determine intensity of illumination and reflection as the angle of the laser changes.

Changing the angle of illumination also changes the magnitude of the intensity incident on the target due to the inverse relationship the intensity has with the incident angle.

Case IV: In this case motion of the target and scanning the laser are combined to produce an intensity curve across the scanned target at every position. Scanning occurs across a range of angles to measure the change in delivered and detected intensity.

Case V: The final case adds additional sensors, spatially separated by a known distance to allow comparison of the intensities incident on each sensor. For this study two sensors are used, but multiple sensors can be simulated. The sensors are spaced linearly along the transmitter-sensor baseline. Off axis sensors added to the simulation would need the addition of the appropriate angle measures from the baseline to calculate the corresponding reflected range for each particular sensor. With the addition of multiple sensors in this case, it is here where range can be estimated and is demonstrated.

For all cases considered, simulation was completed across a range of environmental attenuation factors and depths corresponding to typical coastal characteristics, particularly the South Florida area. Attenuation was selected between 0 and 1 and depth up to 60 meters. Open, deep water conditions were not considered for this study, though the simulation can support the analysis. Experimental analysis and verification of the simulations was not performed, it is left for additional effort to compare results with experimental data.

3.6 Simulation Construction

Simulations were constructed and analyzed in MATLAB. Each case was individually programmed for flexibility and ease of use. The cases can be adjusted as necessary to change and examine parameters such as transmitter-detector baseline, number

of sensors, start and end position of the target, target length, attenuation, and noise. A primary consideration in construction was to use the simulation as both a theoretical analysis and design tool.

4 Results

The purpose of modeling is to develop a theoretical framework for optical tracking by applying known scientific and mathematical principles described by Lambertian reflection, radiance, environmental effects, and the considered geometry of the operating system. Analysis of simulation results develops an approximation of how the system responds under real conditions and can aid in hardware design, signal processing, and integrating components.

Results are organized by case, except for Case I which is neglected due to the lack of meaningful results. Case I is used primarily for initial model development with no dynamic aspects of the target or laser incorporated. It is a single scan and receive point. Cases II through V provide more meaningful results due to dynamic aspects of the target and laser individually (Cases II and III, respectively), combined dynamics (Case IV), and the addition of multiple sensors and range estimation (Case V). These four cases provide a set of results which can be analyzed for trends to describe general principles and response of the operating system. A set of principles is developed through the course of model progression and analysis of the results.

In this section, case analysis focuses on three levels of environmental attenuation: no attenuation (ideal conditions, $k = 0$), a typical level for South Florida Atlantic coastal waters ($k = 0.25$), and extreme conditions ($k = 1$). Depth analysis is considered for typical coastal depths at z equals 10, 20, and 30 meters, levels which correspond to possible depths for initial testing for the prototype system. Additional results for Case V, which includes

attenuation levels 0.5 and 0.75, and depths up to 60 meters, are included for reference in the appendix. Results beyond these environmental parameters can be obtained through additional simulation.

4.1 Case II Results

Case II examines intensity delivered to a sensor when the transmitted laser signal is incident on a moving target. The case is designed for laser incidence to occur at the midpoint of the target resulting in an equal angle of incidence and reflection. The angle of incidence is therefore different for each target position, starting with a large angle when the target is in the starting position, 1 meter from the transmitter-detector baseline, and ending with a small angle at the final position, 21 meters from the baseline.

4.1.1 Ideal Transmission

First consideration in the simulation is modeling intensity response under ideal attenuation conditions. Here $k = 0$, so no signal attenuation occurs. Results are shown in the graph below.

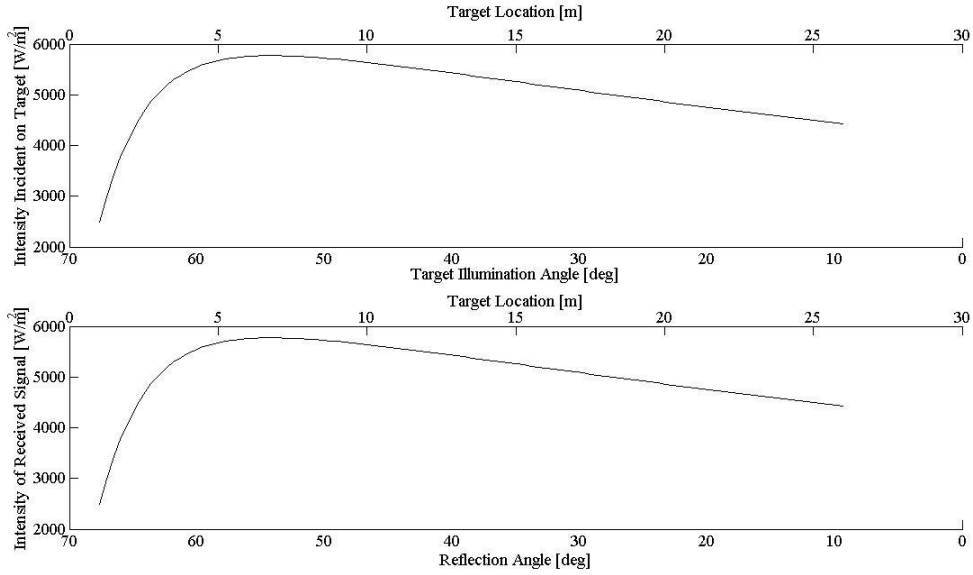


Figure 5 Case II: Target illumination and reflection intensities for ideal attenuation, $k = 0$ and depth $z = 10$ meters. Results are for a single scan point of the target at each position starting at 1 meter from the transmitter-detector baseline to 21 meters

Figure 5 shows ideal results of laser transmission with no attenuation according to the geometry described. Increasing irradiance from position 1 to position 7 is not expected. This is a consequence of the decreasing incident angle as target position increases. At close range, position 1, the average angle of illumination on the target is 67.5 degrees. Since the cosine of the angle approaches 0 as theta approaches 90 degrees this limits the intensity at position 1. At position 7 the average angle decreases to 19.6 degrees, greatly increasing irradiance at the target. Moving beyond position 7 to position 21, the average illumination angle decreases at a slower rate, down to 6.8 degrees and increased illumination area due to beam divergence dominates behavior. An important aspect of beam divergence is the location of the beam waist, the minimum spot area of the beam. Due to collimation, the beam initially decreases in area after transmission to the location of the beam waist, then diverges to greater illumination area afterwards. For a 100 [mm] focal length lens, the

location of the beam waist is 22.5 [mm] from the point of transmission. This coincides with theoretical values for a solid state diode laser [23]. The assumption for beam divergence in this study, from the point of transmission, provides results appropriate to determine the characteristics of tracking a target. No diminishment of signal magnitude from illumination to reflection is observed due to the lack of attenuation.

4.1.2 Attenuation at Constant Depth

The next set of graphs, present results obtained by varying the environmental attenuation coefficient while maintaining a constant depth. Attenuation is modeled with increasing attenuation at depth $z = 30$ meters.

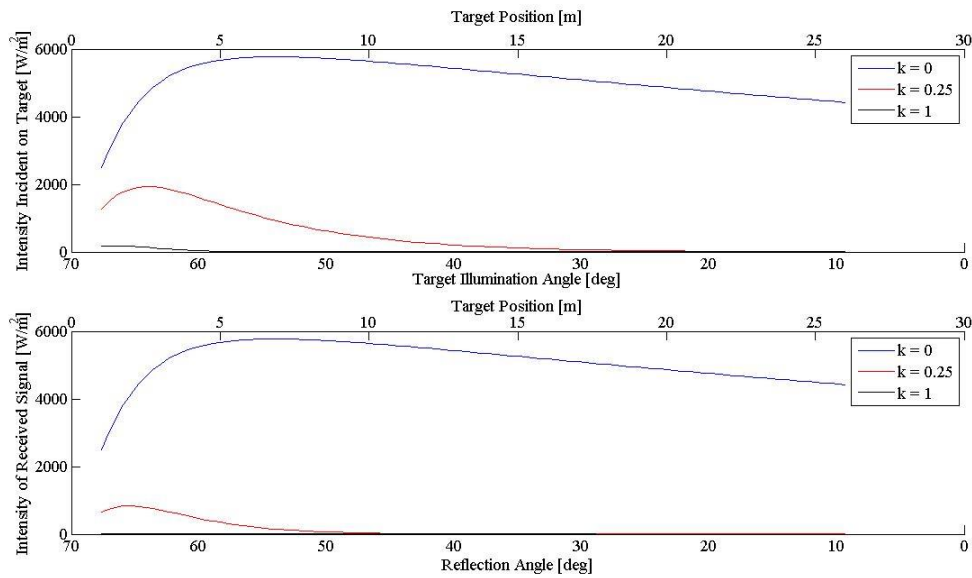


Figure 6 Case II: Intensity delivered to target and sensor at depth $z = 30$ meters and varying attenuation coefficient, $k = 0, 0.25, 1$. The top graph is target illumination and the bottom is reflection intensity.

Adding attenuation and increasing the coefficient in the simulation produces the intuitively expected result for real conditions, decreasing intensity with increasing target distance. For $k = 0.25$, a localized maximum of increased intensity before steadily

decreasing. As the target moves from the 2 meter to 3 meter position, there is a drastic decrease in the illumination angle compared to the change between all other positions. This dramatic change in illumination angle from position to position diminishes over the following positions. Increase in irradiance due to the reduced illumination angle as target position increases is evident on both the illumination and reflection response, though due to attenuation this behavior is not as pronounced as in the no attenuation case. As the rate of change of the angle from position to position reduces beam divergence dominates the response curve, continuing the downward intensity response as range increases. Attenuation at this level suggests maximum tracking range for the laser power modeled, 50 mW in this simulation, is about 10 meters.

In the high attenuation condition, $k = 1$, the resulting curves are expected though bleak for a tracking application. Illumination response is slightly above zero while the reflection response appears to be zero.

4.1.3 Signal to Noise Ratio

The next set of results for Case II describes the signal referenced to ambient noise. Two sets of graphs are presented to illustrate two different principles that will provide a basis to draw conclusions. The first set of graphs describes the SNR at constant depth and varying attenuation.

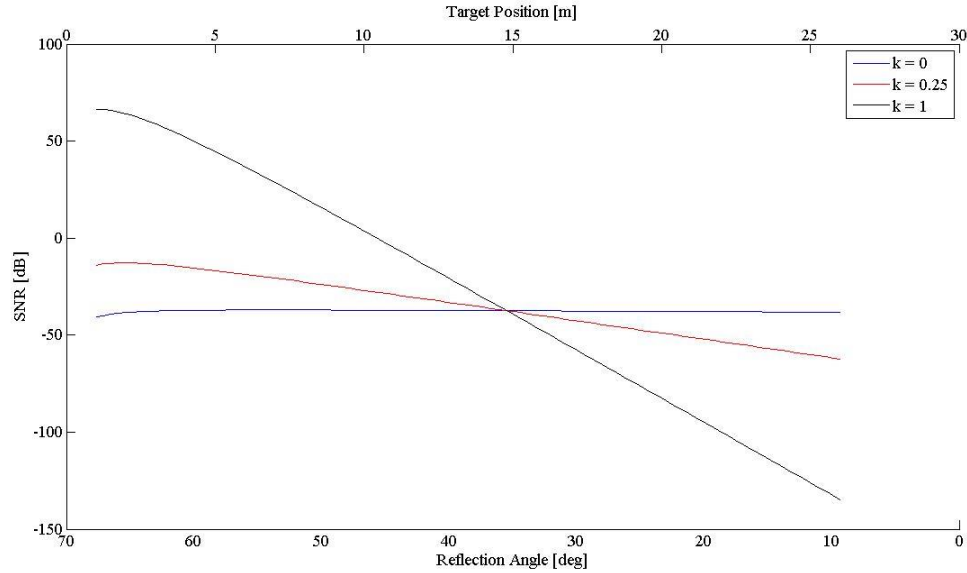


Figure 7 Case II: SNR for constant depth, $z = 30$, and varying attenuation $k = 0$, 0.25 , and 1 .

For SNR at constant depth, the graph compares the associated levels for each position at three attenuation levels. For $k = 0$ and 0.25 attenuation levels the SNR is negative over all positions on the curve, denoting a signal level smaller than the detected noise. Attenuation level, $k = 1$, is not always negative. In the near target positions, signal levels are sufficiently high above the noise level to provide a positive SNR and the possibility for target acquisition. The ratio does become negative after position 11 and continues to degrade. As attenuation level increases, SNR at position 1 increases. Over the path length, in this case depth, solar irradiance at the surface down-welling to the sensor decreases as the increased attenuation factor reduces the noise level. In general, increased attenuation over constant depth will improve SNR, which is desired despite a tradeoff with reduced laser illumination. SNR in this condition is driven by attenuation of noise.

In the second set of SNR graphs the attenuation coefficient remains constant and the depth is varied to study the change in the ratio. The scenario is examined with $k = 0.25$ and depth varying between 10 and 30 meters.

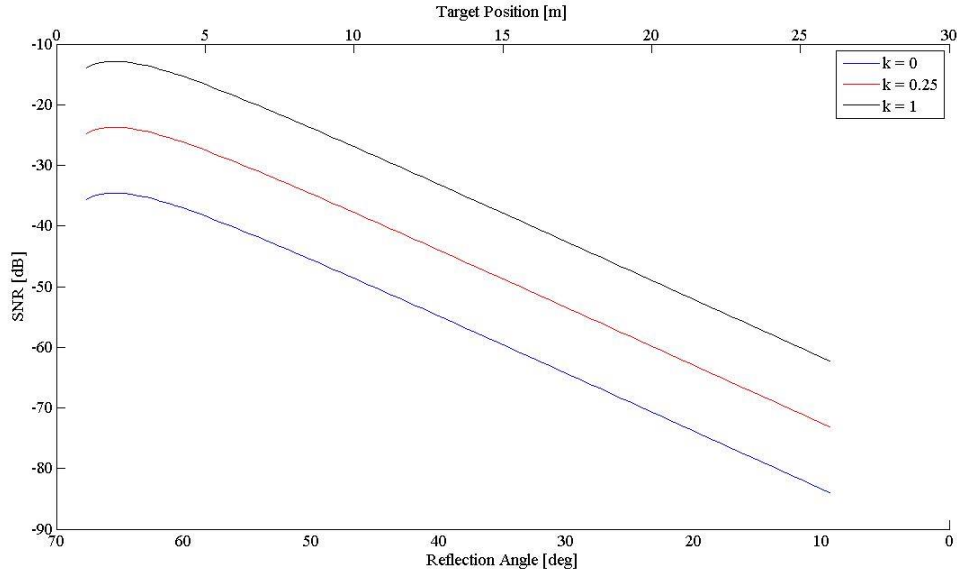


Figure 8 Case II: SNR with constant attenuation, $k = 0.25$, and varying depth, $z = 10, 20,$ and 30 meters

In this second SNR scenario, the response curves all have the same shape. The difference between the results is easily exemplified at two main points. As depth increases, the ratios increase at each position, which is easily viewed at the start and end points of each curve. From the 10 to 30 meter, the SNR at the 1 meter position experiences a 185 percent increase. There is still a declining ratio as target distance increases, but since ambient noise is reduced with increasing depth, the ratio increases for corresponding points from depth to depth. As depth increases, signal attenuation of the laser due to path length becomes the main driver of resultant SNR at the detector.

4.2 Case III Results

The scenario in Case III examines intensity levels as the angle of illumination changes during target acquisition. The target in this case maintains a constant position, 5 meters, allowing only the angle to vary. This allows analysis of intensity levels delivered and received as well as the angles associated with reflection for the established transmitter-detector geometry. Angles of reflection are predicted using trigonometric relationships based on target location at 1 [m], transmitter-sensor baseline of 5 [m], and the illumination angle.

4.2.1 Ideal Transmission

The first set of conditions examined is the ideal transmission case at depth $z = 10$ meters. Here, the general characteristics of energy radiance at the target and sensor is developed. These characteristics will be used for comparison with follow on environmental conditions as attenuation is varied and depth increased.

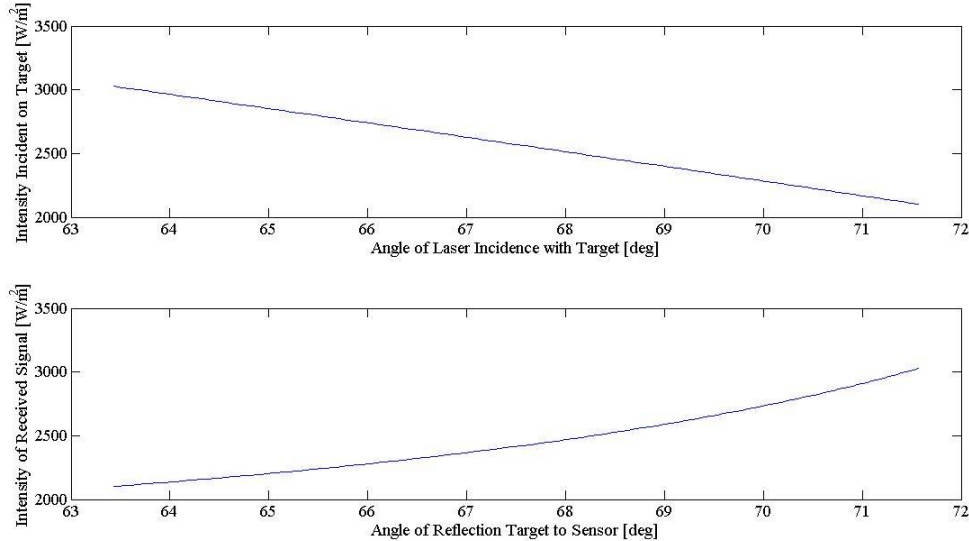


Figure 9 Case III: Laser intensity at the target and sensor under ideal environmental conditions, $k = 0$, at depth $z = 30$ meters. Target is located 1 [m] from the transmitter-sensor baseline.

In the top graph above, target irradiance is displayed. The general characteristic of the curve is decreasing intensity as the angle of illumination increases toward 90 degrees from the normal. This is a result of the direct relationship between intensity and the angle's cosine. As the angle of illumination increases toward the terminal boundary of the target's plane, intensity will decrease. This result is limited to a target scan at a particular position, it does not compare illumination based on angle for different positions. Change in the path length of the laser during a single position scan is differential compared to the change in angle from position to position. Considering beam divergence with illumination angle, for the simulation, both conditions should work together to decrease irradiance as illumination angle increases, so for a positional scan, regardless of target range, the general behavior of decreasing irradiance should be observed. This is the general characteristic to examine, combined with the response from varying attenuation level. Since laser path length increases through the scan, these three components greatly impact signal levels at the final scan point.

In the bottom graph, intensity at the detector is shown. The general characteristic here is increasing intensity as the angle of reflection increases, opposite to the relationship described in the upper graph. What is not intuitive in the graph is the angles are flipped across the axis of the graphs, i.e. the angles of incidence and reflection do not correspond reading the graphs top to bottom. In other words, the angle depicted as the first point (left) in the incident graph does not correspond with the angle depicted at the first point on the reflection graph (left). The corresponding angle to the first, left point on the incident graph, is the last, right point on the reflection graph. Reading the graphs this way provides corresponding angle of incidence, reflection, and intensity levels for every scan point in

the target acquisition. Reflection signal magnitude through the scan does not reduce from the incident intensity due to no attenuation modeled in the result and lack of beam divergence from the diffuse nature of Lambertian reflectance.

4.2.2 Attenuation at Constant Depth

The next set of conditions to examine is the effect of attenuation. Depth remains constant, at $z = 10$ meters, as in the ideal case presented. Attenuation coefficients are $k = 0.25$ and 1 , the same values used in Case II.

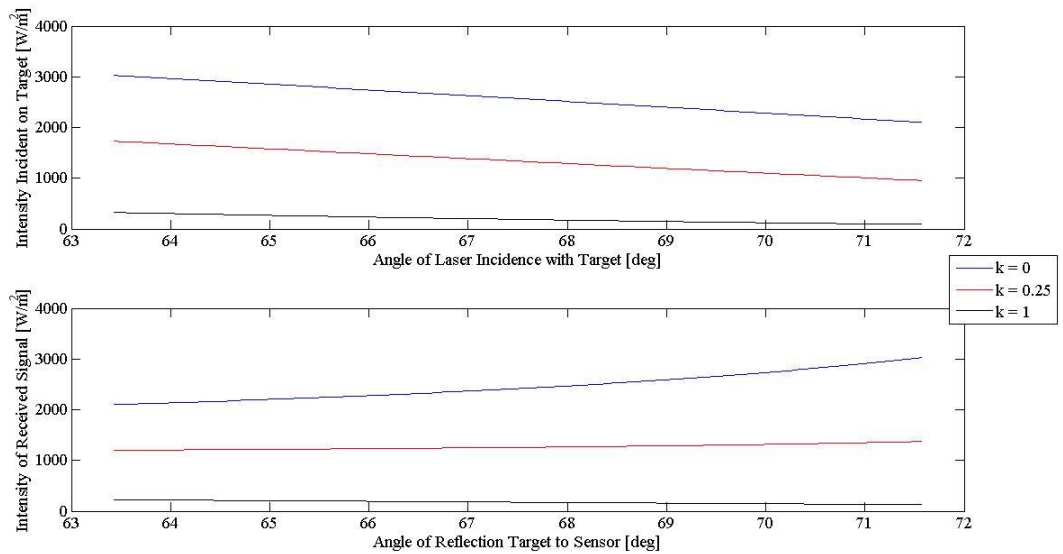


Figure 10 Case III: Intensity levels for varying angles of illumination and reflection with increasing attenuation at depth $z = 30$ meters. Top graph is target irradiance and bottom graph is intensity at the sensor. Target is located 1 [m] from the transmitter-sensor baseline.

As attenuation increases, intensity magnitude decreases as the signal reduces along the path of travel, however the general characteristic of decreasing intensity with increasing angle measure is still present. Transitioning from $k = 0$ to 1 the curves flatten as reflection intensity reduces due to attenuation. In general, as attenuation increases, the reflection response for a positional scan will appear to become constant across target acquisition.

4.2.3 Signal to Noise Ratio

As shown in Case II, SNR varies based on attenuation by reducing signal intensity received by the detector and depth by changing the path length of solar radiance to the system sensor. Although Case II examined SNR at varying angles of illumination indirectly due to the methods utilized in the simulation, these results are not the same as relationships in Case III determined more directly. Case III is more direct due to scan angle being the only varying condition for target positioning.

The first scenario examines SNR at constant depth with varying attenuation in the same manner as before with the same attenuation breakdown.

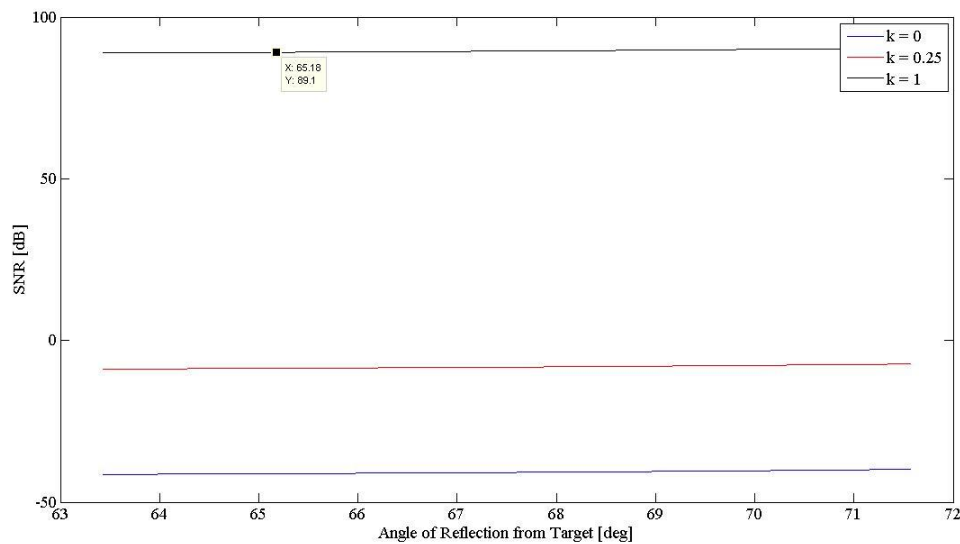


Figure 11 Case III: SNR for increasing attenuation, $k = 0, 0.25,$ and $1,$ at constant depth, $z = 30$ meters. Target distance is 1 [m] from transmitter-detector baseline.

For SNR results with increasing attenuation at constant depth, each condition exhibits the same behavior, increasing ratio with increasing reflection angle. This corresponds with increased intensity levels with increased reflection angle. Specific ratios, for a particular reflection angle, increase as attenuation level increases, attributable to

reduced noise levels at the sensor. The general behavior for each curve is similar regardless of attenuation level and follows the intensity curves.

Conditions for the next scenario are constant attenuation, $k = 0.25$ and varying depth, $z = 10, 20,$ and 30 meters.

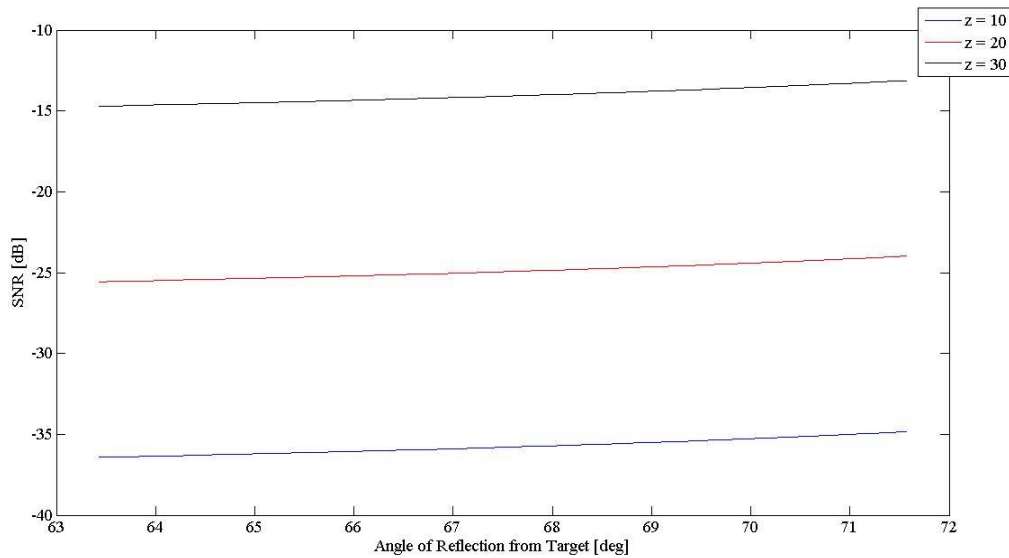


Figure 12 Case III: SNR at constant attenuation, $k = 0.25$, and varying depth, $z = 10, 20,$ and 30 meters. Target distance is 1 [m] from transmitter-detector baseline.

Under constant attenuation, varying depth conditions the SNR curves display similar behavior for the constant depth, varying attenuation condition. The difference here is the magnitude of SNR relative to each depth. As depth increases SNR increases, due to greater noise attenuation.

Case II and III demonstrate the relationship between depth, attenuation, and target position on SNR. For a given laser power level the SNR will be dependent upon environmental attenuation effects on the transmitted signal and noise. Travel distance between the laser source, target, and sensor determines reduction of the signal and sensor depth determines noise reduction, for a given attenuation level. Although attenuation may

not be isotropic, in most cases where mixing results in regular distribution of particles in the environment, assuming isotropic conditions over short operating ranges may be sufficient to estimate signal response. Under this assumption, the SNR will exhibit smooth behavior across varying angles of target acquisition.

4.3 Case IV Results

Case IV represents a scenario much closer to a tracking situation through a volumetric space. In this case the position of the target and laser scan are examined together, providing conclusions closer to a real world measurement.

Explanation is necessary to read the graphs which will be presented in the following subsections. Plots are shown as a function of the angle of illumination and reflection as opposed to position. For each position there is a corresponding curve on the plot that shows intensity versus degree. It is important to keep in mind that the geometry simulated in this study results in low angle measures corresponding with longer ranges and high angle measures corresponding with close ranges. Refer to Figure 3 for a graphic representation of the associated system geometry. Therefore, the final position, 21 meters, has a curve appearing on the extreme left of the graph and the first position, 1 meter, has a curve on the extreme right for 2-D graphs.

4.3.1 Ideal Transmission

The first graph presents results for the ideal case. Attenuation is set to $k = 0$ and depth set to $z = 30$ meters.

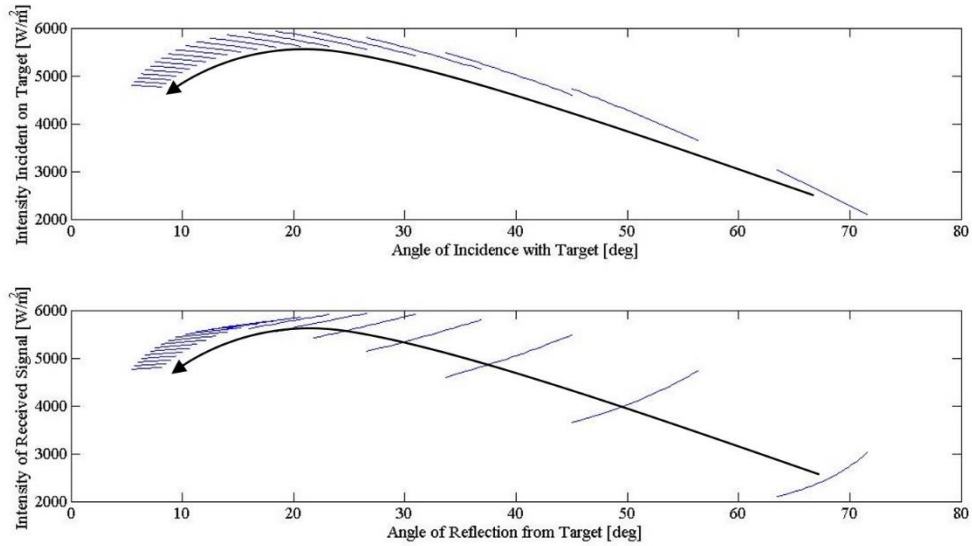


Figure 13 Case IV: Ideal transmission with no attenuation, $k = 0$, at depth $z = 30$ meters. Performance combines varying target position, 1 to 21 meters, and laser scan per position. Curves are plotted Intensity vs Angle with curves on the left of the graph representing results for farthest positions and curves on the right representing closest positions to the transmitter-detector baseline. Arrows in the graphs represent the direction for increasing target position.

In the above figure, characteristics recognized in cases II and III are combined in the simulation results. For this scenario, as in case II, illumination intensity increases to position 7 before decreasing due to initial dominance of the cosine factor. Reflection intensity follows this characteristic. Examining each position independently, intensity decreases as target illumination angle increases and increases as reflection angle increases. To estimate intensity magnitude between the illuminated and reflected results, the following figure is a clearer representation.

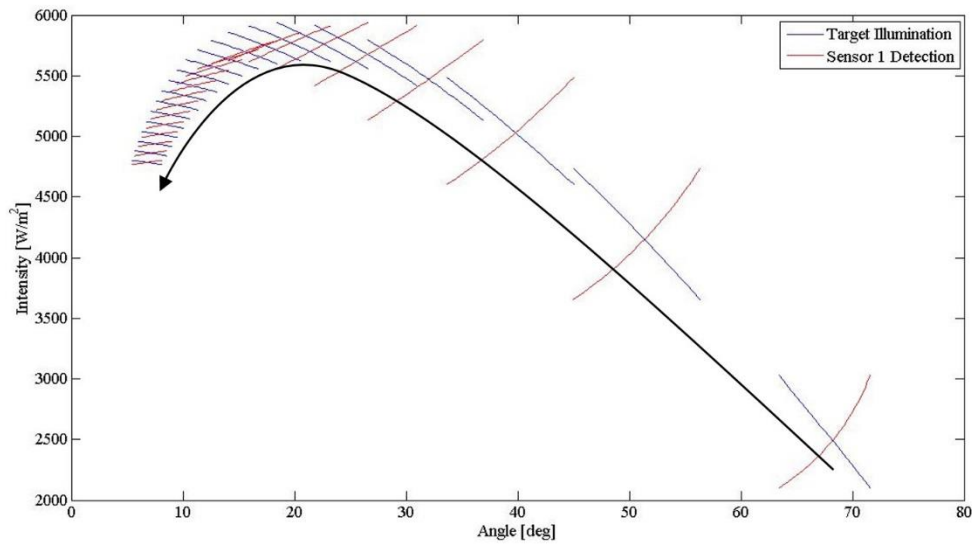


Figure 14 Case IV: Target illumination and reflected intensities per position with no attenuation, $k = 0$, and depth $z = 30$ meters. Arrow indicates direction for increasing target position.

Mapping illumination and reflection results together allows comparison of the magnitudes across all positions. Since no attenuation occurs, there is symmetry between illumination and reflection. This will change as attenuation is introduced in the simulation.

4.3.2 Single Sensor Attenuated Model

Individual positions within full dynamic analysis of the model follow the behavior described in Cases II and III for changing attenuation and depth. Full graphic descriptions are available in the appendix for multi-sensor Case V which can be simplified to the fully dynamic, single sensor case. The following analysis for Case IV is thus limited to changes within the positions for a given attenuation and depth.

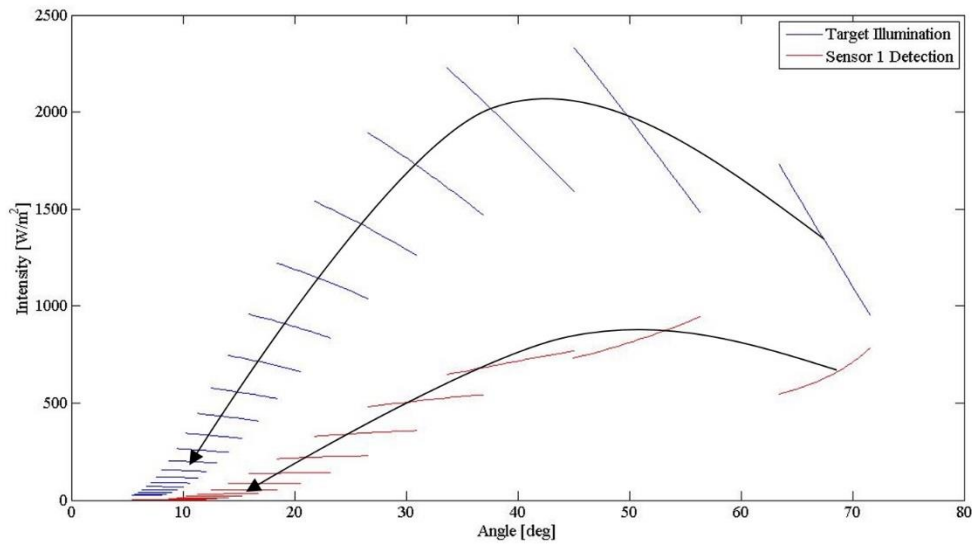


Figure 15 Case IV: Illumination and reflection intensity responses for $k = 0.25$ and $z = 30$ meters. Arrows indicate direction for increasing target position.

Considering attenuation in the full dynamic model, the first noticeable change in response is separation of intensities between illumination and reflection as compared to the ideal transmission case. Symmetry is no longer characteristic in the responses, as attenuation of the reflected signal occurs. Additional attenuation also causes flattening of the reflection response over the position scan. As target position increases and the range of angles in the scan decreases, the reflection response curve approaches a near constant response across the scan. As in Case II, where attenuation caused the position of maximum irradiance to shift, this occurs in the fully dynamic model as well. In the no attenuation case, maximum irradiance occurred at position 7, here it occurs at position 2. Reflection response mirrors this characteristic as position 2 is also the maximum level detected. With increased attenuation, the number of observable positions decreases, as expected for the decrease in signal level as range increases.

4.3.3 Signal to Noise Ratio

In the signal response analysis with dynamic position and laser scanning, SNR now becomes a useful tool for anticipating the operations of a tracking system. Before, a static component existed in the simulation, but now the resulting curves can estimate a signal level as a target dynamically moves in the environment against an angle of illumination.

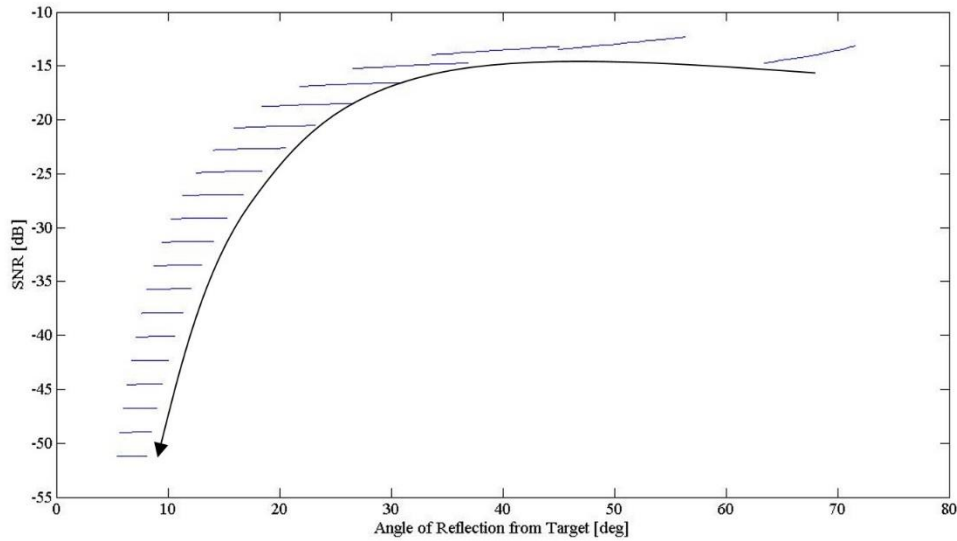


Figure 16 Case IV: SNR for attenuation $k = 0.25$ at depth $z = 30$ meters. Arrow indicates direction for increasing target position.

The SNR graph in the above figure follows the general curvature of the reflection intensity detection shown in Figure 15. Some variance is present through the initial positions as the response curves flatten out at higher positions. Maximum SNR is present at position 2, just as maximum intensity was present under the same conditions. Response here is negative across all positions, indicating noise is dominant in the environment, as opposed to the signal level.

4.4 Case V Results

Case V is a repetition of Case IV with the added component of an additional sensor to estimate intensity response across a defined sensor geometry. The sensor geometry presented is the same as the schematic shown in Figure 4 with a second sensor spaced linearly along the transmitter-detector baseline 1 meter to the right of the first sensor. Additional sensors can be added, with the appropriate ranges and angles defined in the geometry to calculate the appropriate intensity levels. Results presented exhibit the same behavior as previous cases. Complete results for Case V for attenuation levels $k = 0, 0.25, 0.5, 0.75,$ and 1 and depths $z = 10, 20, 30, 40, 50,$ and 60 meters are available in Appendix A for intensity responses and Appendix B for SNRs. The following results present unique aspects of Case V, using the multi-sensor consideration, as opposed to reiterating the characteristics described in the previous cases.

4.4.1 Ideal Transmission

For reference, intensity responses for ideal transmission, $k = 0$ are presented.

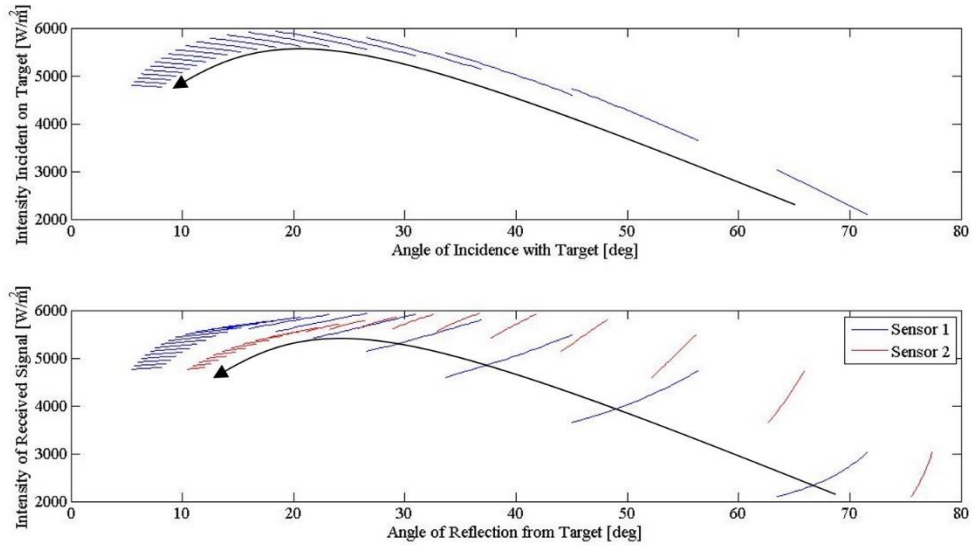


Figure 17 Case V: Target and detector intensity under ideal conditions: attenuation, $k = 0$ at depth $z = 30$ meters. Results at position 1, $r = 1$ meter from baseline is on the far right, while results at position 21, $r = 21$ meters from baseline is on the far left. Top graph is illumination intensity and the bottom graph is intensity incident at the sensors. Arrow in the upper graph indicates direction of increasing target position for both illumination and reflection.

For ideal laser transmission, the graph above exhibits the same behavior for illumination irradiance as displayed in Case IV for the same conditions. For the reflection response, there are now two sets of responses, each with its own average characteristic curve. The response sets are separated in the graph, which is a result of spatial separation of the sensors established in the simulation geometry. Magnitudes of a matched response set remains the same, however, the span of reflection angles is different. A smaller spread in reflection angles for sensor 2 results in a steeper intensity curve compared to sensor 1. This demonstrates a similar characteristic as previously described for the single sensor response. For a target farther away from the transmitter, a position scan has a smaller angle spread from start to finish. Since sensor 2 is farther away from the target than sensor 1, according to the analyzed geometry, the resulting reflection angle spread is smaller.

Finally, the response curve for sensor 2 offset from sensor 1, indicating matched sets will rarely, if ever intersect.

To observe matched response sets and judge magnitudes against another, the following graph is provided.

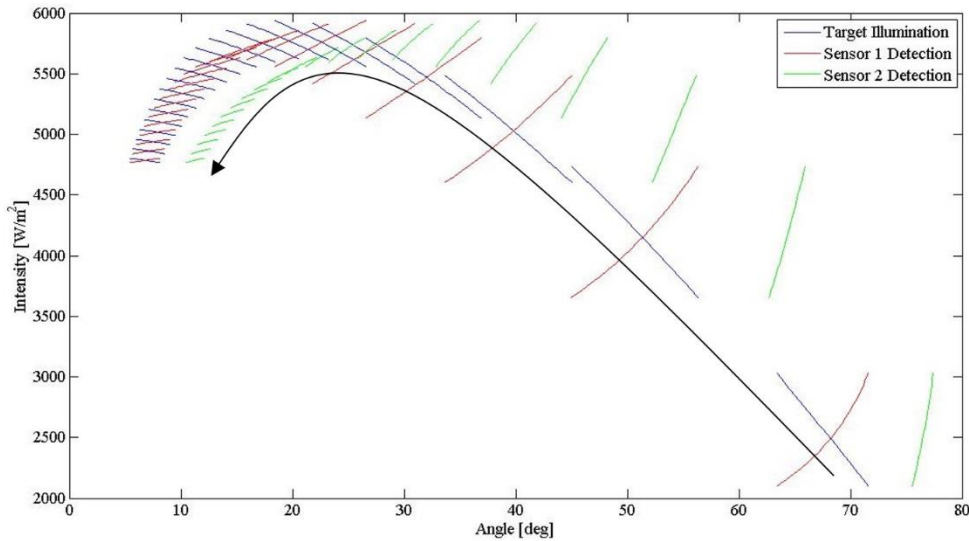


Figure 18 Case V: Illumination and reflection matched sets for ideal transmission. Arrow indicates direction for increasing target position.

Magnitudes from the response curves presented in Figure 18 show equal intensity results for a set as expected with no attenuation. It is also, much easier to see the angular separation between responses as well as the symmetry between target illumination and sensor 1.

Especially for the lower positions, shown on the right of the graph, matched sets are clearly identifiable. Picking out the sets at farther positions is much more difficult due to the narrow range of the response. The concept of a matched set is critical to the tracking problem. Conventional multi-sensor methods for determining target location requires a minimum number of sensors to receive a detectable signal with encoded data. Being able

to differentiate between matched sets aids in characterization of the tracking system and defining maximum operational range for a specific set of conditions and parameters.

To assist in interpretation of the response curves, the 3-D plot below provides the same information with the addition of target position. Individually, the previous and following graphs can be confusing, but used together full understanding of the results can be constructed.

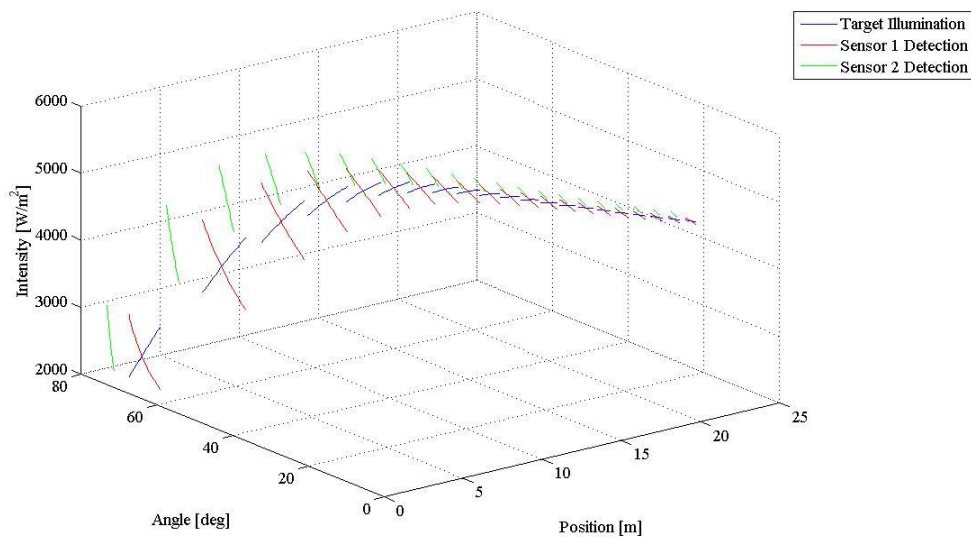


Figure 19 Case V: Illumination and reflection intensities with no attenuation, $k = 0$, at depth $z = 30$ plotted along three axes showing position, angle, and magnitude

4.4.2 Multi-Sensor Attenuated Model

In the next set of graphs, intensity results for multiple sensors under attenuating conditions are presented. Attenuation is $k = 0.25$ and depth is $z = 30$ meters.

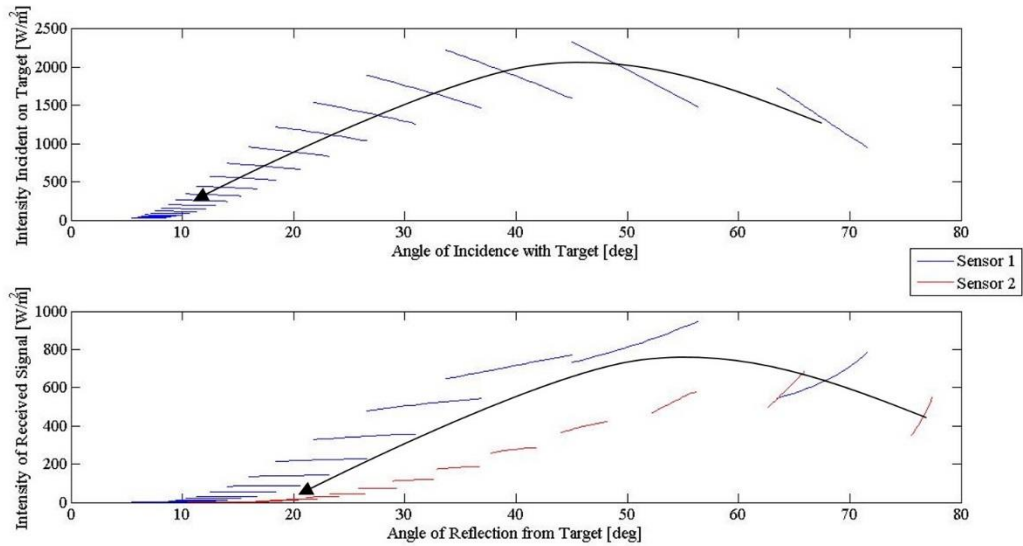


Figure 20 Case V: Multi-sensor attenuated intensity response with attenuation, $k = 0.25$, and depth, $z = 30$ [m]. Top graph is target irradiance and the bottom graph is the intensity response at the sensors. Arrow indicates direction of increasing target position for both illumination and reflection.

Similar to Case IV results, general behavior of the curve is reflective of the characteristics described in the previous cases. The illumination curve on the top is the exact same as the one presented in Case IV for the same conditions.

With attenuation applied to the model, the characteristic difference is present in the sensor response curves. Flattening and reducing in the sensor 2 curve occurs faster than under ideal transmission conditions and the sensor 1 curve, due to the increased path length for the reflected signal. Separation is still apparent between the two sensor responses.

Reflection angle spreads differ between the two sensor results. Difference between the spreads initially results in a steeper response curve at position 1 for sensor 2 compared to sensor 1. In progressive scans at farther positions, the change in the spread for sensor 2 reduces faster than in sensor 1, resulting in a relatively constant response sooner. At the

farthest ranges, angle spreads will approach the limit of being a singular response point for both sensors, limiting range and imagery possibilities for a target.

In the above graphs, relationships between intensity magnitudes are difficult to compare. When intensities are mapped together, such as in the previous section for ideal conditions, these relationships are easier to show. The graphs in the next figure are meant to show these relationships. Under attenuating conditions the reflected intensities are magnitudes lower than the illuminated intensities.

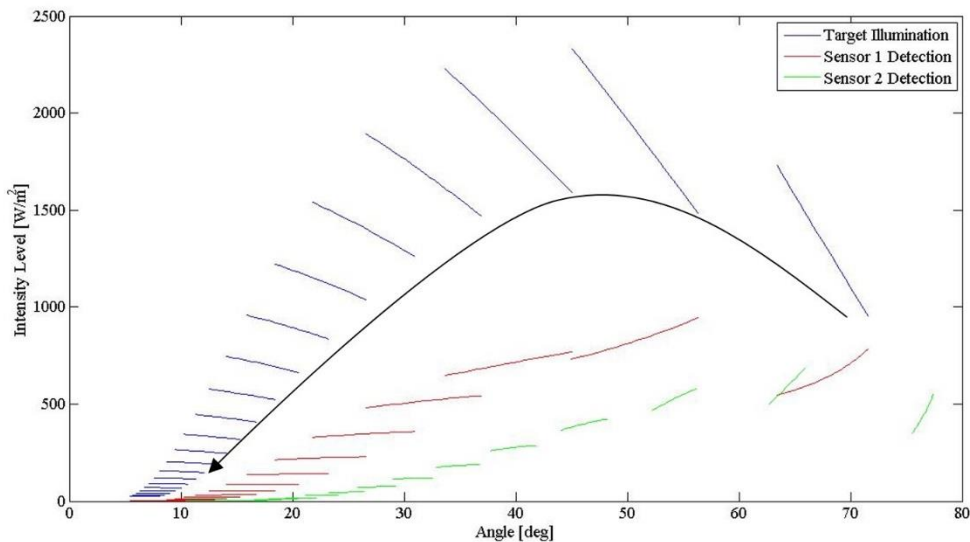


Figure 21 Case V: General relationship between illuminated and reflected intensities at sensors 1 and 2 in an attenuating environment, $k = 0.25$ and 1 , at depth $z = 30$. Arrow indications direction of increasing target position.

Looking again at the results for this condition the important matched response sets are a little more difficult to determine compared to the ideal transmission condition, but discernable. Though many positions are discernable from the target irradiance curves, there are approximately only 10 positions that are viewable from the matched reflection sets. Discerning these matched sets is important as they encode the range data for the

target. Depending on sensor sensitivities, responses at farther ranges which stack at the left side of the graph cannot accurately be estimated. Range ambiguity sets in at the point where at least one of the minimum number of sensors in the network cannot accurately discern between a response at one position and the next.

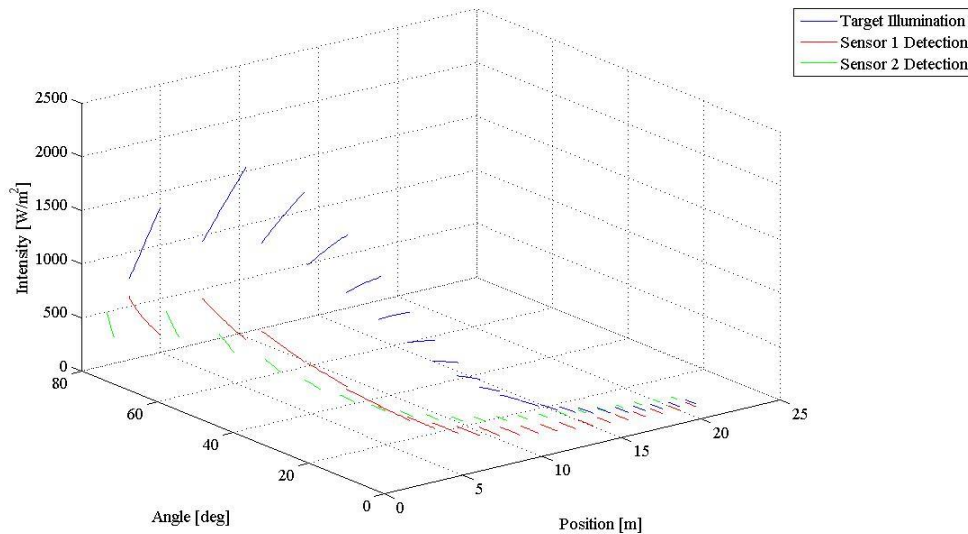


Figure 22 Case V: Illuminated and reflection intensities with attenuation, $k = 0.25$ at depth $z = 30$ along 3 axes showing position, angle, and magnitude.

In the three dimensional plot above, a different perspective of the curve highlights the changing responses based on target position. It is more evident in this perspective of the potential stacking effect of intensities at the farthest positions. From positions 15 to 21, responses are nearly similar for all three curves, suggesting a limit to tracking in actual implementation. Within this range set, the addition of more sensors to meet the minimum number required for a three coordinate solution, range error becomes a real possibility.

4.4.3 Signal to Noise Ratio

To determine the effect of noise in the multi-sensor case, the returned signals were compared to the average noise level provided by down-welling sunlight across the band

pass frequencies of an optical filter. The first graph below is a description of the SNR results for the same conditions as applied to the attenuation graph, $k = 0.25$ at $z = 30$ meters.

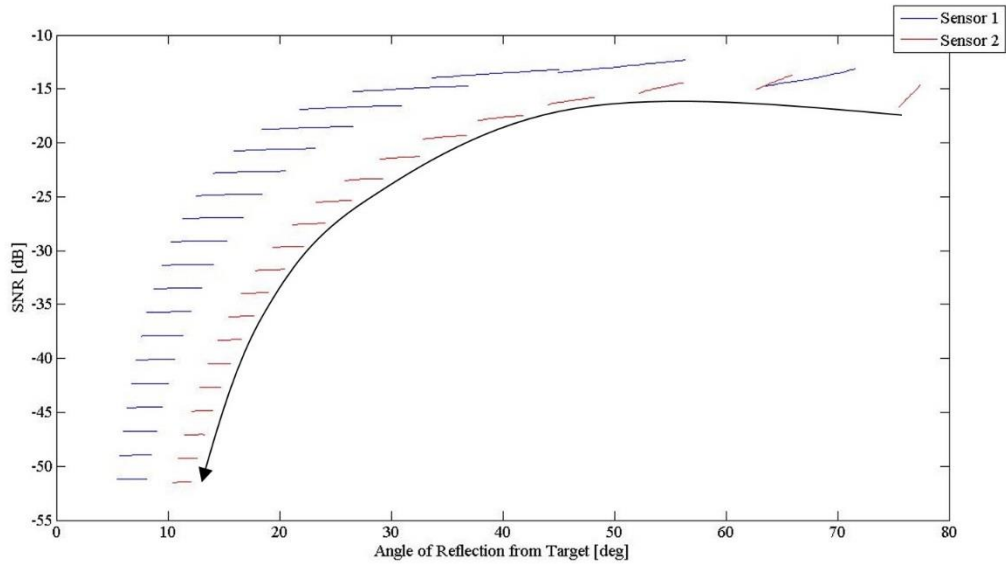


Figure 23 Case V: SNR response curve for attenuation $k = 0.25$ at depth $z = 30$ [m]. Arrow indicates direction of increasing target position.

In the SNR graph above, matched sensor responses are plainly obvious, with no question on which curves pair. Except for the closest positions, the ratios are relatively flat and constant from the initial reflection angle to the last, indicating very little variation in the response across the scan. The ratio varies slightly more in the close positions, at both sensors, leading to the conclusion that SNR will vary more when the target is closer to the detector than farther away. Maximum response is obvious at position 2, which matches the intensity curves previously described.

An issue with this response set, is the magnitude, which is negative across all positions in simulation. If conditions for tracking are generally considered to be positive, discernible matched sensor responses described by SNR, the conditions described thus far result in a no tracking scenario. The question becomes, what are tracking conditions under

these assumptions and does the SNR characteristic response change under those scenarios?

The following graph is an example of possible tracking conditions.

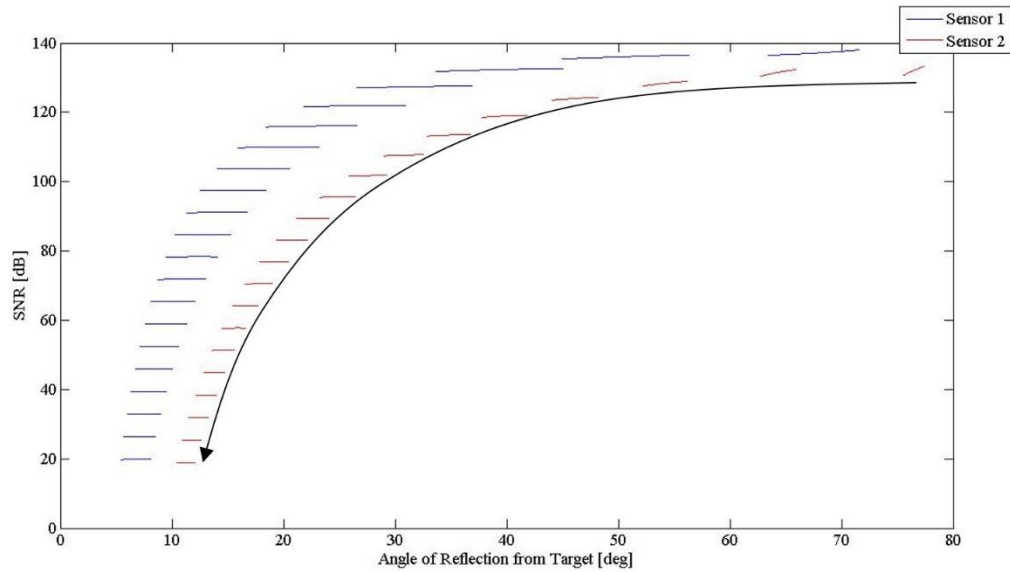


Figure 24 Case V: SNR response curve for a potential tracking condition considering the described laser parameters. Attenuation, $k = 0.75$ at depth $z = 60$ [m]. Arrow indicates direction of increasing target position.

The response curve can be considered a tracking scenario given the conditions described above, mainly positive SNR. All positions are discernable, ascribing to the positive ratios. There is some difference to the response in Figure 24 compared to the previous condition. This is a flatter response per position than before, which is attributable to the increased attenuation condition. In this case, the higher attenuation level and additional depth reduces the noise floor at the sensor, providing the set of positive SNRs.

When considered for tracking, matched discernable sensor sets with positive SNR is a desired characteristic for the system. Careful selection of system parameters can help provide for this characteristic, but attenuation level and deployment depth must also be considered. In the scenarios used as examples, higher attenuation actually becomes a

desirable environmental condition because it pushes the SNRs into the positive regime. However, this is a simplistic reduction. The absolute intensity level may still not be high enough to meet detection thresholds depending on selected sensor sensitivities. Use of both SNR curves and intensity response curves is necessary to estimate signal levels which constitute target acquisition.

4.5 Additional Characteristics and Trends

Analysis of results in Cases II through V developed a set of general characteristics and trends. Trends presented thus far show how intensities and SNRs vary with attenuation, depth, range, and angle, constituting a summary of signal response expectations for a tracking problem. Additional characteristics and trends, peculiar to specific phenomenon are noticeable in the general trends developed in the preceding analysis. These trends are discussed in the following section, along with average trends across Case V.

4.5.1 Tendency of Illumination

In the Case IV and V target illumination results, a specific behavior was identified involving illumination maximum response in the middle range positions. As shown through the constant depth and increasing attenuation factor sections, this behavior changed as attenuation increased, causing the maximum to shift to a lower position at higher attenuation levels. This is attributable to signal reduction across the path length of the laser as target position increases and attenuation increases. Change in this behavior is shown in the figure below. The curves were determined by removing the laser power level for the maximum illumination intensity for a target position and plotting against its

corresponding angle. This leaves the cosine factor and illuminated area as variables for the curves, effectively normalizing the result for any laser power level.

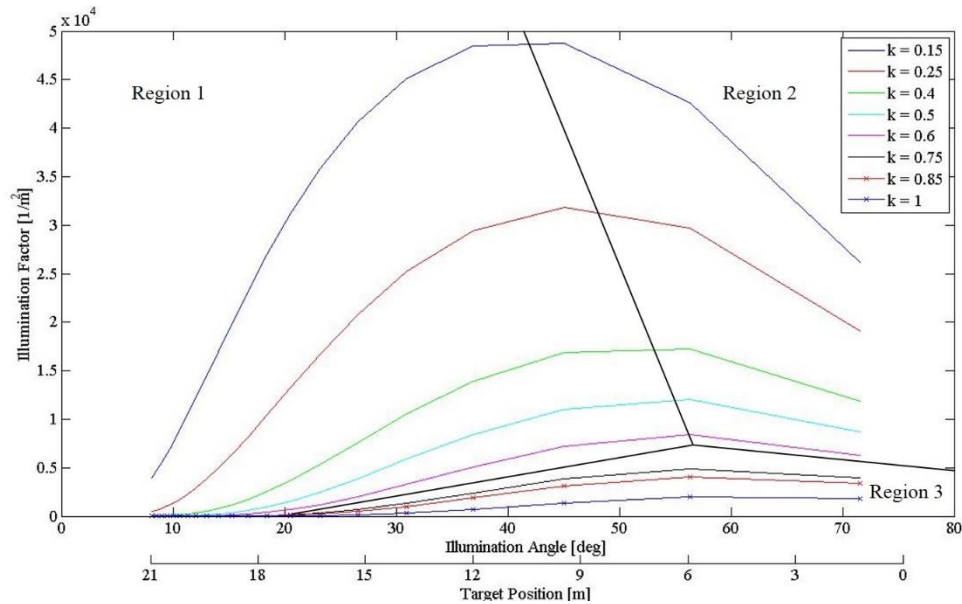


Figure 25 Tendency of illumination for the laser with increasing attenuation factor across all positions and angles. Region 1 is dominated by illumination area through beam divergence, region 2 cosine of the illumination angle, and region 3 attenuation.

At low attenuation levels the described ratio presents a balance of the overall attenuation to target illumination. The global maximum for the $k = 0.15$ line occurs at 45 degrees, but noticeably shifts on the $k = 0.4$ curve to approximately 57 degrees. From here the curves tend to flatten more rapidly, but the maximum stays roughly at the 57 degree mark through the $k = 1$ curve. Presence of the global maximum in the middle of the curve is a function of the decreasing angle which approaches 1 when the cosine is taken. This allows for maximum power applied to illumination when the path is normal to the incident plane of the target. In the region 1 area on the curve, beam divergence leads to a larger illuminated area which dominates the decrease in illumination angle. The maximum represents a balance between the two variables. Although present in all the curves, the

behavior is prominent at low attenuation levels. As attenuation increases, the behavior diminishes, indicating attenuation is the dominate variable in illumination as opposed to angle or beam divergence in region 3.

4.5.2 Average Intensity Response

Average intensity response for target illumination and sensor detection was determined by calculating the mean intensity level and plotted against target position. The results show a summary of the expected responses developed in Case II across varying attenuation and constant depth.

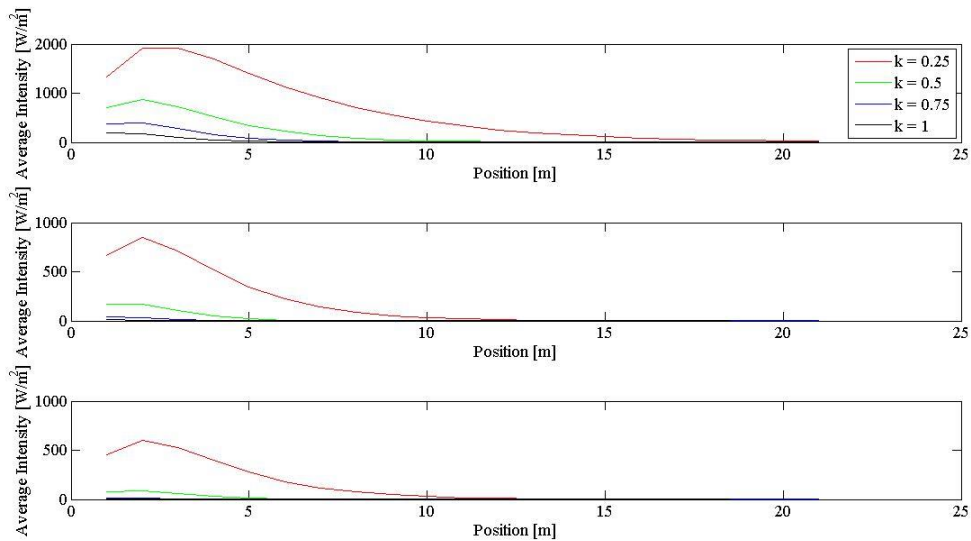


Figure 26 Average target illumination with increasing attenuation at constant depth. Top graph is target irradiance, middle is sensor 1 response, and the bottom is sensor 2 response.

Analyzing average intensity against target position at a low attenuation level, a maximum occurs at the 2 to 3 meter position corresponding with the decreasing angle behavior described in the previous section. This maximum diminishes as attenuation increases as expected and established in the ‘Tendency of Illumination’ graph. Results in

the graph follow the behavior described by the e-folding principle for attenuation, which diminishes the signal as signal path length increases.

Difference between the intensity responses describes the drop off in signal in a different manner. Using these curves, knowing the intensity magnitude at one point, target or sensor, the response at another point can be estimated. The results for the previous conditions follow.

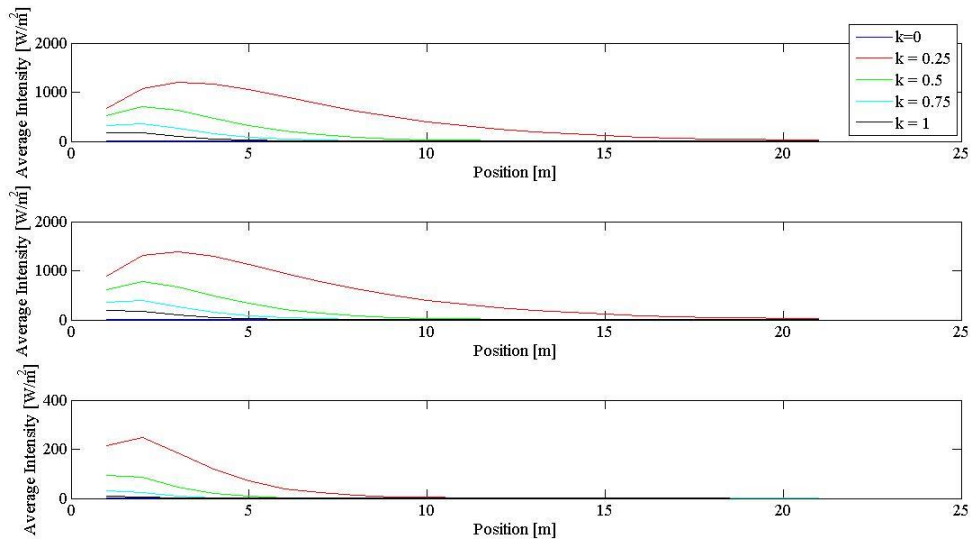


Figure 27 Difference in the average intensity responses for various attenuation levels at depth $z = 30$ [m]. Top: Difference between illumination and sensor 1. Middle: Difference between illumination and sensor 2. Bottom: Difference between sensors.

The difference curves follow the same behavior as the intensity response curves, as expected. Difference is not uniform, however, and changes with increased attenuation levels. Magnitude of the signal difference is greatest at the nearest target positions, maximum at the highest illumination point, and decreases beyond as target position increases.

4.5.3 Average SNR Results

SNR results provide the most useful tool to inform operational parameters and design decisions for a legitimate tracking system. Case V results were averaged and are presented in the same manner as the previous subsection for intensity results. The same conditions apply for the figures presented.

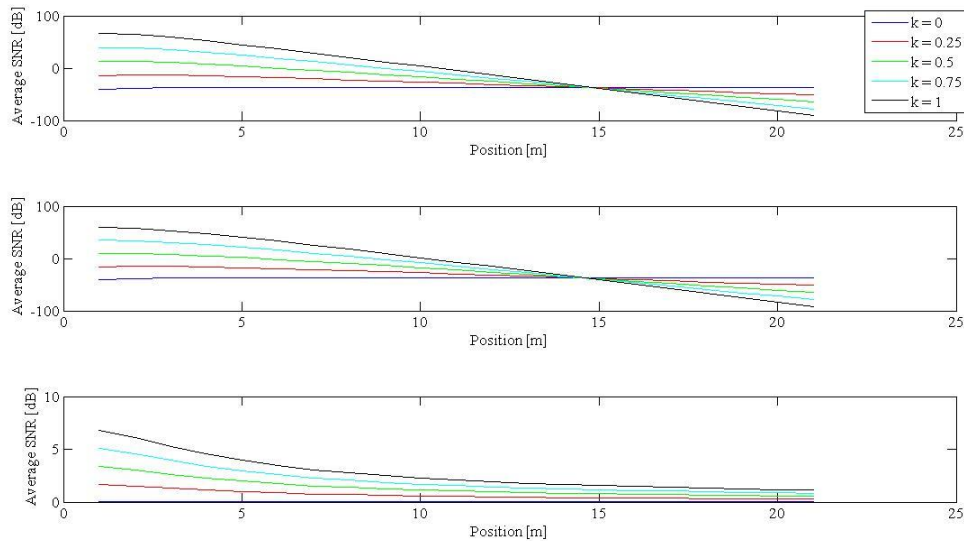


Figure 28 Average SNR results for increasing attenuation results and constant depth, $z = 30$ [m]. Top: SNR for sensor 1. Middle: SNR sensor 2. Bottom: Difference between the sensors.

For the increasing attenuation and constant depth condition, SNR results for both sensors are similar. The main difference is a slightly diminished ratio for corresponding positions between the sensors. Additionally, an intersection point for the various attenuation factors is present. For sensor 1 the intersection occurs at target position 15 meters with an associated SNR of -39.26 [dB] and sensor 2 at 15 meters with SNR -40.81 [dB]. In the SNR difference graph below, the difference in the mean SNR value decreases across positions as range increases. At low attenuation, the difference between SNRs at

sensor 1 and 2 is very small and changes less significantly across the positions. As attenuation increases, the difference in values increases, with greater separation the closer the target position. SNR where $k = 0$ is nearly constant, varying only slightly, but higher attenuation factors exhibit much higher variation, due to greater signal degradation while noise levels at the sensor remain relatively constant.

Results for average SNR with varying depth are shown below.

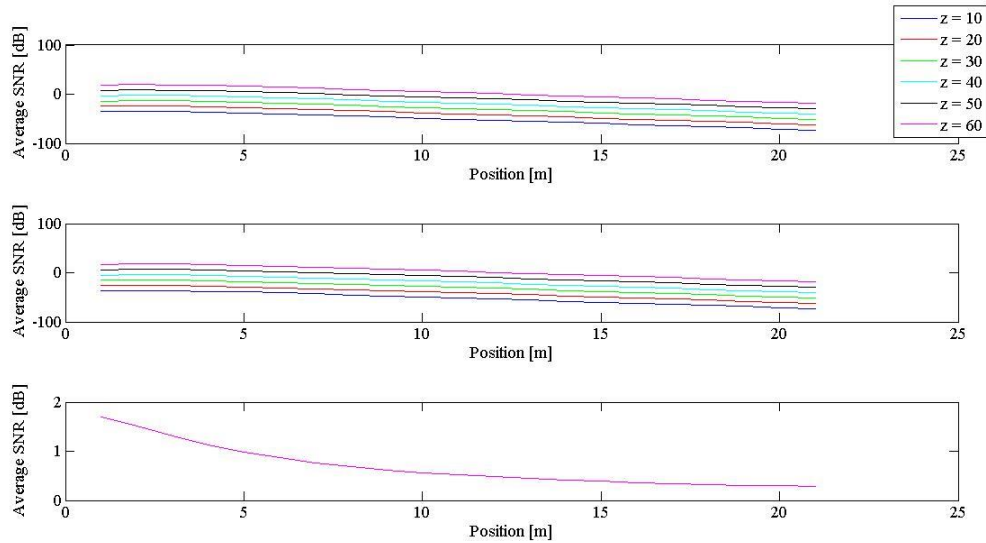


Figure 29 Average SNR results for increasing depth and constant attenuation, $k = 0.25$. Top: SNR sensor 1. Middle: SNR sensor 2. Bottom: Sensor difference.

Average SNR with increasing depth across both sensors shows steadily declining ratios as target position increases from the transmitter-detector. SNR improves with increasing depth, as expected, due to diminished noise levels. No intersecting point is exhibited with changing depth because laser signal levels are not attenuating at a different rate with changing depth. The noise floor is the only level changing due to increased depth. The difference in SNR value between the sensors is very small, with mean difference shown in the third graph. Since the SNRs change at the same rate for a given curve at each

sensor, the difference is the same across all depths resulting in the same difference curve for all depths.

4.6 Range Estimation

Location determination, including range, bearing, and altitude is the ultimate goal for a tracking system. Though this study does not fully examine all aspects to determine target location for tracking, attempts to determine the range were made using the method described in the approach section (3.3), based on the modeled intensity results at each sensor. Estimation using the method was only considered for no attenuation and no beam spreading conditions. Determining range with those added parameters necessitates other methods not considered in this study. Results of the estimates were marginal for short ranges, improving as the position of the target increased.

The method described requires a large number of data points to estimate the range. As the number of scan points increases, the range estimate more closely fits the known range of the target based on the positioning algorithm in the simulation. Using a large number of points is practical due to the step resolution capable by the prototype tracking system. Range was measured as a distance from the transmitter-sensor baseline due to establishing it as the reference coordinating origin throughout the simulation, though the calculation does determine the illumination distance from transmitter to target. Estimating range from one of the sensor positions can be accomplished through one of the triangular geometric relationships after solving for the illumination range.

In addition to no attenuation and beam divergence in the calculation, an assumption had to be made to reduce the number of variables describing the laser path in the overall calculation to one, the illumination range from transmitter to target. A primary assumption

is a ratio between the solid angles describing the reflection path of the laser and sensor observation. This allowed intensity at the sensors to be reduced to the illuminated intensity by eliminating dependency of the solid angle calculations on the range. The ratio was determined through post processing the original simulation data. In reality, this ratio is not constant as it varies with the beam spreading rate, if applied, and very slightly by the change in range from scan point to scan point, however, analysis through the simulation allowed averaging of the ratio to a particular value used in the calculation. When discounting beam spreading, ratio variation is on the order of 10^{-6} . This average is only valid over the operating range of the system. This was done out to a position of 21 meters under the simulation parameters due to operational goals of the proposed prototype system.

Range estimation results through intensity detection are shown in Figure 30. Figure 31 describes the mean square error between the range estimate and actual range per position. The calculation was performed with 20, 50, 100, 250, 500, and 1000 scan points per target position to demonstrate the benefits of data density to fit the estimate to actual conditions.

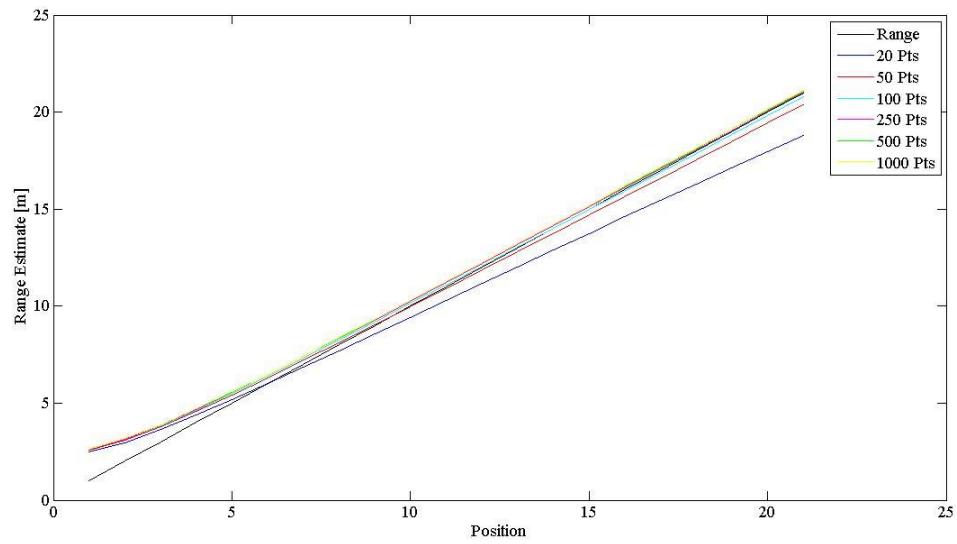


Figure 30 Range estimation results from detected intensity results in Case V, multi-sensor. No attenuation and beam divergence.

From the results, it is readily apparent that scan density improves the calculated range estimate. Except for the estimate with 20 points, the fit also improves with increasing range out to the explored range of the system (21 meters) in the simulation. At close range estimate error is greater.

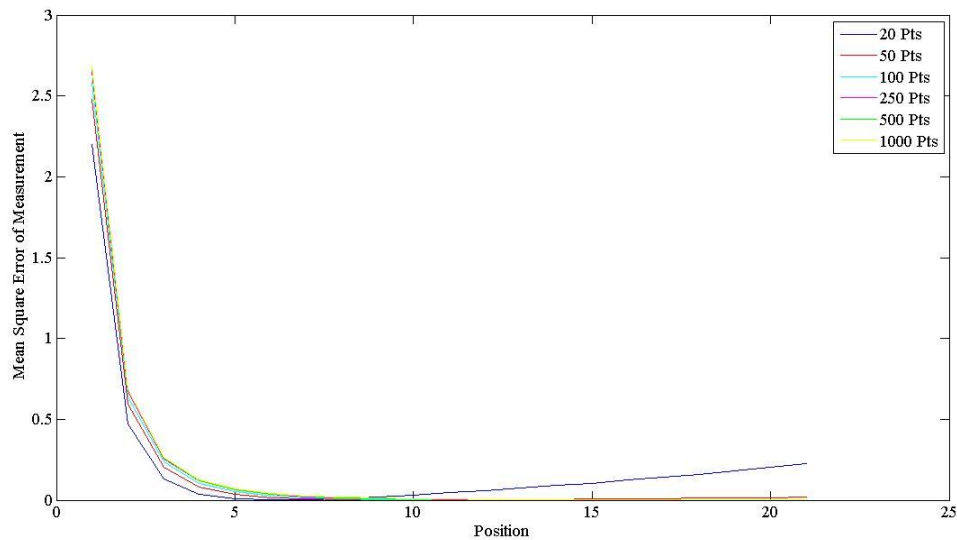


Figure 31 Range estimate error. Error is normalized to target distance from the transmitter-sensor baseline. No attenuation and beam divergence.

Results in Figure 31 show the error between the estimated range and actual range of the target. Error is greatest at the nearest positions and improves with data density at longer ranges. From position 4 on, the estimated error for the 100 and 1000 point simulations is near zero over the operating range of the system.

The method described to estimate range from SNR and hence, received intensity at the sensors was attempted using irradiance rather than radiance calculations. An issue presents using irradiance values because the illuminated target area present in the initial calculation (Equation 1) and Lambert's reflection model cancel, leaving a calculation free of a range variable. Attenuation conditions were inserted to attempt to resolve the issue, however attenuation must be accounted for on both the transmission and reflection sides of the calculation. Since attenuation is dependent on range and the transmission and reflection ranges are not necessarily equal, there was not a typical method available to isolate one of the ranges as a single variable. The calculation would require knowledge of

one of the ranges, effectively negating the purpose of the exercise. Ultimately, the solution involved determining the laser transmission solid angle and converting irradiance to radiance, resulting in the range calculation shown.

4.7 Target Tracking

The summation of this study is to characterize laser performance in order to track a dynamic target underwater. Laser characteristics have been developed so far, without regard to this objective. This section applies the findings of the study to answer the fundamental question.

Since this study does not consider all of the variables necessary for target tracking, such as sensor sensitivity and specific signal characteristics, the conclusions will be limited purely to relative signal levels: SNR and intensity. Extrapolation of the simulation will be considered for attenuation $k = 0.25$, a typical value described in literature for the waters in South Florida at depths $z = 30$ and 60 meters.

4.7.1 Laser Power

Laser specifications have primary importance to determine intensity and SNR levels in the study. Secondary is sensor sensitivity to delivered energy. For the purposes of applying simulation characteristics to determine appropriate laser power, SNR will need to be positive with an intensity level above $10 \text{ [W/m}^2\text{]}$ for a trackable situation.

Simulation conditions considered laser power at 50 [mW] , which is insufficient to track a target at the 21 [m] position. Extrapolating the data for 30 meter depth, under the SNR and intensity assumptions, a laser with power at 10 [kW] is necessary for tracking out to 20 [m] in the described attenuation environment. Considering depth at 60 meters, laser power drops to 5 [W] , demonstrating the benefit for system deployment at greater depths.

4.7.2 Detector Distribution

Location of detectors plays a large part in the received intensity level and end SNR at individual sensors. Geometric relationships between the transmitter, target, and detector change the total signal path length and levels. Strategic placement of detectors can reduce signal path length and improve detected signal levels. Additional considerations for detector numbers and placement are economics, system complexity, and infrastructure installation and maintenance.

The simulation considered one sensor or set of sensors. To develop a three coordinate target fix a minimum of four sensors are needed, a condition well developed in literature. Additional sensors in a detector would add redundancy in establishing a target location. Regardless of the number of sensors, placement in relation to each other is important. The simulation demonstrates that spatial separation creates distinct responses at individual sensors. Separate and distinct responses are critical to the location process. Without regard to specific signal characteristics, sensor spacing should be far enough to provide distinct responses, but close enough to maintain detectable signal levels. The one meter spacing simulated provides these distinct responses, but analysis shows instances where one sensor provides a detectable signal while the second is undetectable. One meter spacing should constitute the maximum spacing between any two sensors in a detector. Closer spacing will result in overlapping in the characteristic curves between sensors when viewed in their entirety across a positional scan, but will limit sensors dropping out of a target fix. This result is not an issue as spatial separation will provide distinct responses at each sensor for an individual point scan of the target. Only when sensors exist in the same space will the responses be identical.

The second consideration for detectors is the total number and placement (detectors are considered to be a collection of four or more individual sensors). The simulation did not consider detector placement which would result in target detection anywhere along the circumference of a 20 meter radial volume. Additional detectors are necessary for total volume tracking. Strategic placement of detectors will cover the total volume, but also limit total signal path length, improving sensor response. The longest path length for a target located at a 20 meter radius within a hemisphere exists at an angle bisecting two detectors. Detector placement towards maximum target range improves path length, but at a cost to near target path length. Geometric analysis suggests two sets of detector placement would be suitable for tracking to reduce maximum range path length and minimize near target path length cost without creating extra complexity in the system. These detector placements are the Staggered-6 and Staggered-8, with 6 and 8 detectors respectively. Detectors are placed in two rings with an equal number of detectors per ring, dividing the circle into equal sectors. The outer ring is placed to minimize the maximum signal path length, while an inner ring is placed at an intermediate distance between the transmitter and outer ring along the bisecting radial between the two outer sensors. For a 20 meter maximum range the resulting geometries indicate estimated path lengths as shown in the following table.

Detector Geometry	Outer Ring 12.5 [m] (Path length for target at 20 [m])	Inner Ring 5 [m] (Path length for target at 1 [m])
Stagger-6	37.5 [m]	13.03 [m]
Stagger-8	34.2 [m]	12.8 [m]

Table 2 Detector geometry path lengths

5 Conclusions

Over the course of five cases, a number of general characteristics are apparent for laser performance in a tracking situation. These characteristics developed during simulation progression, but remained consistent and provide expected response curves to enhance development of a tracking system. In general these characteristics describe the intensity as illumination angle and target distance vary through the framework of Lambert's Reflection Model. Both attenuation and beam divergence function to reduce the magnitude of the response, however attenuation can also enhance signal characteristics when considering ambient noise levels. The ultimate objective of a tracking system, extracting target location, is achievable from the intensity response detected at the sensor network, though the method used is limited to the most ideal circumstances.

Comparing the ideal case with no attenuation to real conditions where attenuation is a factor, the results indicate a change in intensity as both location and angle vary. In the ideal case intensity magnitudes were greatest at a transition point which balanced the illumination angle with area, the latter increasing as range increased due to the spreading condition. When attenuation is considered, illumination continues to follow the same behavior, however, the maximum point tended to shift toward a shorter range until attenuation dominated both the angle and area factors resulting in a flat response curve.

As illumination angle varies, the intensity at both the target and detector varies. While intensity increases as illumination angle decreases, generally, this is not the case for reflection intensity. Maximum illumination results in maximum reflection magnitude,

though the corresponding angles are not necessarily equal. For the geometry analyzed, the corresponding reflection angle for maximum illumination was the highest reflection angle in the scan, occurring when the illumination angle was minimum. This relationship was constant regardless of target position, though increasing target position resulted in diminishing variance in the angles of illumination and reflection. As position increased, the resulting intensity level's variance also diminished, approximating a constant level at the farthest positions. Reflection intensity exhibited this same behavior, though reduced in magnitude due to attenuation. The highest reflection intensity occurred at the position where illumination intensity was maximum, regardless of attenuation.

In multi-sensor Case V, analysis shows the same results for the second sensor as the first in relation to the illumination intensities for the general characteristics described. Two noticeable differences do exist between the sensors. Variation in reflectance angles is reduced in sensor two from sensor one and intensity magnitude is reduced. These are both a result of increased distance from the target for sensor two. Increasing target position corresponded with reduced variation in the independent variables governing a target scan. The resultant illumination and reflected intensity variation also reduced. In general, when comparing the responses of two sensors, as sensor distance increases variation in reflection angle and intensity magnitudes will reduce. These effects are magnified as target position increases from the transmission source.

SNR tends to exhibit it's own behavior, though it closely relates to the reflection intensity response. SNR at the sensor tends to follow the typical response curves shown by the reflection intensity. Where detected laser intensity did not vary according to depth and was only effected by the environmental attenuation condition, SNR does vary

according to both conditions. Increasing attenuation and depth has a tendency to increase the SNR by reducing the level of ambient noise. However, as target position increases there is a balance between path length of transmission and reflection. SNR tended to be negative where limited attenuation occurs to the noise floor. An inflection point for the transition between positive and negative SNRs occurs where total path length of the laser (total of transmission and reflection path) results in a detected intensity that is equal to the attenuated noise level. This point suggests a maximum operating range for a laser tracking system based purely on SNR analysis without consideration of signal processing and target detection techniques.

Range determination from detected intensity levels is possible, though not practical, based on mature techniques utilized in acoustics and radar applications which can be applied to optical methods. Still, under the most ideal conditions range can be found with minimal error through an averaging process of high density scan data. This method was most effective as target position increased with minimal error between the estimated and actual position. At short range, error was the greatest.

Applying these results and conclusions to the tracking problem, specific characteristics evidently affect decisions in which a system is designed and operated. Foremost, is determination of maximum range of a system. Maximum range for an operating system is not just described by the minimum signal level detectable by a sensor for a set power level and specific attenuation level, but is also described by the relative level of noise at the sensor. In effect, this is what SNR results show in the analysis, the reflected signal not only needs to be above a minimum detectable level, but also discernable against the noise floor observed by the sensor. This suggests reduction of the maximum

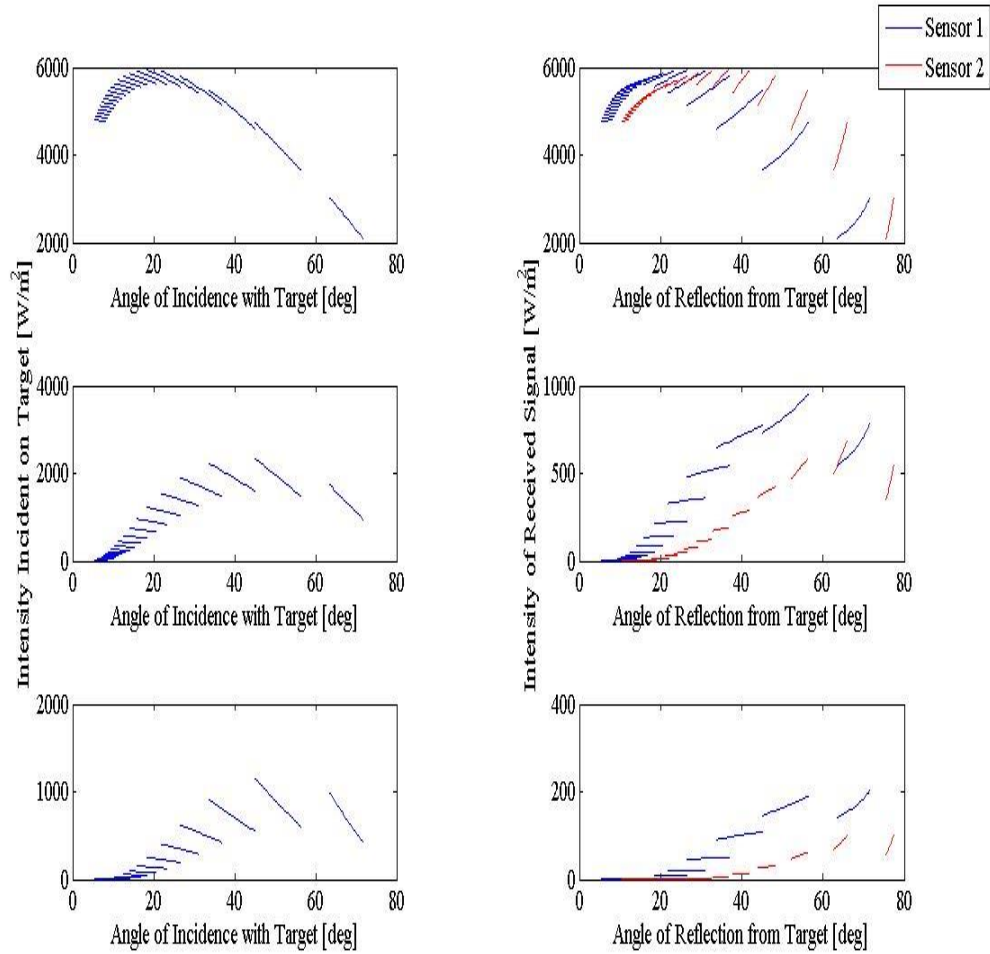
operating range of a system based on local ambient noise in the environment. Second, quite obvious in post analysis, is the drop off in signal between sensors due to spatial separation. Difference in the received signal level has one immediate impact, specifically at maximum range of an operating system. For a target located at maximum operating range, reflection signals maybe undetectable by one or more sensors in the network, due to the signal drop off resulting from additional attenuation based on the added range from the target. In the coordinate solution process, an individual non-detecting sensor can lead to reduced location resolution and loss of whole dimensional coordinates for the fix. These specific conclusions concerning application to tracking suggest careful consideration of environmental conditions, system geometry, and operational objectives in design and deployment.

Lambert's Reflection Model applied to an underwater optical tracking problem results in response curves capable of suggesting operation and potential design considerations for a practical system. Utilization of the curves and models should provide decisive data to specify processing architecture which can maximize the characterization of a laser operating under the proscribed conditions. These conditions, however, simplified the simulation a great deal, leaving opportunities for additional research. Proposed research in the future could include experimental confirmation and validation of the simulated model, sensor network geometry optimization, signal optimization, utilization of a more complex reflection model, target effects on reflection (such as material and geometry), multiple target acquisition, target positioning determination, target imagery extraction, and target pattern recognition.

Appendices

Appendix A Case V Intensity Results

Figures in this appendix represent results from the simulation in Case V for target illumination and reflected intensities at the sensors. They are organized by attenuation ($k = 0, 0.25, 0.5, 0.75, 1$) and increasing depth, ($z = 10, 20, 30, 40, 50, 60$ [m]).



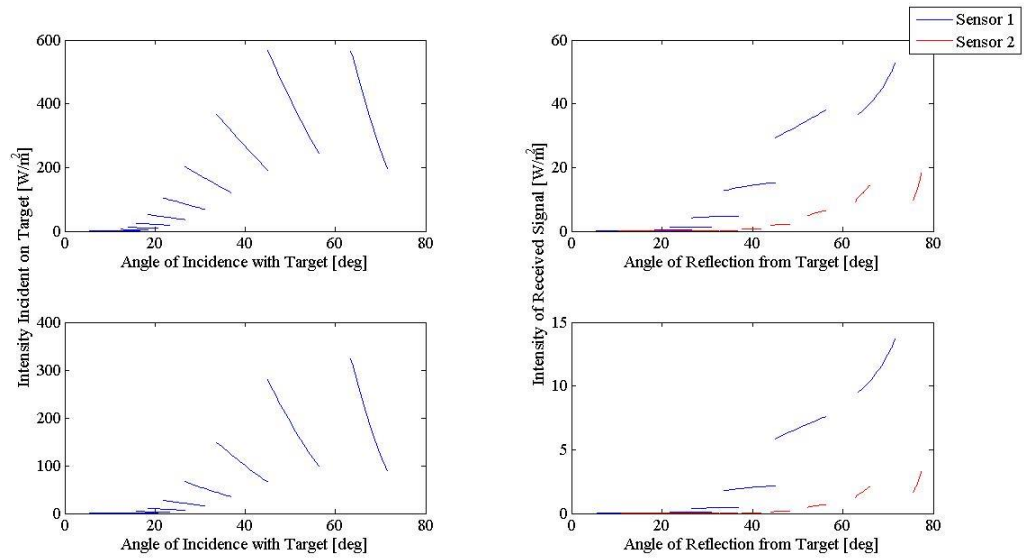
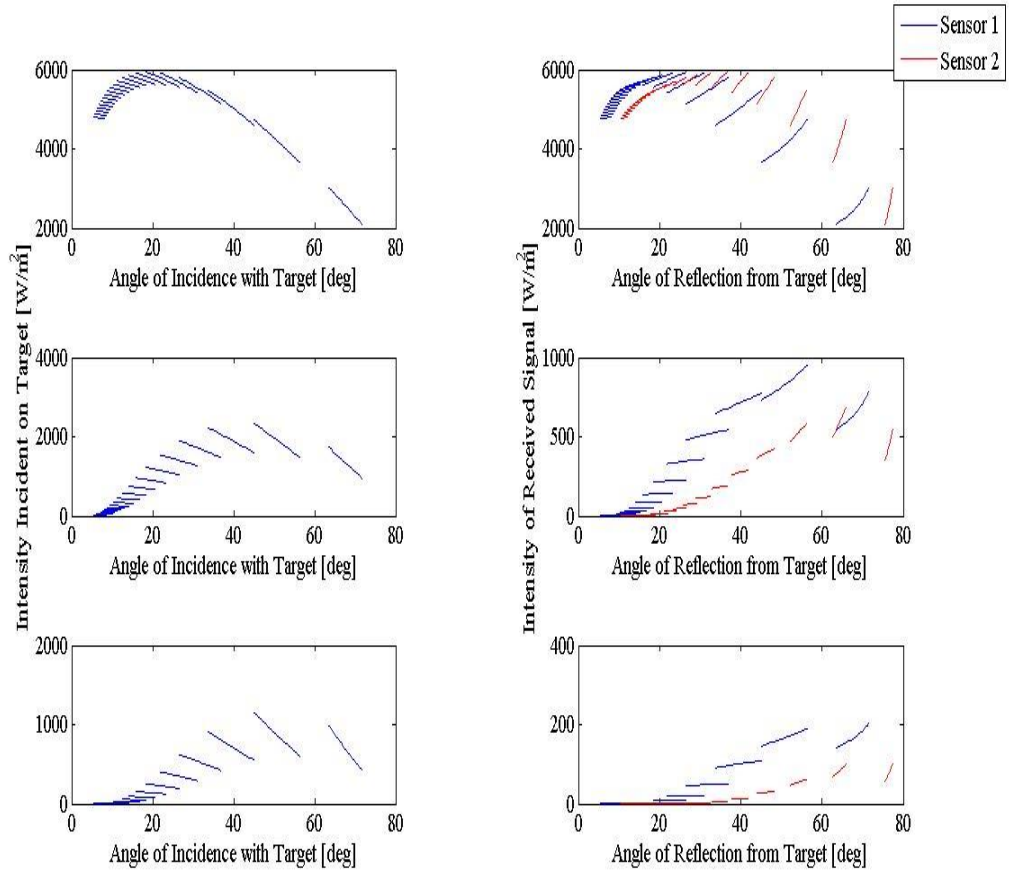


Figure 32 Case V illumination and intensity results for increasing attenuation at depth $z = 10$ [m]. From top to bottom $k = 0, 0.25, 0.5, 0.75, 1$.



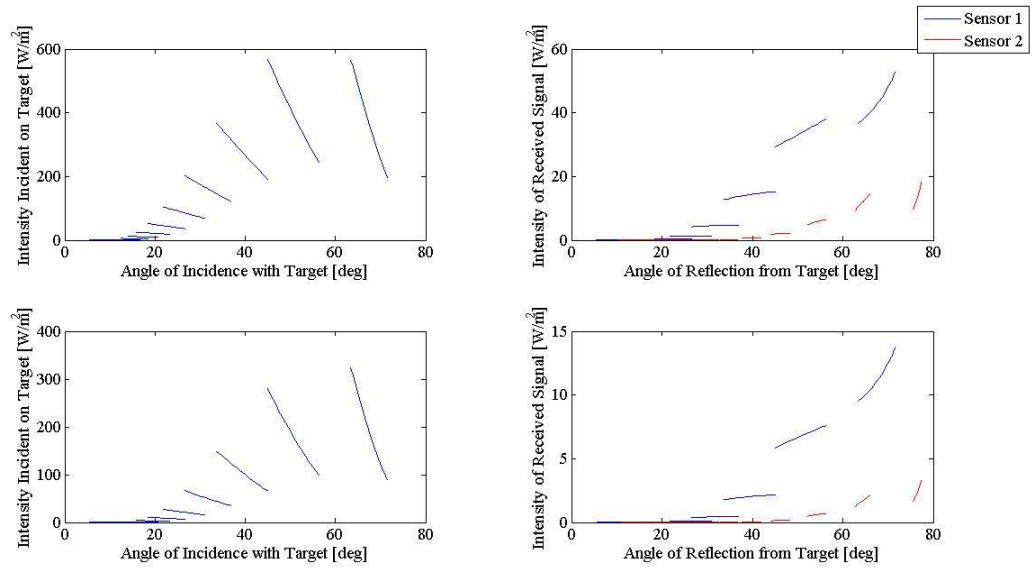
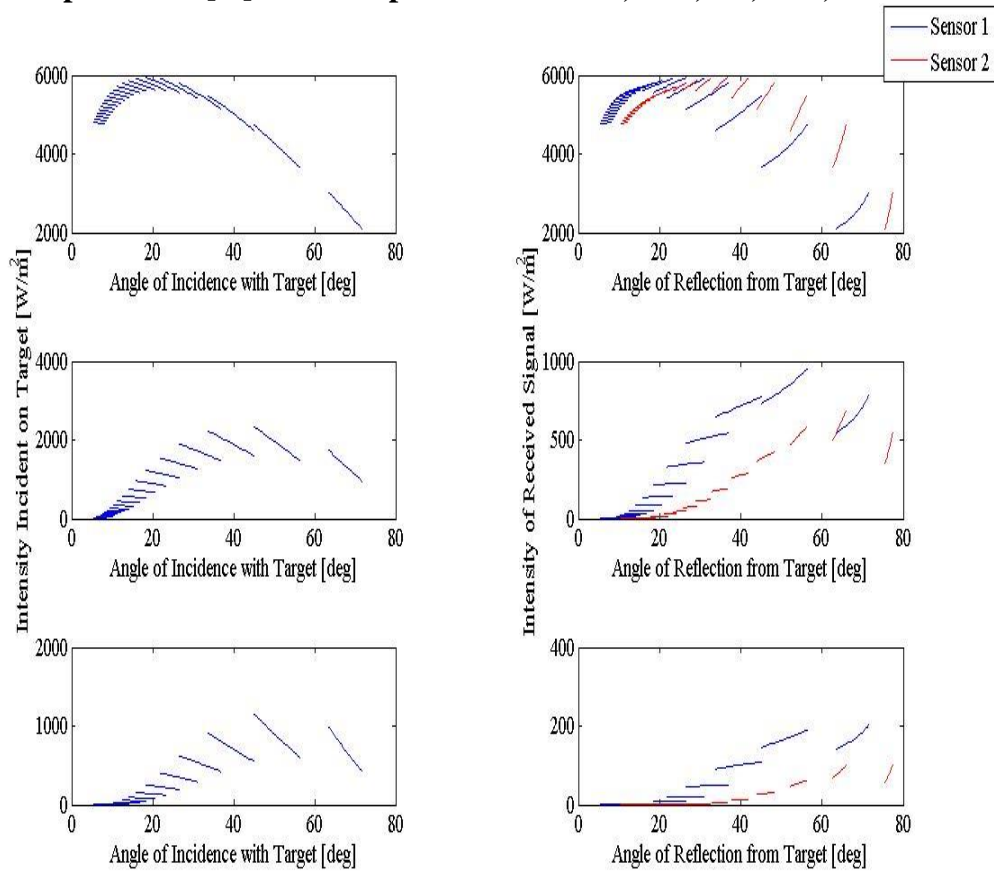


Figure 33 Case V illumination and intensity results for increasing attenuation at depth $z = 20$ [m]. From top to bottom $k = 0, 0.25, 0.5, 0.75, 1$.



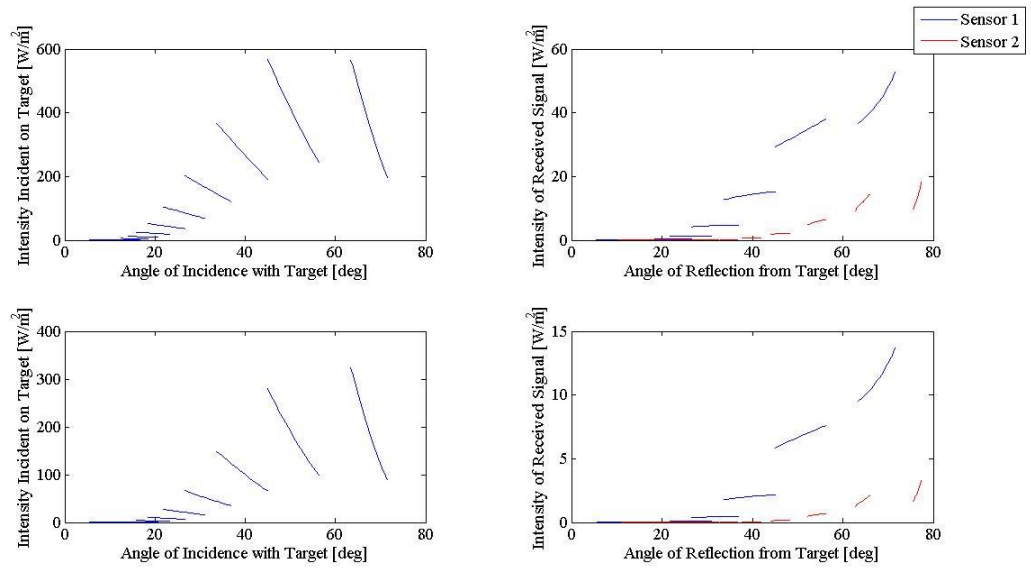
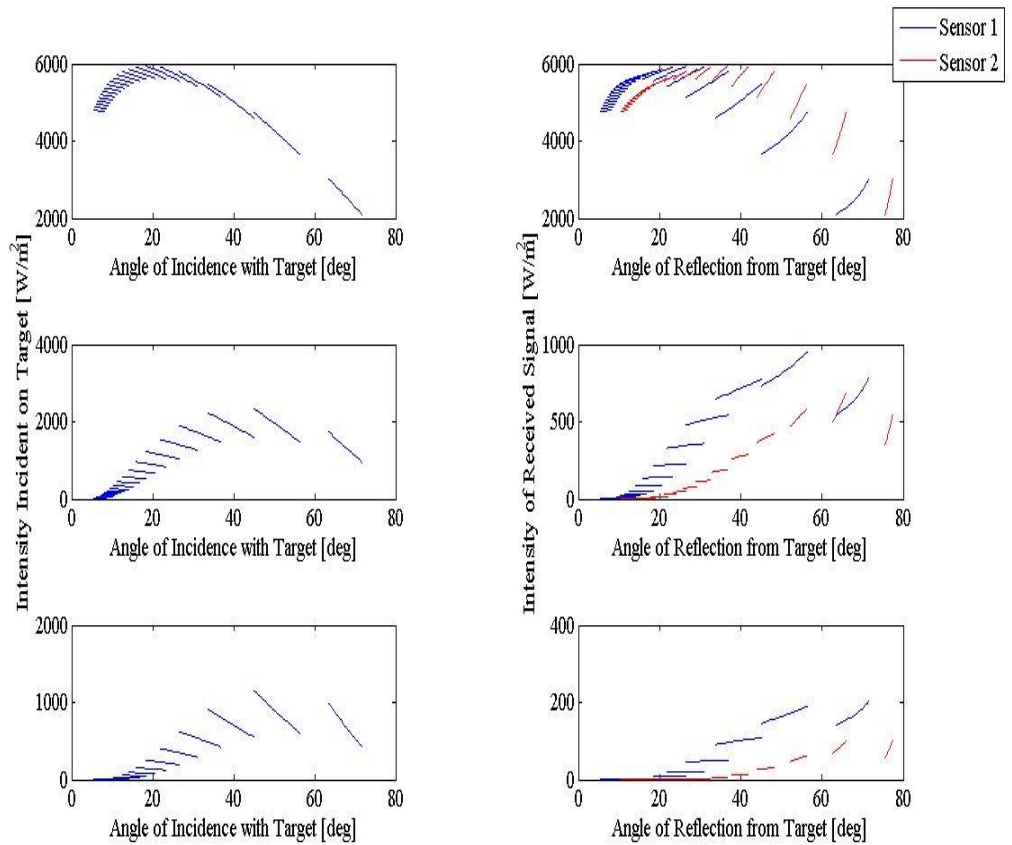


Figure 34 Case V illumination and intensity results for increasing attenuation at depth $z = 30$ [m]. From top to bottom $k = 0, 0.25, 0.5, 0.75, 1$.



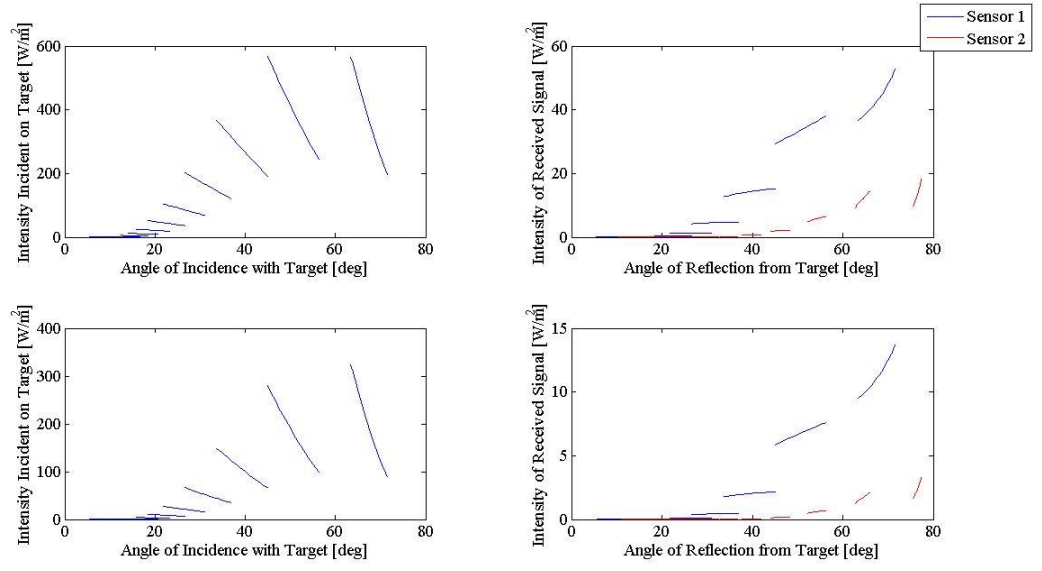
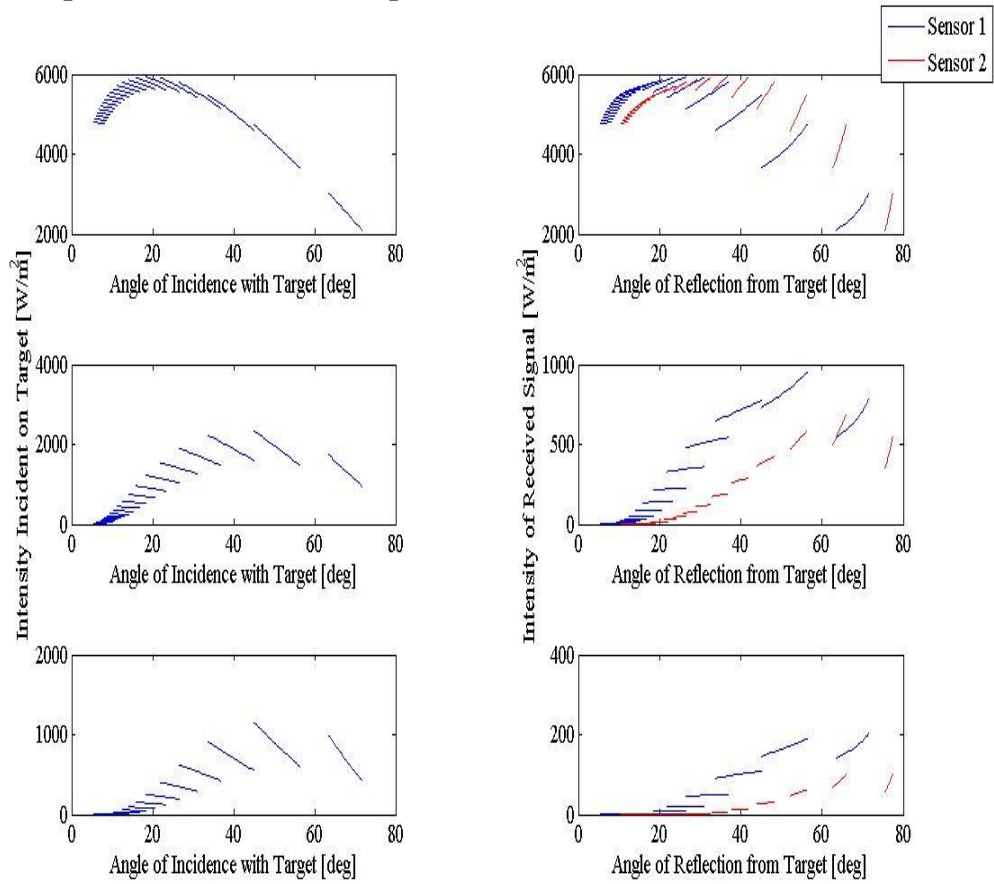


Figure 35 Case V illumination and intensity results for increasing attenuation at depth $z = 40$ [m]. From top to bottom $k = 0, 0.25, 0.5, 0.75, 1$.



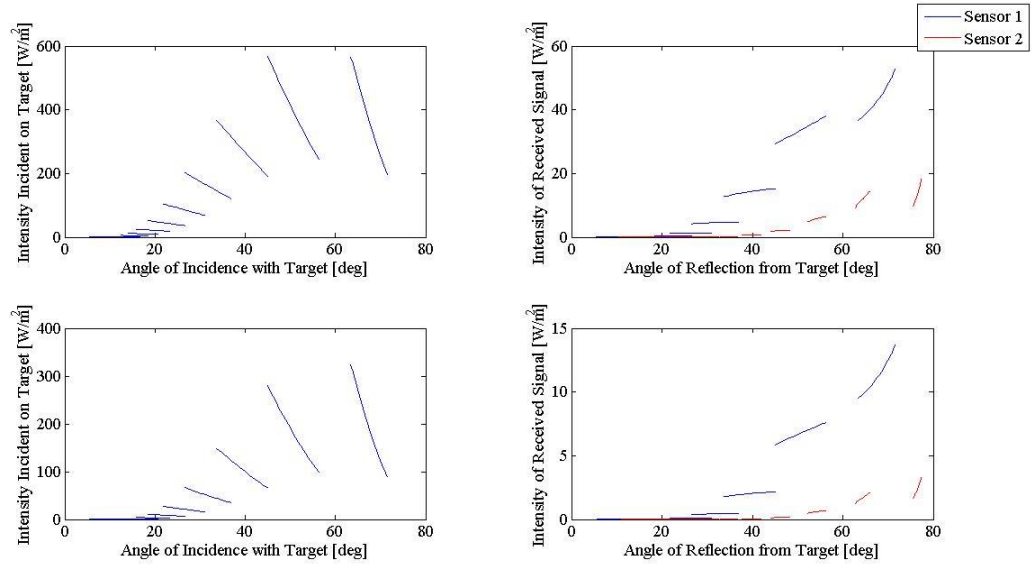
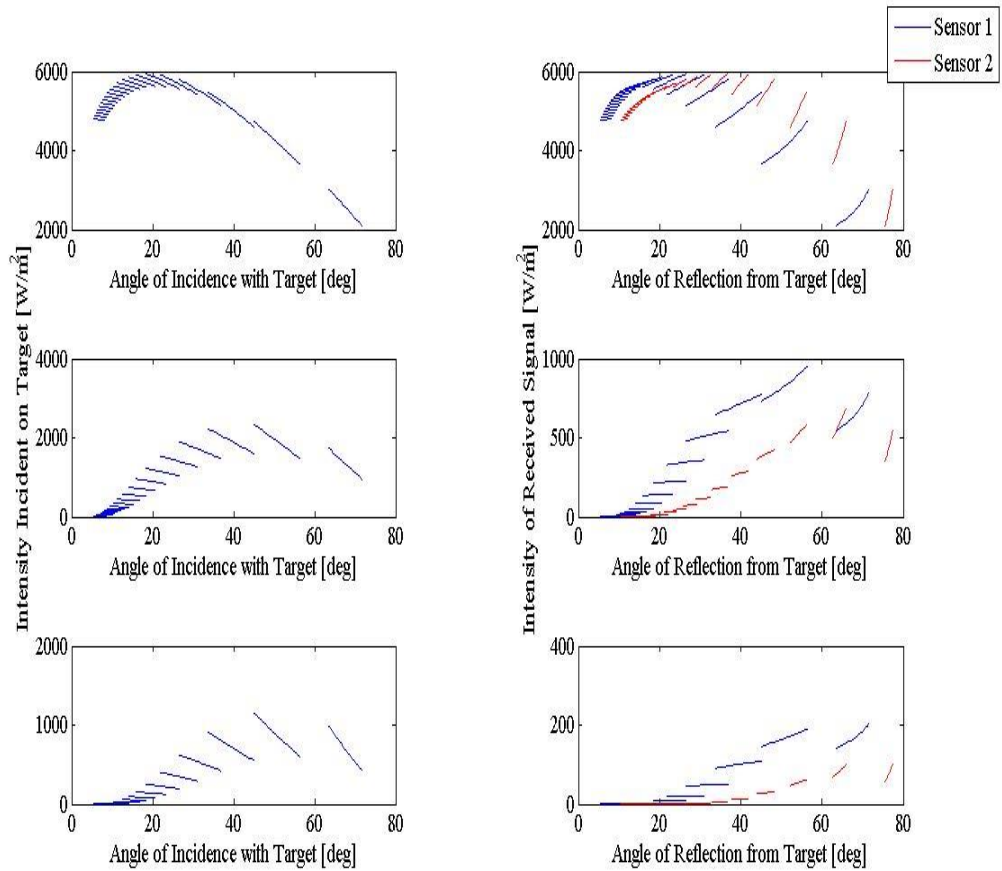


Figure 36 Case V illumination and intensity results for increasing attenuation at depth $z = 50$ [m]. From top to bottom $k = 0, 0.25, 0.5, 0.75, 1$.



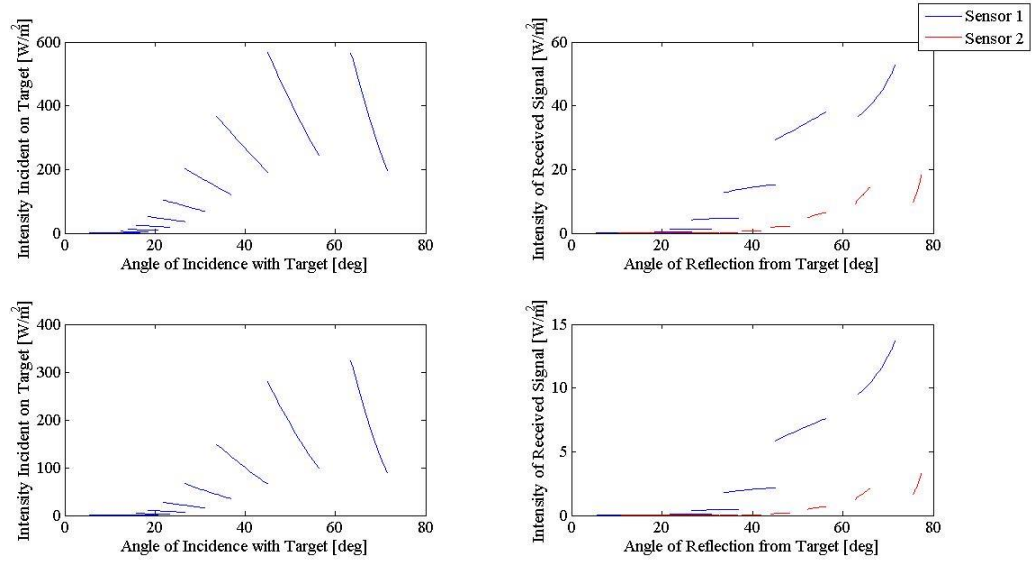


Figure 37 Case V illumination and intensity results for increasing attenuation at depth $z = 60$ [m]. From top to bottom $k = 0, 0.25, 0.5, 0.75, 1$.

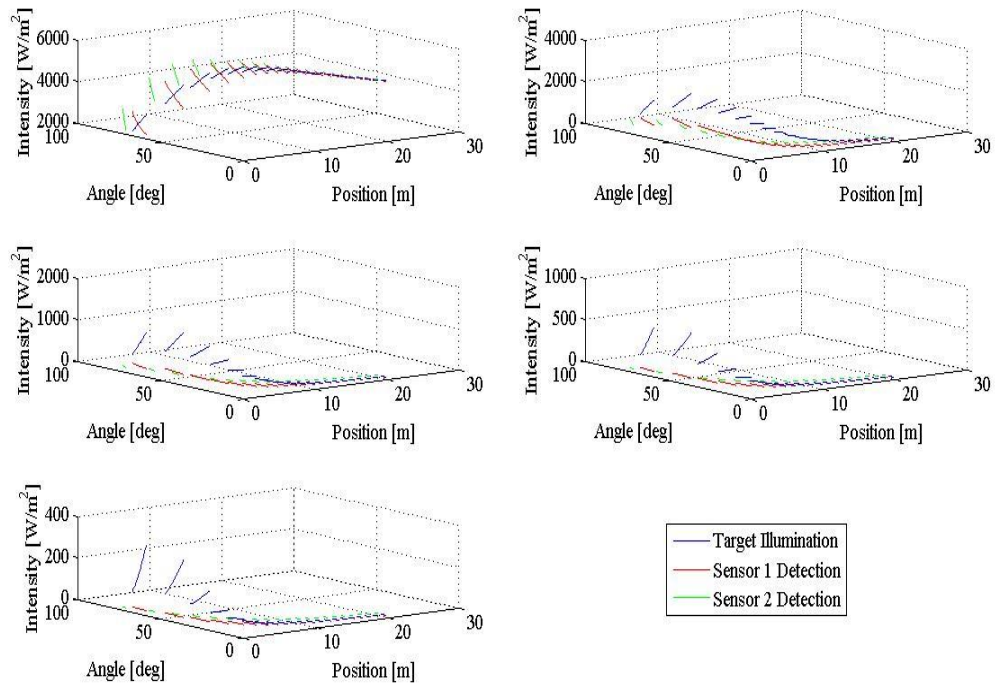


Figure 38 Case V 3D illumination and intensity results for increasing attenuation at depth $z = 10$ [m]. From top to bottom, left to right $k = 0, 0.25, 0.5, 0.75, 1$.

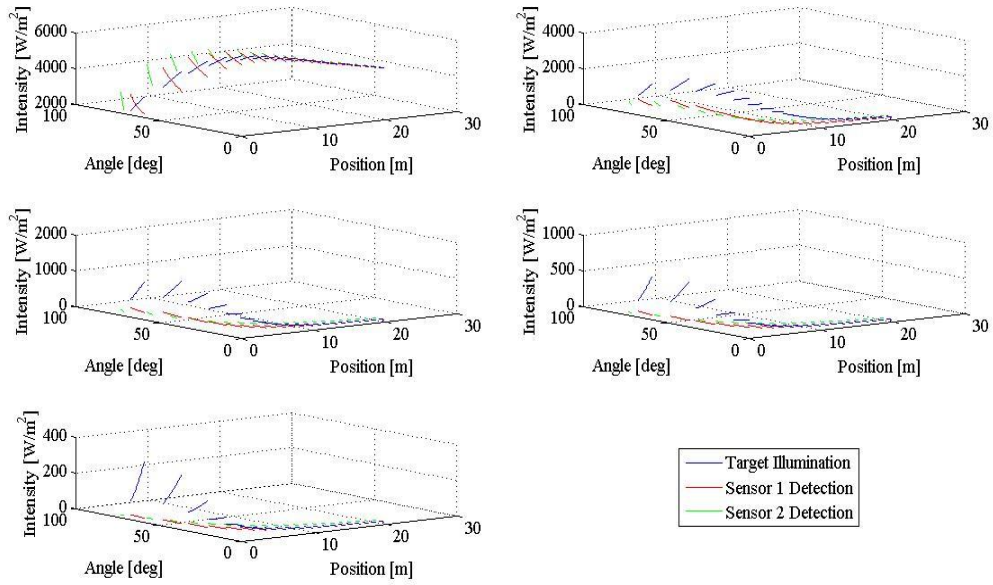


Figure 39 Case V 3D illumination and intensity results for increasing attenuation at depth $z = 20$ [m]. From top to bottom, left to right $k = 0, 0.25, 0.5, 0.75, 1$.

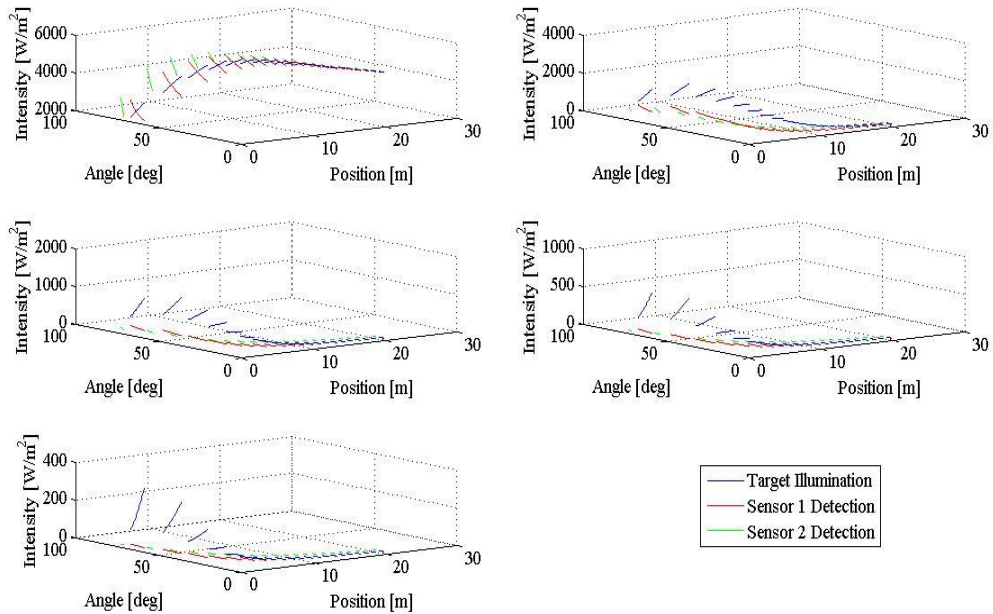


Figure 40 Case V 3D illumination and intensity results for increasing attenuation at depth $z = 30$ [m]. From top to bottom, left to right $k = 0, 0.25, 0.5, 0.75, 1$.

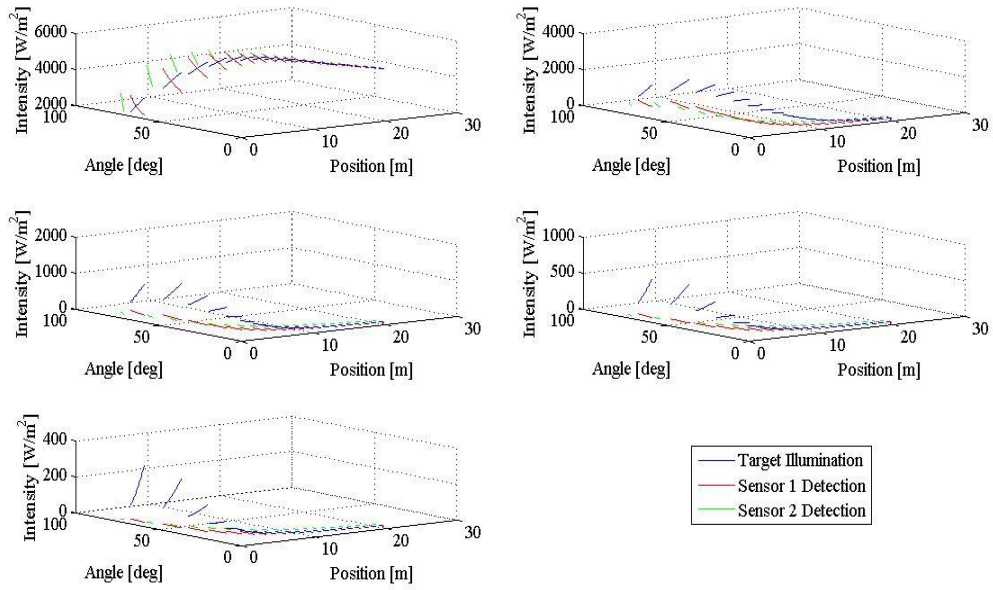


Figure 41 Case V 3D illumination and intensity results for increasing attenuation at depth $z = 40$ [m]. From top to bottom, left to right $k = 0, 0.25, 0.5, 0.75, 1$.

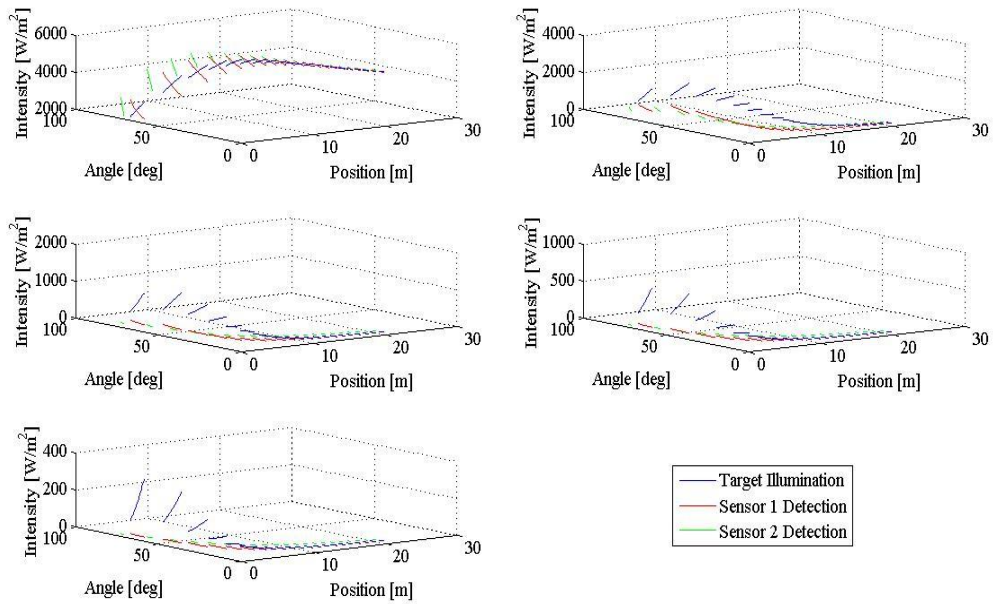


Figure 42 Case V 3D illumination and intensity results for increasing attenuation at depth $z = 50$ [m]. From top to bottom, left to right $k = 0, 0.25, 0.5, 0.75, 1$.

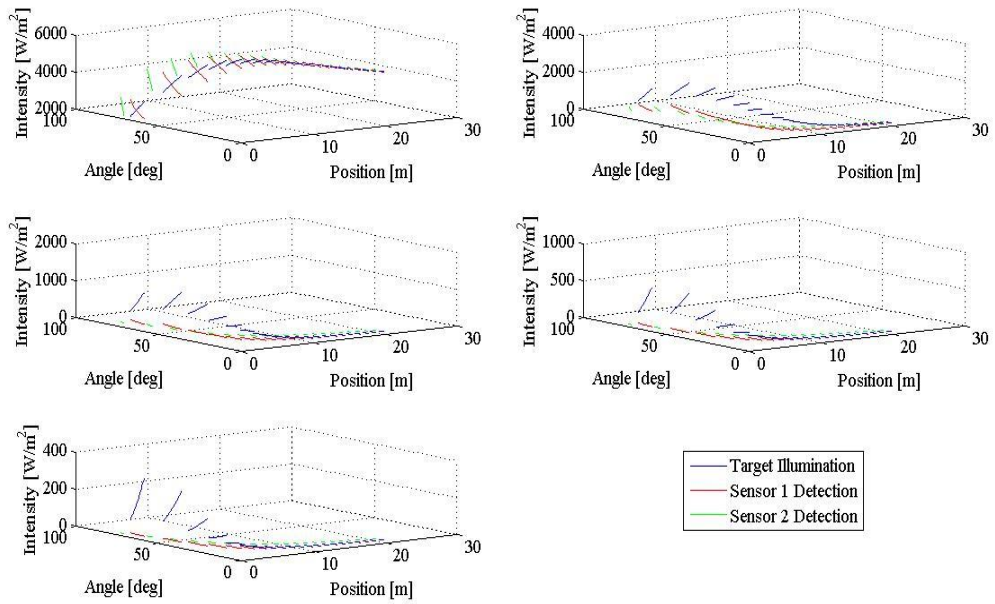


Figure 43 Case V 3D illumination and intensity results for increasing attenuation at depth $z = 60$ [m]. From top to bottom, left to right $k = 0, 0.25, 0.5, 0.75, 1$.

Appendix B Case V SNR Results

Results in this section represent the associated signal to noise ratios for the scenarios and results described in section 6.1. They are listed in sets by attenuation ($k = 0, 0.25, 0.5, 0.75, 1$) and increasing depth ($z = 10, 20, 30, 40, 50, 60$ [m]).

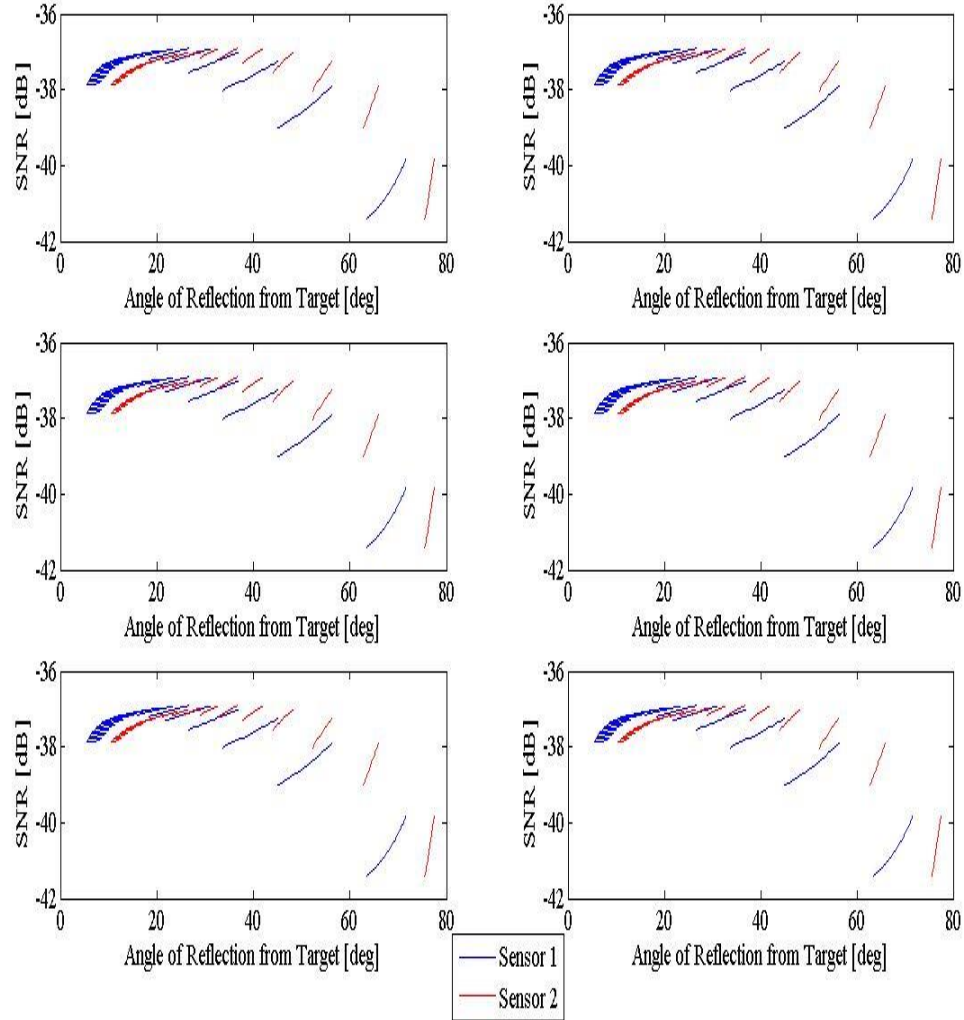


Figure 44 Case V: Multi-sensor SNRs for attenuation $k = 0$ and (from top to bottom, left to right) depth $z = 10, 20, 30, 40, 50$ and 60 [m]

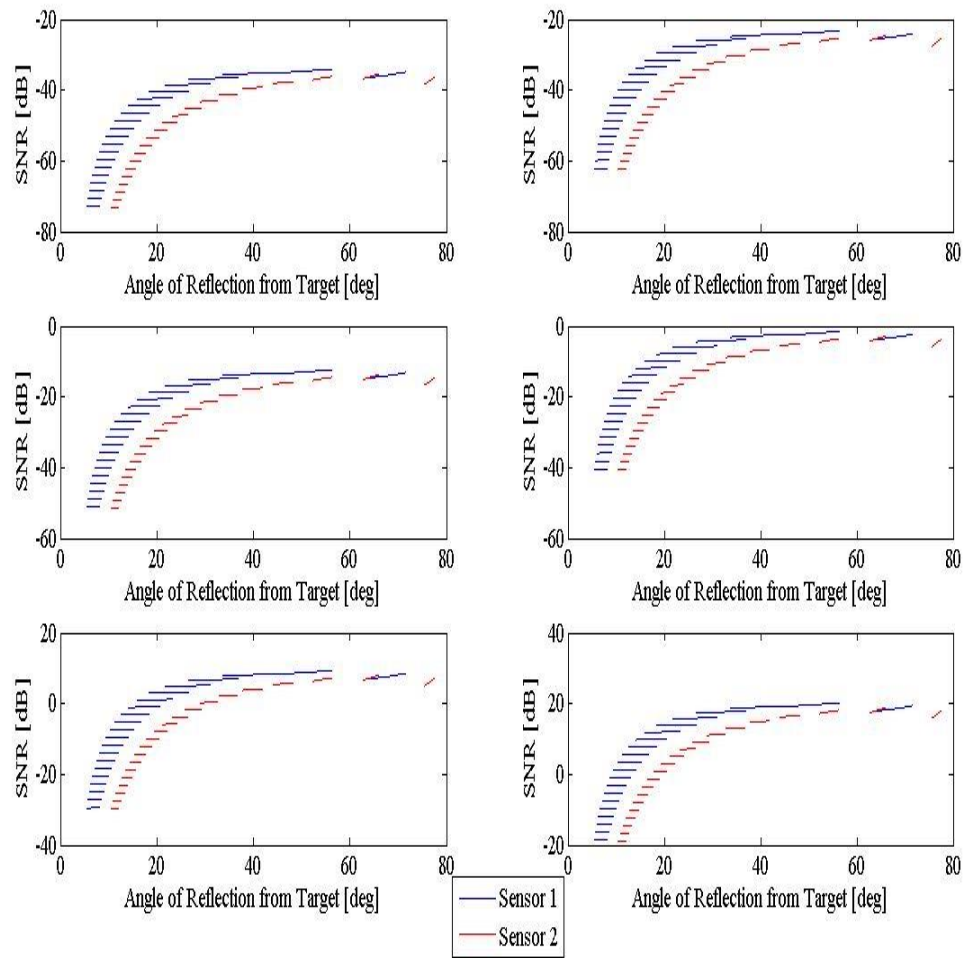


Figure 45 Case V: Multi-sensor SNRs for attenuation $k = 0.25$ and (from top to bottom, left to right) depth $z = 10, 20, 30, 40, 50$ and 60 [m]

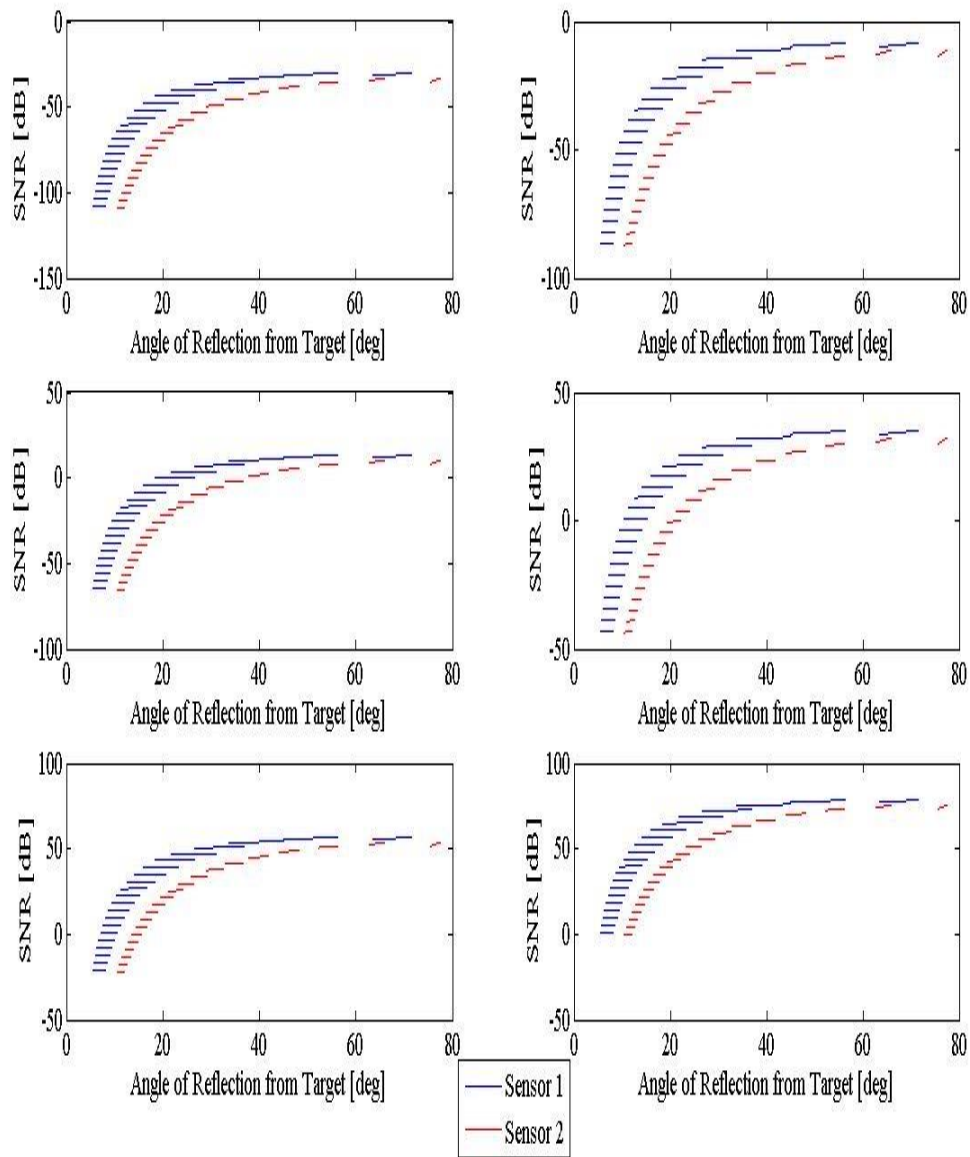


Figure 46 Case V: Multi-sensor SNRs for attenuation $k = 0.5$ and (from top to bottom, left to right) depth $z = 10, 20, 30, 40, 50$ and 60 [m]

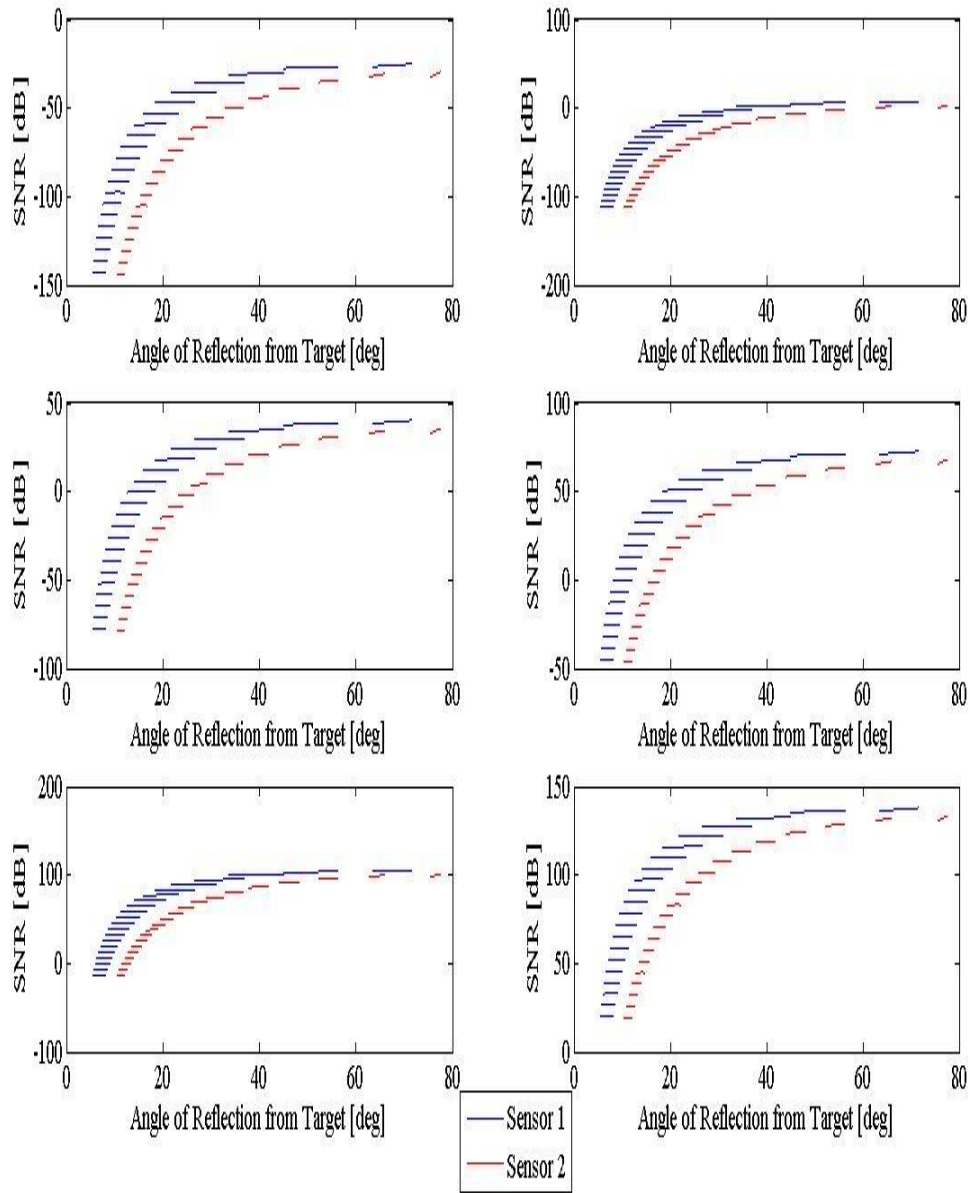


Figure 47 Case V: Multi-sensor SNRs for attenuation $k = 0.75$ and (from top to bottom, left to right) depth $z = 10, 20, 30, 40, 50$ and 60 [m]

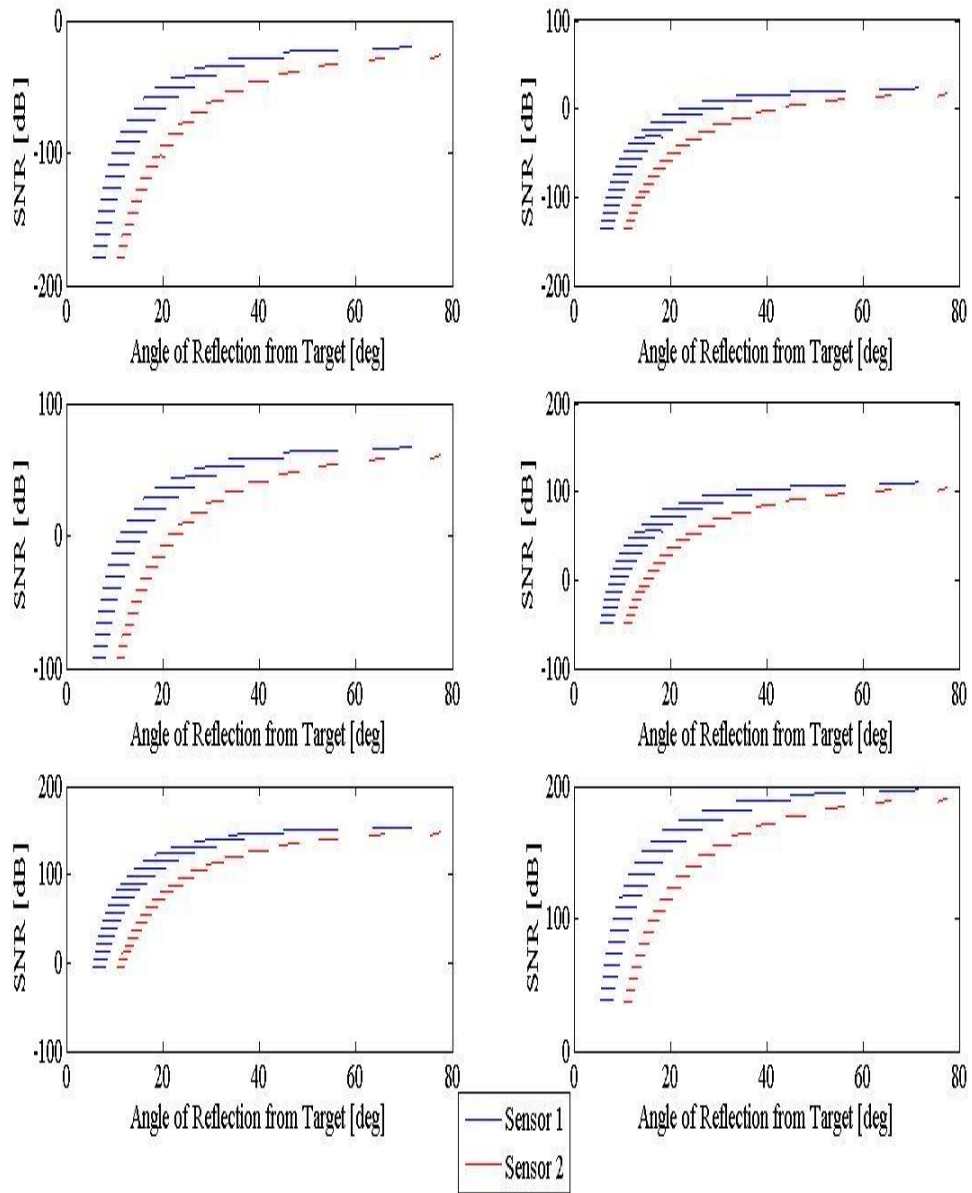


Figure 48 Case V: Multi-sensor SNRs for attenuation $k = 1$ and (from top to bottom, left to right) depth $z = 10, 20, 30, 40, 50$ and 60 [m]

References

- [1] Stann, B., Giza, M., Robinson, D., Ruff, W., Sarama, S., Simon, D., and Sztankay, Z., (April 1999), "A scannerless imaging lidar using a laser diode illuminator and FM/cs radar principles", *Conference on Laser Radar Technology and Applications IV, April 1999, Orlando, FL, SPIE*, vol 3707.
- [2] Wojtanowski, J., Mierczyk, Z., and Zygmunt M., (2008), "Laser remote sensing of underwater objects", *Proc of SPIE*, vol 7105.
- [3] Ricci, R., Francucci, M., De Dominicis, L., Ferri de Collibus, M., Fornetti, G., Guarneri, M., Nuvoli, M., Paglia E., and Bartolini, L., (8 Feb 2010) "Techniques for effective optical noise rejection in amplitude-modulated laser optical radars for underwater three-dimensional imaging", *EURASIP Journal on Advances in Signal Processing*.
- [4] Farr, N., Chave, A.D., Freitag, L., Preisig, J., White, S.N., Yoerger, D., and Sonnichsen, F., (2006), "Optical Modem Technology for Seafloor Observatories", *IEEE 1-4244-0115-1/06*.
- [5] Zhao, J., Barnes, B., Melo, N., English, D., Lapointe, B., Muller-Karger, F., Schaeffer, B., Hu, C., (2013), "Assessment of Satellite-Derived Diffuse Attenuation Coefficients and Euphotic Depths in South Florida Coastal Waters", *Remote Sensing of Environment*, 131 38-50, pp 38-49.

- [6] Dalgleish, F.R., Caimi, F.M., Vuorenkoski, A.K., Britton, W.B. and Ramos, “Experiments in Bistatic Laser Line Scan (LLS) Underwater Imaging”, Proceedings Marine Technology Society/IEEE Oceans Conference 2009, Paper 090710-001.
- [7] Alley, D., Mullen, L., and Laux, A., “Compact, Dual-Wavelength, Non-Line-of-Sight (NLOS) Underwater Imager”, EO and Special Mission Sensors Division NAVAIR, Patuxent River, MD.
- [8] Tan, C., Seet, G., Sluzek, A., and He, D., (1 Oct 2004), “A novel application of range-gated underwater laser imaging system (ULIS) in near-target turbid medium”, *Optics and Lasers in Engineering*, vol. 43, pp 995-1009.
- [9] Dalgleish, F.R., “Multilateration for localization of modulated or pulsed optical illuminators”, Harbor Branch Oceanographic Institute, Florida Atlantic University.
- [10] Hu, P., Tan, J., Yang, H., Zhao, X., and Liu, S., “Phase-shift laser range finder based on high speed and high precision phase-measuring techniques”, The 10th International Symposium of Measurement Technology and Intelligent Instruments: 29 June – 02 July 2011
- [11] Bucher, R., and Misra, D., (2002), “A Synthesizable VHDL Model of the Exact Solution for Three-dimensional Hyperbolic Positioning System”, *VLSI Design*, vol 15 (2), pp 507-520.
- [12] BeauJean, P., Mohamed, A., and Warin, R., (2007), “Acoustic positioning using a tetrahedral ultrashort baseline array of an acoustic modem source transmitting frequency-hopped sequences”, *Journal of the Acoustic Society of America*, vol 121 (1), pp 144-157.
- [13] Bakhoun, E., (2006), “Closed-Form Solution of Hyperbolic Geolocation Equations”, *IEEE Transactions of Aerospace and Electronic Systems*, Vol 42, pp 1396-1404.

- [14] Sen, Z. (2008), “Solar Energy Fundamentals and Modeling Techniques: Atmosphere, Environment, Climate Change and Renewable Energy”, Springer-Verlag London Limited, pp 77.
- [15] Li, J., Zhao, B., Tang, L., and Zhao, X., (2009), “Digital Signal Processing Method and Implementation for Pulse Laser Rangefinder”, The Ninth International Conference on Electronic Measurement & Instruments.
- [16] Mourad, B., and Pramod, K., (1989), “Decentralized CFAR Signal Detection”, *IEEE Transactions on Aerospace and Electronics Systems*, Vol AES-25 No 2, pp 141-149.
- [17] Mahafza, B.R., (2013), “Radar Systems Analysis and Design Using MATLAB, 3rd Ed”, CRC Press, Boca Raton.
- [18] Magaz, B., Belouchanri, A., and Hamadouche, M., (2011), “Automatic Threshold Selection in OS-CFAR Radar Detection Using Information Theoretic Criteria”, *Progress in Electromagnetics Research B*, Vol 30, pp 157-175.
- [19] Tait, P., (2005). “Introduction to Radar Recognition”, *Institute of Engineering and Technology*, Michael Faraday House, United Kingdom, pp 77-78.
- [20] Oren, M., and Nayar, S. K., (1994). “Generalization of Lambert’s Reflectance Model”, *SIGGRAPH 94 Proceedings of the 21st Annual Conference on Computer Graphics and Interactive Techniques*, pp 239 -246.
- [21] Janecek, M., and Moses, W. W., (2009). “Optical Reflectance Measurements for Commonly Use Reflectors”, *Lawrence Berkley National Laboratory*, pp 1 – 7.
- [22] Ryer, A., (1997). “Light Measurement Handbook”, International Light, Inc, Newbury, MA, p 27.
- [23] Peterman, D., (2005). “The Misunderstood M Squared”, *SPIE OEMagazine*, p 30.